Organusulfur catalysis with reduced molybdenum sulfides containing the Mo_6S_8 cluster

by

Thomas Jay Paskach

A dissertation submitted to the graduate faculty

in partial fulfillment of the requirements for the degree of

DOCTOR OF PHILOSOPHY

Major: Chemical Engineering

Program of Study Committee:
Glenn L. Schrader, Major Professor
Dennis Vigil
Kurt Hebert
Marc Porter
Dennis Johnson

Iowa State University

Ames, Iowa

2002

Graduate College
Iowa State University

This is to certify that the doctoral dissertation of

Thomas Jay Paskach

has met the dissertation requirements of Iowa State University

Glenn L. Schrader
Major Professor

Charles E. Hladky
For the Major Program

For the Graduate College

TABLE OF CONTENTS

CHAPTER 1. GENERAL INTRODUCTION

Introduction

Organosulfur compound synthesis

Industrial synthesis of sulfur-containing organic chemicals basically focuses on the broad categories of mercaptans (thiols), alkylsulfides (thioethers), polysulfides, and thiophenes. Of the organo-sulfur compounds produced, by far the most important in terms of quantities produced is methyl mercaptan (methanethiol or MeSH), which is produced mainly for the downstream production of methionine and methanesulfonyl chloride. Higher thiols are also used in the manufacture of rubber and plastics as polymerization regulators, chain transfer agents, or initiators. Other important organosulfur chemicals are dimethyl sulfide (DMS) and dimethyl disulfide (DMDS), both of which are used extensively for presulfiding of industrial hydroprocessing catalysts, and substituted thiophenes which are used as intermediates for production of agrochemicals, dyes, and pharmaceuticals.

Thiols are produced commercially at the rate of about 10^4 ton/yr from hydrogen sulfide (H_2S) and alcohols or olefins, using homogeneous free-radical synthesis, or heterogeneous catalysts based on solid acids or supported metal oxides and/or sulfides. Despite this large production rate, and the industrial importance of the organosulfur compounds, only limited research has been devoted to the development of new catalytic materials for their synthesis. Additionally, for most organosulfur catalytic reactions, only limited information exists about reaction mechanisms, active sites, adsorbed surface species, and especially the nature of the catalysts under reaction conditions.

Catalysts containing the Mo_6S_8 cluster

Since the discovery of their catalytic activity in the 1980's, research has been devoted to studying the properties of reduced molybdenum sulfides containing the Mo_6S_8 cluster (Fig. 1), especially with regard to their unique activity and selectivity as hydrodesulfurization (HDS) catalysts. It has recently been discovered that these materials are also active for organosulfur synthesis. Materials based on the Mo_6S_8 cluster include: 1) crystalline ternary molybdenum sulfides, $M_x(Mo_6S_8)$, 2) amorphous ternary molybdenum sulfides, $M_x^{n+}(Mo_6S_8)S_{2x/n}$, and 3) ligated molecular complexes, $Mo_6S_8L_{6-x}$, where M is the ternary metal, and L is a ligand such as pyridine. The materials are referred to as reduced molybdenum sulfides since the oxidation state of the molybdenum atoms in this overall neutral cluster, $(Mo_6S_8)^0$, is +2.67; Mo is reduced with respect to the common sulfides MoS_2 (+4) or Mo_2S_3 (+3).

The crystalline ternary materials are known as Chevrel phases (1) and have been studied extensively for HDS (2,3,4,5) including mechanistic studies (6,7,8). This is due in part to the fact that a range of these materials can be prepared with different ternary metals, but all having the same basic crystal structure. This allows for easier characterization and determination of the role of the ternary metal in their catalytic function. They are generally produced by solid state techniques and have low surface areas (~1 m^2/g).

The recent discovery of the new synthesis route to high surface area (up to 200 m^2/g) amorphous ternary molybdenum sulfides has allowed further understanding of the Mo_6S_8 materials. These materials are prepared by a low temperature route synthesis of an amorphous sodium-containing material, $Na_x(Mo_6S_8)S_{2x/n}$, x = 2 or 3. In a subsequent step, the sodium material is contacted with a metal salt in solution, where the metal replaces the

sodium by ion exchange. A wide variety of ternary metals have been successfully incorporated into this structure, including Pt, resulting in a previously unknown material; $Pt(Mo_6S_8)S$ (9).

The ligated molecular complexes, $Mo_6S_8L_{6-x}$, are produced via similar chemistry as the amorphous ternary materials, but with the addition of the ligand molecule to the first step, resulting in partial ligation of the clusters. This category includes amorphous $Na_x(Mo_6S_8)L_{6-x}$, amorphous $(Mo_6S_8)L_{6-x}$, and crystalline $(Mo_6S_8)L_6$. The latter, fully ligated material is often soluble in the ligating solvent, which may allow for a simple impregnation procedure to produce the materials on a support such as alumina.

Research Goals

This research focused both on the extension of our knowledge of materials containing the Mo_6S_8 cluster, including preparation of new materials, and the study of their catalytic properties in reactions with organosulfur compounds. Since the materials represent a new family of catalysts, this research focused on answering the three basic questions of concern for any new catalyst: activity, selectivity, and stability. These questions are answered by performing reaction studies with these catalysts to determine their activity and selectivity with regard to specific reactions and side reactions. The question of catalyst stability is one that requires study of the reactions over time, as well as characterization of the catalyst itself to determine if any important structural changes occurred during the reaction. The organosulfur reactions of interest include HDS of thiophene and synthesis of low molecular weight thiols.

Explanation of Dissertation Format

This dissertation consists of six chapters and one appendix. Figures and references are located at the end of each chapter. Chapter 1 is a brief overview of organosulfur catalysis, with emphasis on thiol synthesis. Chapter 2 is an in-depth literature review, focusing on research done by others in the area of thiol synthesis. Chapters 3 and 4 are articles published (or submitted) by the author in refereed journals. Chapter 5 is a paper in a format suitable for journal submission. Chapter 6 contains general conclusions and recommendations for future work on the subject of organosulfur catalysis over the reduced molybdenum sulfides studied in this work. The appendices contain information on the nomenclature of sulfur-containing compounds and recommendations for their safe handling, and an in-depth explanation of the methods used to estimate thermodynamic properties and equilibrium constants.

References

1 Chevrel, R. and Sergent, M., Topics in Current Physics, (Ø. Fischer and M. B. Maple, Eds.), **32** (Ch. 2), Springer-Verlag, Heidelberg (1982).

2 Hilsenbeck, Shane J., McCarley, Robert E., Thompson, R. Kirk, Flanagan, Lucy C., and Schrader, Glenn L., *Journal of Molecular Catalysis A: Chemical* **122** (1997) 13-24.

3 McCarty, K. F. and Schrader, G. L., *Ind. Eng. Chem. Prod. Res. Dev.*, **23** (1984), 519.

4 McCarty, K. F., Anderegg, J. W., and Schrader, G. L., *J. Catal.*, **93** (1985), 375.

5 Eckman, M. E., Anderegg, J. W., and Schrader, G. L., *J. Catal.*, **117** (1989), 246.

6 Huckett, S. C., Angelici, R. J., Eckman, M. E., and Schrader, G. L., *J. Catal.*, **113** (1988), 36.

7 Markel, E. J., Schrader, G. L., Sauer, N. N., and Angelici, R. J., *J. Catal.*, **116** (1989), 11.

8 Sauer, N. N., Markel, E. J., Schrader, G. L., and Angelici, R. J., *J. Catal.*, **117** (1989), 295.

9 Paskach, T. J., Hilsenbeck, S. J., Thompson, R. K., McCarley, R. E., and Schrader, G. L., *J. Alloys and Compounds*, **311** (2000) 169-180.

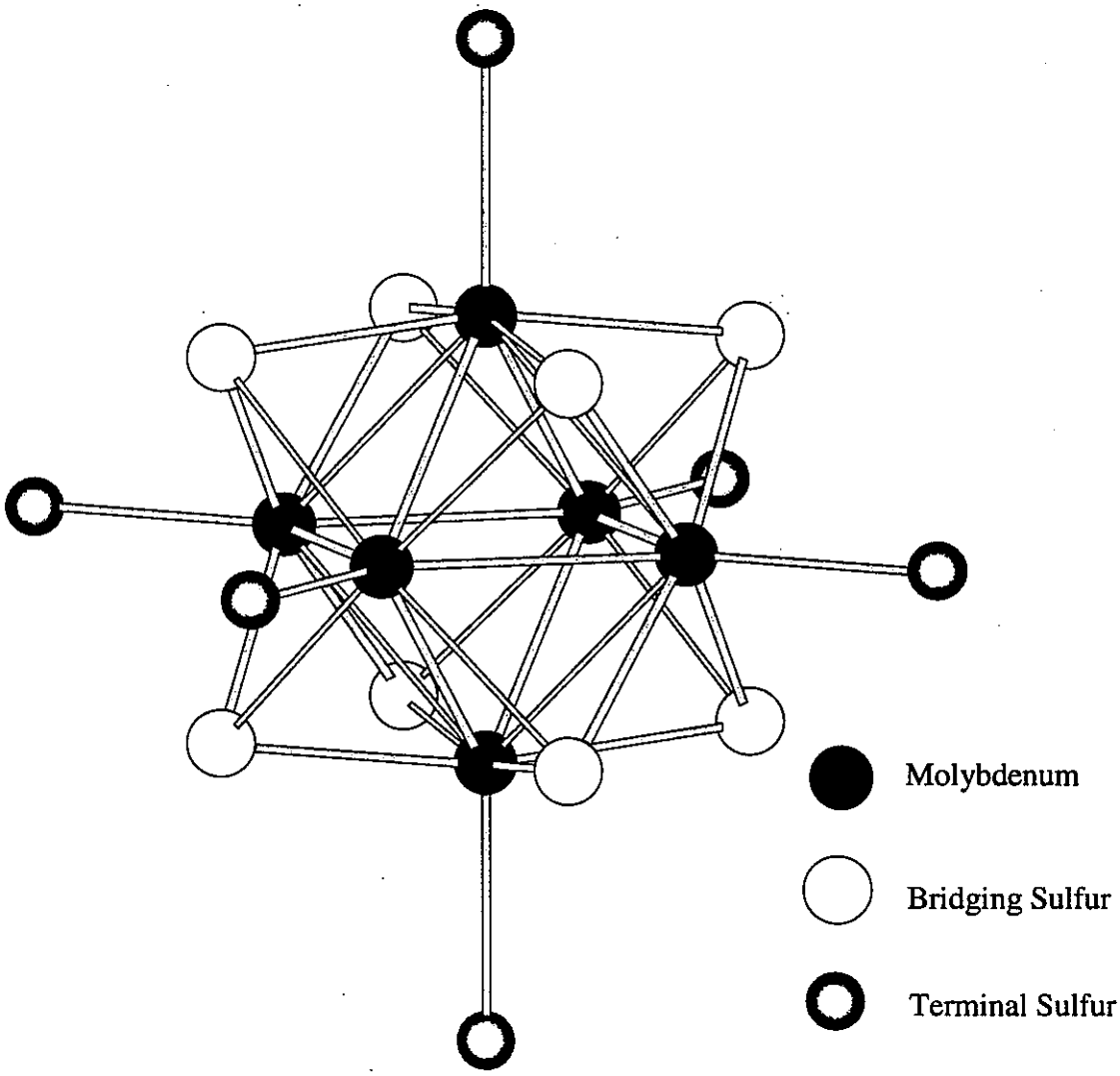

Figure 1. Structure of the Mo_6S_8 hexanuclear cluster unit which is formed by a molybdenum octahedron and eight triply bridging sulfur atoms capping each face. Additionally, six terminal positions are located at the vertices of the octahedron and are occupied by either organic ligands or sulfur atoms.

CHAPTER 2. LITERATURE REVIEW

Thiols can be made from H_2S and olefins, alcohols, or carbonyl compounds on heterogeneous catalysts or by free radical synthesis by ultraviolet radiation or homogeneous initiator catalysts. The heterogeneous catalysts basically fall into two categories. First there are the strictly acidic catalysts, which includes materials like dry solid anion-exchange resins or $AlCl_3$. Second are the metal oxides, which includes aluminum oxides, magnesium oxides, etc. This category also includes materials such as the oxides of W, Mo, Ni, Co, Fe, Pb, Cu, Re, impregnated on a support such as alumina or silica-alumina or unsupported as the massive metal oxide itself. The literature review is divided into discussions of the chemical reactions and thermodynamics, followed by more information regarding the catalysis of these reactions.

Industrial Processing Routes

Free-radical Processes

Photosynthesis with UV radiation is used for production of thiols from olefins and H_2S. Generally primary thiols are produced from α-olefins (anti-Markownikoff addition). The reaction gives ~90% selectivity to the primary thiol. The major side product is the secondary thiol. Most 1-BuSH is produced commercially via this route, starting with 1-butene.

Recently discovered have been certain homogeneous catalysts (1) that can also form free-radicals with H_2S which react with olefins forming thiols. This reaction is more selective, for example up to ~97% for n-octanethiol, so may be commercialized soon.

Solid Acid Catalytic Processes

Solid acid catalysts are used in thiol synthesis also. This group of heterogeneous catalysts includes dry cation-exchange resins containing bound sulfonic acid groups, $AlCl_3$, BF_3 or BF_3-H_3PO_4, H_3PO_4 on kieseghur (solid phosphoric acid), silica-alumina, filtrol clays, and zeolites. Starting with α-olefins and H_2S, the major product is the secondary thiol, in a reaction that follows Markownikoff addition. For example, starting with 1-butene on dry cation exchange resin, 2-butyl mercaptan (2-BuSH) is produced at about 70% selectivity. The alkylsulfide is produced at about 30% selectivity, but what is important is that no 1-BuSH is made, since separation of 1-BuSH and 2-BuSH is not industrially practical. Commercial preparation of tertiary thiols relies exclusively on solid acid catalysts.

Metal Oxide (sulfide) Catalytic Processes

By far the most important catalysts industrially for primary thiol synthesis are the so-called metal oxide catalysts. This group includes catalysts such as γ-alumina, exchanged zeolites, or oxides of Ni, Mo, W, Co, and less importantly Cu, Fe, Pb, Mn, Ag, U, and Re. They are typically promoted with bases such as alkaline or alkaline earth metal oxides, carbonates, or hydroxides, or prepared with group I salts of the metal oxides. These types of materials have been studied extensively and found to catalyze the production of thiols from almost every thinkable feedstock: olefins, alcohols, alkylsulfides, alkyldisulfides, CS_2, carbonyl compounds (aldehydes, ketones, and carboxylic acids), and even carbon oxides (CO and CO_2).

Alcohols and H_2S as Feedstocks

Early work in catalytic organo-sulfur synthesis was summarized by Weisser and Landa (2). The first example of the use of heterogeneous catalysis for thiol synthesis from

alcohols and H_2S was in 1910 by Sabatier. The catalyst was ThO_2 which was later supported on pumice (3). In the 1950's, alumina began to be used as a catalyst, and by the 1970's, catalysts consisted of Ni, Mo, W, Co, Cu, Fe, Pb, Mn, Ag, and U, or combinations of these. These were usually prepared in oxide form supported on alumina, and usually promoted with potassium oxide. At that time, the temperatures required for high alcohol conversion on the heterogeneous catalysts were high, and yield of the thiol was poor. Carbonyl compounds could be converted to thiols more efficiently at higher temperatures, and for this reason, carbonyl compounds or mixtures of alcohols and carbonyl compounds were preferred (4).

The first *commercial* catalysts for thiol synthesis were potassium tungstate promoted γ-alumina (K_2WO_4/γ-Al_2O_3), although the range of catalysts studied include the sulfides (or oxides which become sulfides) of W, Mo, Ni, Co, Fe, Pb, Cu, Re, supported or not. Though hardly mentioned in the literature, these catalysts are expected to undergo sulfidation with H_2S to various extents at conditions normally employed for the synthesis reactions, so that the active form of the catalyst is either a metal oxysulfide or a more extensively sulfided form.

Today primary thiols are mainly produced on metal oxide catalysts from H_2S and primary alcohols. The use cheaper α-olefin feedstocks on metal oxides is also possible, but the major product is the secondary thiol. The most recently patented catalysts are actually potassium hydroxide (KOH) promoted commercial HDS catalysts, which consist of Ni-Mo, Ni-W, Co-Mo, or Co-W, supported on alumina (5), sulfided α- or β-alumina trihydrate formed by KOH treating γ-Al_2O_3[6], K_2WO_4 with KOH on alumina, or just KOH on alumina (7). These catalysts are very active and selective for primary thiol production from primary alcohols and H_2S. Starting with MeOH and H_2S, the major side products include DMS,

DME, and methane. Starting with the secondary alcohol on the metal oxide catalysts largely leads to dehydration (8), with formation of α and β-olefins.

Sulfur-containing Feedstocks

The metal oxide catalysts have also been studied for the production of thiols from various related compounds such as alkylsulfides and disulfides. The sulfides, especially DMS, are obtained as byproducts of thiol production. This is a very active area of research since the sulfide byproducts are the major byproducts and produced well in excess of demand (9,10,11,12,13). The use of disulfides to form thiols, especially DMDS to MeSH, has also been extensively studied more recently since DMDS has much lower toxicity and handling problems relative to MeSH (14,15,16,17,18).

Carbon Oxides as Feedstocks

The carbon oxides have been studied as feedstocks to MeSH (19), starting with synthesis gas (CO and H_2) or a mixture of CO_2 and H_2. Sulfur sources were either H_2S or elemental sulfur. Catalysts for these processes were W-K/Al_2O_3 (20) and various other metal oxides (Cr, Ni, Zn).

The industrial production of thiols has made use of various feedstocks. Basically, we have two choices to make: 1) choice of sulfur source, and 2) choice of carbon source. Almost all work in this area has been with the use of H_2S as the sulfur source, owing to its reactivity and availability, and despite its drastic toxicity.

For MeSH production, there are several possible choices (Table 1, Fig. 1) for the carbon source. Carbon disulfide (CS_2) as a feedstock was patented in 1975 by Phillips Petroleum Co (21). Carbonyl sulfide (COS) is not preferred due to its toxicity, price, and hydrogen (H_2) requirements. The aldehyde is unattractive, since the price of this materials is high ($0.37/lb

for formaldehyde, compared to $0.38/*gallon* for methanol [MeOH] (22)). Methane is very stable and does not react with H_2S over any known catalysts at reasonable temperatures. Therefore, MeOH is the remaining choice. Not surprisingly, MeOH is the commercially preferred feedstock for MeSH synthesis.

Thermodynamics of Thiol Synthesis

Examination of the thermodynamics of the reactions involved in thiol synthesis is useful to help decide which reactions are favorable at various temperatures. Reactions that are unfavorable thermodynamically can sometimes then be eliminated from consideration, simplifying the eventual discussion of kinetics. Determination of reaction equilibrium constants at temperatures other than 298 K requires knowledge of the Gibbs energy of reaction at the reaction temperature. See Appendix C for a detailed description of this calculation method.

Starting with MeOH and H_2S, several reactions (Table 2, Fig. 2) are possible. The important side reactions are DMS and dimethylether (DME) production, each of which can occur in two ways, with the elimination of either H_2O or H_2S. COS and CS_2 formation could become important at high temperatures. The heat of reaction and Gibbs energy of reaction are listed at 25°C (23).

To produce a higher thiol, other types of feedstocks can be considered, such as olefins. An overview of the chemistry and thermodynamics (Tables 3, 5, Figs. 3, 5) involved for production of EtSH and BuSH starting with various C_2 and C_4 feedstocks have been assembled. The heat of reaction and Gibbs energy of reaction are listed at 25°C.

Thermodynamics dictates that starting with the olefins, the temperature must be kept low (<200°C) for reasonable conversion (24). The use of alcohols allows slightly higher

temperatures (up to 350°C) since the reaction is less temperature dependent. Aldehydes extend this analogy further and allow even higher reaction temperatures. However, as the temperature is increased further to about 600°C, thiophenes are favored by dehydrocyclization reactions, which are highly endothermic. Addition of excess H_2S (up to ~200% excess) is known to favor the H_2S addition reaction also, and tends to improve selectivity to the thiol vs. the sulfide.

Starting specifically with the alcohols and H_2S, important side reactions are possible, (Tables 4, 6, Figs. 4, 6). The heats of reaction and Gibbs energies of reaction are listed at 25°C.

Kinetics, Catalysis, and Mechanisms for Thiol Synthesis on Metal Oxides

Mashkina *et al.* performed extensive work in characterizing the acid-base properties of metal oxides and sulfides, including zeolites, (Si, Be, Mg, Zr, Ti, Al, V, W, HNaY, HZSM-5, NaX) that are potential catalysts for thiol and alkylsulfide synthesis (25,26,27,28,29). Carbon monoxide TPD was generally used to probe the quantity and strength of basic sites, and ammonia or pyridine was used with IR to determine the quantity and types of acid sites (30). These data were later summarized and used to correlate the relative strength and type of acid and base sites on these catalysts with their activity and selectivity for thiol and alkylsulfide synthesis (31). Their discussion was framed in terms of the types of catalytic sites: 1) protonic acid sites (Brønsted sites), 2) Lewis acid sites, and 3) basic sites. In this work, Mashkina *et al.* concluded that the catalysts which contained strong Lewis acid sites (e.g. Al^{3+} in the most common alumina catalyst) had to also have coordinated basic sites, in order to activate the H_2S and alcohol.

Ziolek *et al.* have also studied the production of MeSH with MeOH and H_2S over various metal oxides (32) and the production of C_2 and C_3 thiols over various zeolites (33,34). In their work on metal oxides, they studied TiO_2, Al_2O_3, $MgAl_2O_4$, CeO_2, and MgO. Their experiments involved the IR characterization of chemisorbed MeOH and H_2S on these oxides, IR determination of the strength of basic sites by adsorption of probe molecules (SO_2 for basic sites), and activity measurements through reactor studies. They concluded that their research had confirmed the work of Mashkina in that what was required for an active catalyst was a pairing of strong Lewis acid sites and medium strength basic sites.

Kinetic studies by Mashkin (35), were done for DMS and MeSH synthesis on alumina helped to elucidate the mechanism further. In this work it was postulated that the formation of MeSH from MeOH and H_2S follows the mechanism below. X_1 is the initial vacant site, X_2 is the methylated (or methoxylated) site, and X_3 is a site poisoned with H_2O. The sites referred to by X_1, X_2 and X_3 are the basic sites (surface oxygen atoms). This model incorporated the fact that pairs of acid and base sites are needed for activation of alcohol and H_2S by assuming that acid and base sites are always adjacent; a surface site was mathematically equivalent to a pair of acid and base sites.

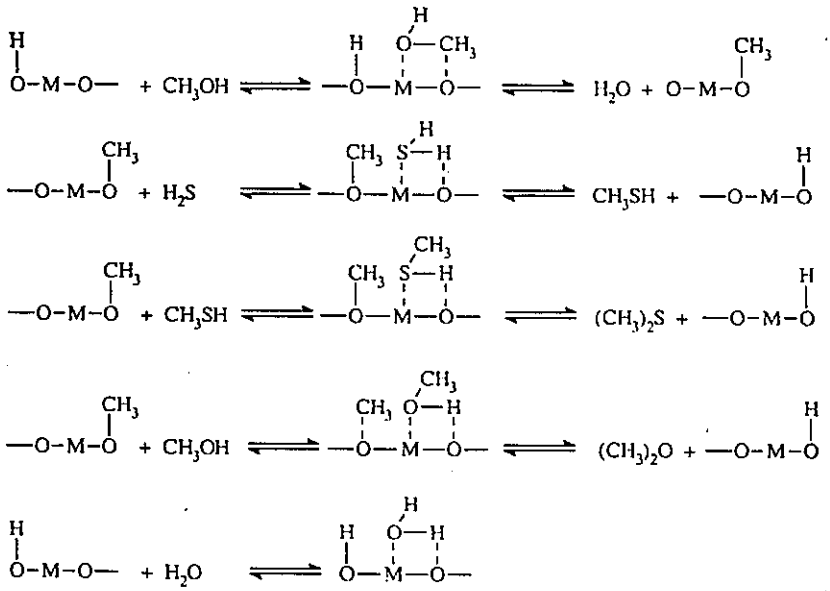

1. $CH_3OH + [X_1] \Leftrightarrow [X_2] + H_2O$

2. $H_2S + [X_2] \Leftrightarrow [X_1] + CH_3SH$

3. $CH_3SH + [X_2] \Leftrightarrow [X_1] + (CH_3)_2S$

4. $CH_3OH + [X_2] \Leftrightarrow [X_1] + (CH_3)_2O$

5. $H_2O + [X_1] \Leftrightarrow [X_3]$

Fitting of the experimental data required the assumption that the heat of adsorption varied linearly with coverage. This was thought to be because the surface had a distribution of adsorption site strengths. This gave rise to fractional exponents in the rate expressions. After numerical fitting of the site strength distribution parameters, the exponents always turned out to be 0.5. The author concluded that the alcohol is activated by dissociative chemisorption with formation of a surface alkoxide group. Similarly, H_2S was thought to be activated by dissociative chemisorption and formation of a surface sulfhydryl (-SH) group. The surface alkoxide and sulfhydryl group then reacted to form the thiol, which then

desorbed. The -OH and -H left on the surface also reacted to form H_2O. The surface alkoxidation was extended to higher alcohols, so that the same type of mechanism is expected for those cases as well. This result had direct impact on the proposed mechanism for ethanethiol synthesis (see chapter 5).

The author found experimentally that by weakening the Lewis acid sites and strengthening basic sites with an alkali metal such as potassium, the formation of DME and DMS were suppressed. This meant that reactions 3 and 4 above could be ignored and the kinetic model simplified. The resulting simplified model fit experimental data reasonably well.

In another part of the study, Brønsted sites were considered. In the proposed mechanism, the formation of DMS and DME involved these sites through hydrogen bonding with the proton.

From this mechanism, it was proposed that the most effective catalyst for MeSH synthesis should have a pairing of acid-base sites on the surface, where the alcohol and H_2S can be activated, respectively. This allows close association of these activated species so they can react with each other. Further, in order to have a selective catalyst for thiol synthesis, reactions involving the thiol with another thiol or a surface alkoxide to form alkylsulfide, and alkoxyl groups reacting with each other to form ether should be suppressed. For this to occur, the protonic sites should be poisoned and Lewis acid sites should be weakened. Basic sites should be strong in order to increase the rates of reactant activation.

The work by Mashkin and Mashkina both ignore the fact that the metal oxide catalysts under study will react with H_2S in the reaction environment. Often, metal oxide catalysts that are exposed to H_2S become significantly sulfided and may even become

pyrophoric. Therefore, the catalyst that is characterized by adsorption of tracer molecules in air, without H_2S present, could be significantly different than the material that is the actual catalyst involved in the reaction. For the investigation of the nature of active sites involved in the reaction, it is important to at least consider this fact, or better yet, characterize the catalysts *in situ* or after reaction without exposure to atmospheric oxygen. In addition, some of the surface mechanisms proposed have improbable steps involving the simultaneous formation of multiple bonds and requiring the coordination of ensembles of surface sites. For example, in reactions involving Brønsted acid sites, H_2S is thought to not dissociate on adsorption, so the formation of MeSH proceeds via an intermediate species that requires 3 surface bonds[3]:

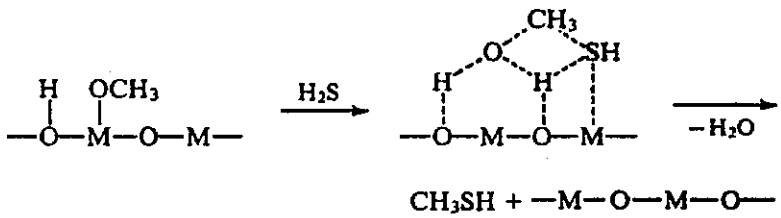

Nonetheless, it is interesting to note that the most recent metal oxide catalysts in use for industrial synthesis of thiols seemed to follow the results of this work. All of them made use of potassium hydroxide to promote an alumina base, which would be expected to poison Brønsted sites and weaken the remaining Lewis acid sites. Basic sites should be strengthened by this KOH addition also. It is unclear what effect the addition of KOH would have on the hydrogenation/ dehydrogenation function of the Co-Mo-S, Ni-Mo-S, or K_2WO_4 remaining. It is also interesting to note the work by Clark and Elkins[5] wherein the active catalyst was similarly KOH treated alumina, but in this case it was treated in H_2S without

first calcining in air. It is possible that there were aluminum oxysulfides formed on the surface from the aluminum trihydrate surface gel produced during the initial KOH treatment. We should expect the same effect for the transition metal catalysts supported on alumina and treated with KOH, and used after drying, but without calcination.

References

1 U.S. Patent 5,741,934 to Sandler, Stanley R., Peerce-Landers, Pamela J., and Forquy, Christian. (1998)

2 Otto Weisser and Stanislav Landa: Sulphide Catalysts, Their Properties and Applications, Pergamon Press, Oxford, NY, 1973.

3 A. V. Mashkina, *Russian Chemical Reviews*, **64** (12), (1995) 1131-1147.

4 U.S. Patent 3,994,980 to Phillips Petroleum Company (1976).

5 U.S. Patent 5,898,012, to Phillips Petroleum Company (1999).

6 European Patent Application 564 706 A1 to Elf Atochem North America, Inc. (1992).

7 U.S. Patent 5,874,630 to Occidental Chemical Corporation (1999).

8 C. Forquy, E. Arretz, *Stud. Surf. Sci. Catal.* **41** (1988), (*Heterog. Catal. Fine Chem.*), 91-104.

9 U.S. Patent 4,005,149 to Phillips Petroleum Company (1977).

10 U.S. Patent 4,059,636 to Phillips Petroleum Company (1977).

11 U.S. Patent 4,396,778 to Pennwalt Corporation (1983).

12 S. N. Koshelev, E. A. Paukshtis, N. A. Verkhoturova, and A. V. Mashkina, *Kinetics and Catalysis,* **29**(2) (1988), 326-330.

13 U.S. Patent 4,927,972 to Elf Aquitaine Production (1990)

14 Emmanuel Cadot, Michel Lacroix, Michele Breysse, and Emmanuel Arretz, *J Catal.*, **164** (1996), 490-492.

15 U.S. Patent 5,493,058 to Elf Aquitaine Production (1996)

16 S. N. Koshelev, E.A. Paukshtis, R. S. Sagitullin, A. V. Bezrukov, and A.V. Mashkina, *React. Kinet. Catal. Lett.*, **27**(2) (1985), 387-391.

17 A. V. Mashkina, V. N. Yakovleva, and L. G. Sakhaltueva, *React. Kinet. Catal. Lett.*, **53**(2) (1994), 363-368).

18 A. V. Mashkina, B. P. Borodin, and V. Yu., Mashkin, *Kinetics and Catalysis,* **36**(2) (1995), 251-255.

19 U.S. Patent 4,410,731 to Pennwalt Corporation (1983).

20 J. Barrault, M. Boulinguiez, C. Forquy, and R. Maurel, *Appl. Catal.* **33** (1987), 309-330

21 U.S. Patent 3,880,933 to Phillips Petroleum Company (1975).

22 Chemical Market Reporter, March, 2000

23 T. E. Daubert and R. P. Danner, Physical and Thermodynamic Properties of Pure Chemicals: Data Compilation, Hemisphere Publishing Corp., NY (1989)

24 Otto Weisser and Stanislav Landa, Sulphide Catalysts, Their Properties and Applications, Pergamon Press, Oxford, NY, 1973.

25 V. M. Kudenkov, E. A. Paukshtis, and A.V. Mashkina, *React. Kinet. Catal. Lett.*, **38**(1) (1989), 199-203.

26 A. V. Mashkina, E. A. Paukshtis, and V. N. Yakovleva, *Kinetics and Catalysis,* **29**(5) (1988), 1014-1020.

27 S. N. Koshelev, E. A. Paukshtis, N. A. Verkhoturova, A. V. Mashkina, *Kinetics and Catalysis,* **29**(2) (1988), 326-330.

28 A. V. Mashkina, E. A. Paukshtis, V. N. Yakovleva, *Kinetics and Catalysis,* **29**(3) (1988), 514-520.

29 A. V. Mashkina, E. A. Paukshtis, E. N. Yurchenko, V. N. Yakovleva, and A. V. Popov, *React. Kinet. Catal. Lett.*, **34**(2) (1987), 407-412.

30 E. A. Paukshtis and E. N. Yurchenko, *Russian Chemical Reviews*, **52**(3) (1983), 242-258.

31 A. V. Mashkina, *Russian Chemical Reviews*, **64**(12) (1995), 1131-1147.

32 M. Ziolek, J. Kujawa, O. Saur, and J. C. Lavalley, *J. Phys. Chem.*, **97** (1993), 9761-9766.

33 M. Ziolek, J. Kujawa, and P. Decyk, *Zeolites*, **8**(Jan) (1988), 54-59.

34 M. Ziolek and J. Kujawa, *Zeolites*, **10**(Sept/Oct) (1990), 657-661.

35 V. Yu. Mashkin, *Applied Catalysis A: General*, 109 (1994), 45-61.

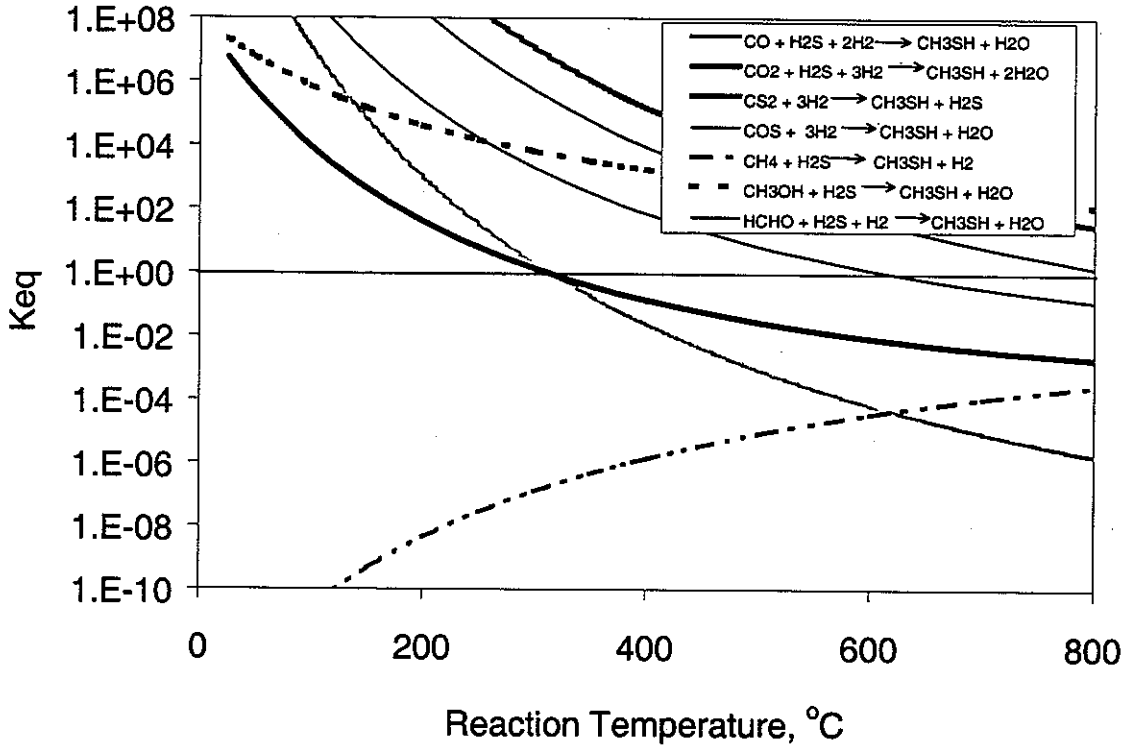

Figure 1: Equilibrium constants for the various C_1 feeds.

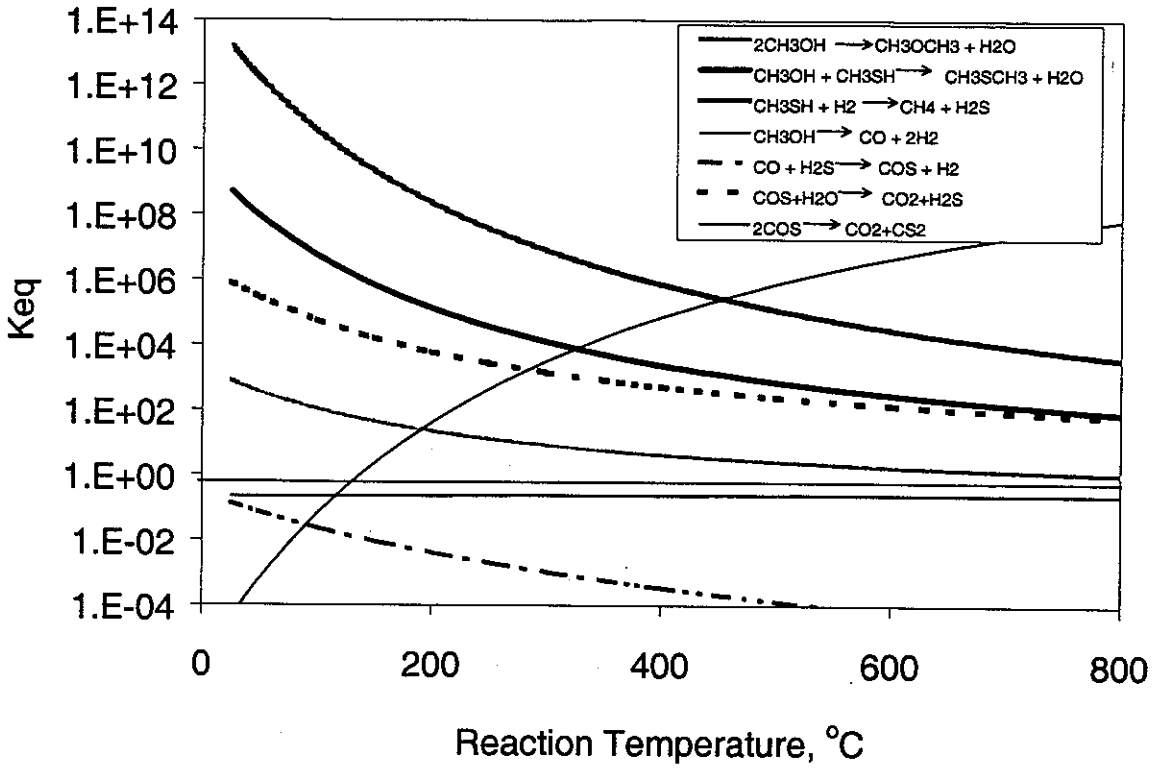

Figure 2: Equilibrium constants for various side reactions involved in MeSH synthesis, starting with MeOH.

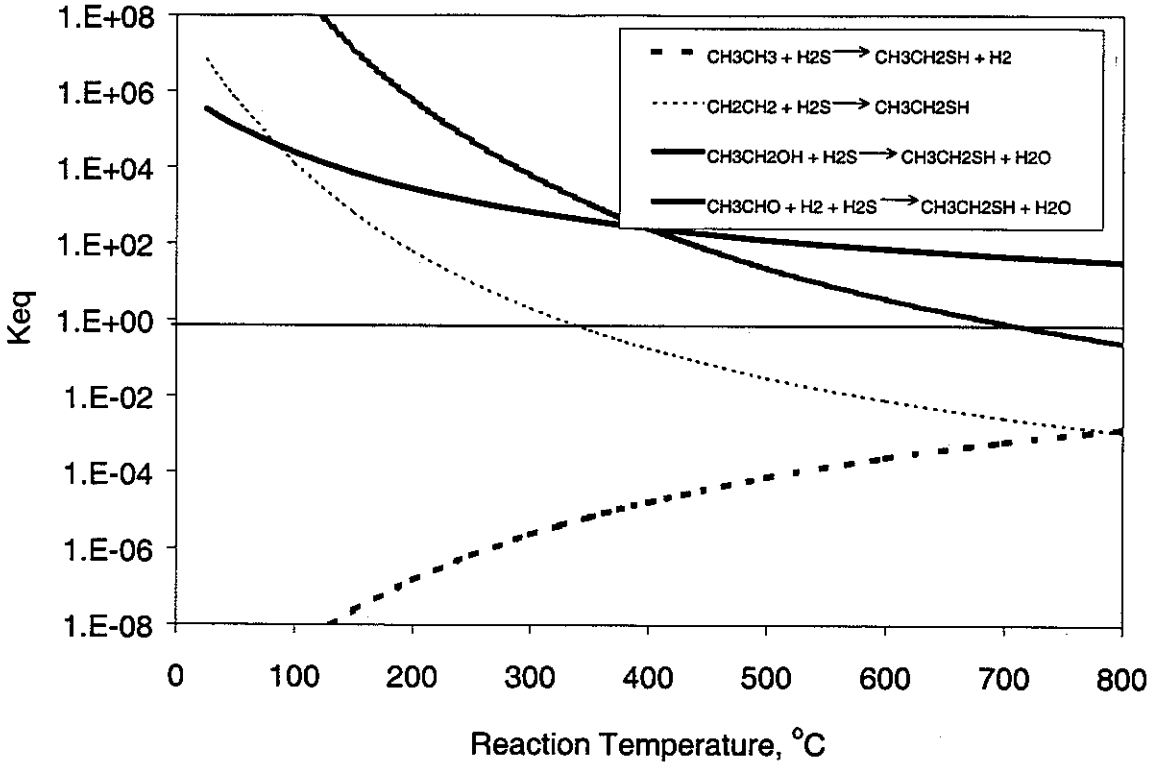

Figure 3. Equilibrium constants for the various C_2 feeds.

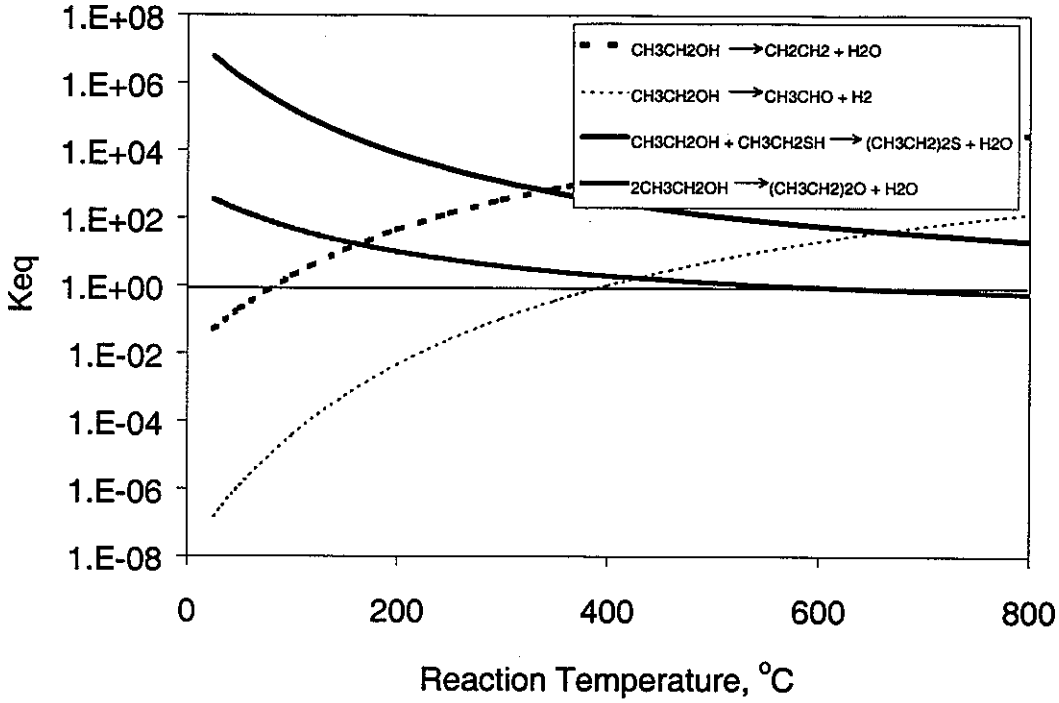

Figure 4: Equilibrium constants for various side reactions involved in EtSH synthesis.

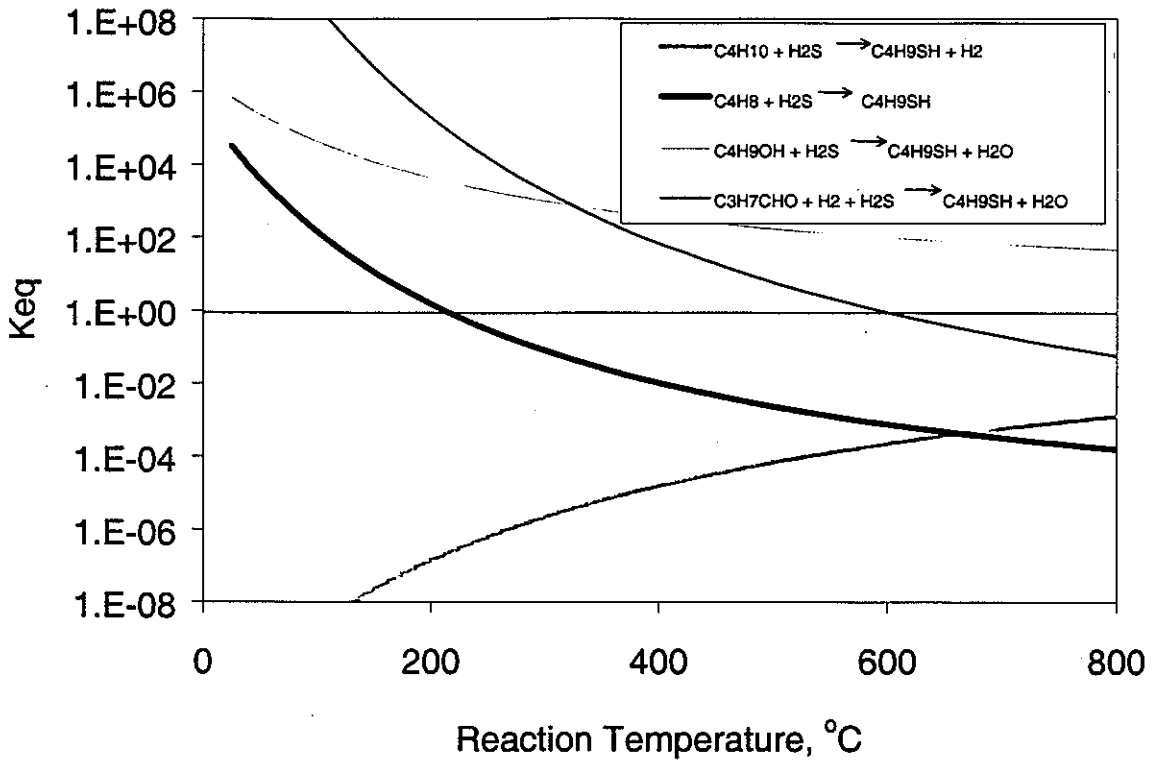

Figure 4: Equilibrium constants for 1-BuSH synthesis, starting with various hydrocarbon feedstocks.

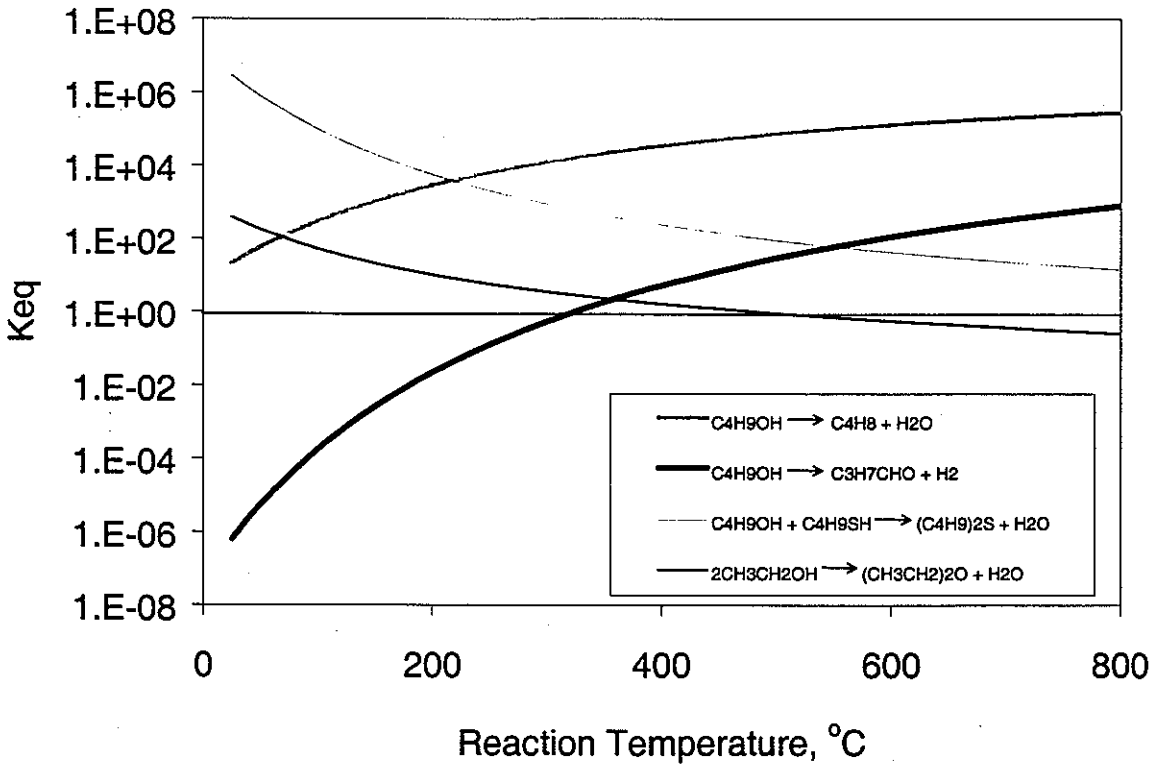

Figure 5: Equilibrium constants for reactions involved in 1-BuSH synthesis.

Table 1: The various C_1 feedstocks for MeSH synthesis.

Feedstock	Stoichiometry (all species in gas phase)	ΔH°_{298} kJ/mol product	ΔG°_{298} kJ/mol product
CO	$CO + H_2S + 2H_2 \rightarrow CH_3SH + H_2O$	-132.92	-67.15
CO_2	$CO_2 + H_2S + 3H_2 \rightarrow CH_3SH + 2H_2O$	-91.75	-38.49
CS_2	$CS_2 + 3H_2 \rightarrow CH_3SH + H_2S$	-159.96	-109.51
COS	$COS + 3H_2 \rightarrow CH_3SH + H_2O$	-125.67	-72.11
Methane	$CH_4 + H_2S \rightarrow CH_3SH + H_2$	73.22	75.10
MeOH	$CH_3OH + H_2S \rightarrow CH_3SH + H_2O$	-42.78	-41.89
Formaldehyde	$HCHO + H_2S + H_2 \rightarrow CH_3SH + H_2O$	-127.60	-94.41

Table 2. Side reactions for MeSH synthesis from MeOH and H_2S. $\rightarrow$

Reaction	Stoichiometry (all species in gas phase)	ΔH°_{298} kJ/mol product	ΔG°_{298} kJ/mol product
Etherification	$2CH_3OH \rightarrow CH_3OCH_3 + H_2O$	-24.53	-16.55
Dialkylsulfide synthesis	$CH_3OH + CH_3SH \rightarrow CH_3SCH_3 + H_2O$	-56.09	-49.64
Thiol hydrogenolysis	$CH_3SH + H_2 \rightarrow CH_4 + H_2S$	-73.22	-75.097
CO formation	$CH_3OH \rightarrow CO + 2H_2$	90.14	25.26
COS formation	$CO + H_2S \rightarrow COS + H_2$	-7.25	4.96
CO_2 formation	$COS+H_2O \rightarrow CO_2+H_2S$	-33.92	-33.62
CS_2 formation	$2COS \rightarrow CO_2+CS_2$	0.37	3.78

Table 3. The various feedstocks for EtSH synthesis.

Feedstock	Stoichiometry (all species in gas phase)	ΔH°_{298} kJ/mol product	ΔG°_{298} kJ/mol product
Alkane	$CH_3CH_3 + H_2S \rightarrow CH_3CH_2SH + H_2$	58.71	61.12
Alkene	$CH_2CH_2 + H_2S \rightarrow CH_3CH_2SH$	-77.43	-38.95
Alcohol	$CH_3CH_2OH + H_2S \rightarrow CH_3CH_2SH + H_2O$	-32.53	-31.52
Aldehyde	$CH_3CHO + H_2 + H_2S \rightarrow CH_3CH_2SH + H_2O$	-100.77	-70.51

Table 4. Side reactions involved in EtSH synthesis from EtOH and H_2S.

Reaction	Stoichiometry (all species in gas phase)	ΔH°_{298} kJ/mol product	ΔG°_{298} kJ/mol product
Dehydration	$CH_3CH_2OH \rightarrow CH_2CH_2 + H_2O$	44.89	7.43
Dehydrogenation	$CH_3CH_2OH \rightarrow CH_3CHO + H_2$	68.24	38.99
Alkylsulfide formation	$CH_3CH_2OH + CH_3CH_2SH \rightarrow (CH_3CH_2)_2S + H_2O$	-45.09	-38.64
Ether formation	$2CH_3CH_2OH \rightarrow (CH_3CH_2)_2O + H_2O$	-25.09	-14.54

Table 5. The various feedstocks for 1-BuSH synthesis.

Feedstock	Stoichiometry (all species in gas phase)	ΔH°_{298} kJ/mol product	ΔG°_{298} kJ/mol product
Alkane (n-butane)	$C_4H_{10} + H_2S \longrightarrow C_4H_9SH + H_2$	58.21	61.05
Alkene (1-butene)	$C_4H_8 + H_2S \longrightarrow C_4H_9SH$	-66.90	-25.75
Alcohol (1-butanol)	$C_4H_9OH + H_2S \longrightarrow C_4H_9SH + H_2O$	-34.58	-33.31
Aldehyde (butanal)	$C_3H_7CHO + H_2 + H_2S \longrightarrow C_4H_9SH + H_2O$	-103.20	-68.71

Table 6. Side reactions involved in 1-BuSH synthesis from 1-BuOH and H_2S.

Reaction	Stoichiometry (all species in gas phase)	ΔH°_{298} kJ/mol product	ΔG°_{298} kJ/mol product
Dehydration	$C_4H_9OH \longrightarrow C_4H_8 + H_2O$	32.32	-7.56
Dehydrogenation	$C_4H_9OH \longrightarrow C_3H_7CHO + H_2$	68.62	35.40
Alkylsulfide formation	$C_4H_9OH + C_4H_9SH \longrightarrow (C_4H_9)_2S + H_2O$	120.93	-88.85
Ether formation	$2CH_3CH_2OH \longrightarrow (CH_3CH_2)_2O + H_2O$	-25.36	-14.81

CHAPTER 3. SYNTHESIS AND CHARACTERIZATION OF A NOVEL PLATINUM MOLYBDENUM SULFIDE CONTAINING THE MO_6S_8 CLUSTER

A paper published in the Journal of Alloys and Compounds[1]

Thomas J. Paskach[a,c], Shane J. Hilsenbeck[a,b,c], R. Kirk Thompson[a,c],
Robert E. McCarley[b,c], and Glenn L. Schrader[a,c2],

Department of Chemical Engineering[a],
Department of Chemistry[b], and
Ames Laboratory-USDOE[c]
Iowa State University
Ames, Iowa 50011

Abstract

Our previously discovered, low-temperature route for the preparation of ternary molybdenum sulfide cluster compounds containing the Mo_6S_8 structure has been used to synthesize a new Pt (PtMoS) material. Ion-exchange of amorphous NaMoS with $[Pt(NH_3)_4]Cl_2$ led to incorporation of the $[Pt(NH_3)_4]^{2+}$ cation yielding $[Pt(NH_3)_4](Mo_6S_8)S{\bullet}x(H_2O/MeOH)$, as confirmed by infrared and x-ray photoelectron spectroscopic (XPS) characterization. XPS indicated that this new platinum material had the reduced molybdenum oxidation state characteristic of ternary molybdenum sulfides containing the Mo_6S_8 structural unit. The surface area of the new PtMoS material was as high as 135 m^2/g. Attempts to convert the PtMoS material to a crystalline Chevrel phase $PtMo_6S_8$ by H_2 reduction at elevated temperatures were unsuccessful. However, H_2 treatment at 400°C provided material retaining the Mo_6S_8 cluster, probably as amorphous

[1] Reprinted with permission of J. of Alloys and Compounds,
[2] Author for correspondence

$Pt(Mo_6S_8)S$. The latter material is a very active hydrodesulfurization (HDS) catalyst, with much higher activity compared to other more stable compounds containing the Mo_6S_8 cluster unit.

1. Introduction

For many years, reduced ternary molybdenum chalcogenides have generated special attention because of their interesting structures and physical or chemical properties. Among these, the Chevrel phases [1], $M_xMo_6Q_8$ (with M = either a main group, transition or lanthanide metallic element and Q = S, Se or Te), have attracted the most attention. The common structural motif in these compounds [2] is the 3-dimensional cross-linking of Mo_6Q_8 cluster units by sharing Q atoms, as indicated in the formula $M_x(Mo_6Q_2Q_{6/2})Q_{6/2}$. The ternary metal atoms, M, reside in interstitial sites created by this network and transfer n electrons to the framework as in $M_x^{n+}(Mo_6Q_8^{xn-})$ [3,4]. Up to 4 electrons per Mo_6Q_8 unit may be transferred [5,6] so xn ranges from 1 to 4. Generally, frameworks with 4 transferred electrons (24 metal-metal bonding electrons per Mo_6Q_8 unit) are semiconducting while those with $xn<4$ are metallic – and often superconducting [2,7,8]. The variable valence of the Mo_6Q_8 cluster units is important to both the superconducting and catalytic properties of these compounds. The members of the family $LnMo_6S_8$ (with Ln = La to Lu) have been characterized as excellent hydrodesulfurization (HDS) catalysts for removal of organosulfur compounds found in petroleum [9,10,11,12,13].

Synthesis of stable phases $M_xMo_6Q_8$ generally can be achieved by direct combination of the elements, at temperatures typically in the range 900-1300°C. Metastable phases such as $HgMo_6S_8$ [14], $TlMo_6S_8$ [15], and others must be obtained by indirect methods, such as electrochemical [16] or direct insertion of M into the binary Mo_6S_8 [17]. The latter is itself a

metastable phase obtained by demetalation of $NiMo_6S_8$ [17] or $Cu_2Mo_6S_8$ [14,15]. Among the ions of metallic elements M^{n+} that have not yet been incorporated into the sulfide phases $M_xMo_6S_8$ are the group 8-10 members Ru, Rh, Pd, Ru, Ir and Pt. In the present paper, as a step towards the preparation of the latter phases, we show that a platinum-containing derivative, $[Pt(NH_3)_4]Mo_6S_9(H_2O)_m$, can be prepared by ion exchange of $[Pt(NH_3)_4]^{2+}$ with amorphous $Na_2Mo_6S_9$ [18].

2. Experimental

Materials

Since the reagents and products have been generally found to be air sensitive, all manipulations were performed using an inert-atmosphere drybox, a high-vacuum manifold, and Schlenk equipment, unless otherwise stated. High yields of amorphous ternary sodium molybdenum sulfide, $Na_2(Mo_6S_8)S{\bullet}y$MeOH (y = 4 to 5) (denoted as NaMoS[MeOH]*), were prepared by the reaction of Mo_6Cl_{12} with NaSH and NaOEt in refluxing *n*-BuOH followed by MeOH washing to remove the NaCl by-product [18]. Solvents were degassed by boiling for 5 min followed by immediate isolation. Methanol and butanol were also dried prior to use with 4Å Molecular Sieve. UHP (zero) nitrogen and zero hydrogen were used for temperature programmed desorption/ temperature programmed reduction (TPD/TPR), H_2 treatment, and HDS studies. Thiophene (99+% purity) was supplied by Aldrich and used as received.

Analytical

Molybdenum was determined gravimetrically as the 8-hydroxyquinolate [19]. Chlorine was analyzed by potentiometric titration with a standardized silver nitrate solution. Quantitative

---

* Since the composition of these materials depends on the stoichiometry of the reaction and solvent utilized, we indicate the formula of $Na_2(Mo_6S_8)S{\bullet}4$MeOH prepared in MeOH as NaMoS[MeOH], PtMoS[H_2O] for $Pt(NH_3)_4(Mo_6S_8)S{\bullet}4H_2O$ prepared in water, etc. PtMoS[5%H_2O] refers to PtMoS prepared in a 5% water / 95% MeOH mixture.

elemental analyses for Pt, Mo, and S were performed with an ARL SEMQ microprobe. The instrument was equipped with wavelength dispersive spectroscopy detectors and was operated at 10 kV and 25 nA. Powder samples were loaded in a dry box on double-stick carbon discs and placed in a sealed sample holder designed for air-sensitive samples. Peak profiles and backgrounds were determined for standards immediately before the analyses. At least ten regions for each sample were examined, and the compositional data were averaged.

Additional quantitative elemental analysis for Pt, Mo, S were performed by inductively coupled plasma (ICP) spectroscopy. Solutions were prepared by dissolving samples with hot *aqua regia* (50:50 concentrated HCl and HNO_3) followed by dilution to standard volume with deionized water. Analyses for Na were performed on the same solutions by atomic absorption spectroscopy (AAS). Solid samples were first degassed under vacuum at 150°C overnight to remove about 5 wt % volatile solvent.

Preparation of the Ternary Platinum Molybdenum Sulfide

Three methods were used to synthesize the ternary platinum molybdenum sulfides PtMoS[H_2O], PtMoS[MeOH], and PtMoS[5%H_2O]. NaMoS[MeOH] (1.00 g) and $[Pt(NH_3)_4]Cl_2 \cdot H_2O$ (0.34 g) were placed into a 100-mL Schlenk reaction flask in the drybox. Three variations in the preparation procedure involved addition of different solvents: 1) 50 mL of degassed H_2O, 2) 50 mL of dried, degassed MeOH, or 3) 57 mL of degassed MeOH and 3 mL of deoxygenated water. After the mixture was stirred at room temperature for 1-2 days, a black solid and faintly colored solution were obtained. The black solid was then filtered from the solution. For the preparations involving MeOH, the solid was rinsed 3-6 times with 20-30 mL aliquots of dried, deoxygenated MeOH. All PtMoS samples were dried under vacuum overnight and stored in the drybox.

Characterization Methods

Materials were characterized by x-ray photoelectron spectroscopy (XPS), infrared spectroscopy (FTIR), laser Raman spectroscopy (LRS), and x-ray diffraction (XRD). XPS data were obtained with a Physical Electronics Industries 5500 multitechnique surface analysis system using a monochromatic MgK_α source; binding energies were calibrated with adventitious C (C 1s = 284.6 eV). Infrared spectra (4000-200 cm^{-1}) were recorded in Nujol mulls with a Bomem MB-102 Fourier transform infrared spectrometer equipped with CsI optics. Laser Raman spectra were obtained in backscattering mode with a Kaiser Holospec f/1.8 spectrometer. A Coherent 532-50 diode-pumped solid state laser was used as the source (532 nm, 50 mW at the source) and a Princeton Instruments CCD (1100x330) was used with Winspec software for data acquisition and processing. XRD data were collected only on air-stable samples, in air using a Scintag 2000 θ–θ powder XRD instrument with CuK_α radiation at 45 kV bias and 30 mA emission current.

The surface areas of the compounds were determined according to the BET method using a Micromeritics ASAP 2010 instrument. N_2 at 77.35 K was the adsorbate.

H_2 Treatment and Temperature Programmed Desorption/Reduction

For H_2 treatment, PtMoS powder was placed in an alumina boat inside a quartz tube and heated to the desired temperature (200-1000°C) in a flow of pure H_2; this temperature was maintained for 2-4 h. After cooling under this flow, the product was stored in an inert-atmosphere drybox.

TPD studies were performed by heating 250 mg samples to 800°C (10°C/min) in a flow of pure N_2 (10 sccm). Temperatures were controlled using an Omega 2010 programmable temperature controller.

Temperature programmed reduction (TPR) studies were conducted using a 6mm O.D. 4mm I.D. quartz reactor. TPR experiments were performed after samples had undergone TPD to 800°C. A mixture of 1 sccm H_2 and 10 sccm N_2 was used in these studies, and a heating rate of 10°C/min achieved an acceptable resolution and signal-to-noise ratio. During TPR, the effluent passed through Teflon-lined stainless steel tubing to a Varian 3600CX gas chromatograph having a thermal conductivity detector and to a UTI 100C residual gas analyzer. Product separation by gas chromatography was achieved with an 8 foot glass lined Hayesep-Q column.

Catalytic Studies for Thiophene HDS

HDS studies were performed at atmospheric pressure using thiophene as the model organosulfur compound. The reactor system used in these experiments has been described previously [20]. A 0.25 inch stainless steel reactor was loaded with 150 mg of catalyst in the drybox and heated to 400°C in a mixed He (19 sccm) and H_2 (22 sccm) gas flow. At 400°C, this flow was replaced by a continuous flow of 2% thiophene in H_2 (22 sccm). Gas chromatograph analyses were performed after 20 min and after each hour for the 10 h reaction study. After the HDS measurements, the catalyst was cooled under flowing He and stored in the drybox.

3. Results and Discussion

Stoichiometry

The platinum ammine salt used for the ion exchange reaction, $[Pt(NH_3)_4]Cl_2 \cdot H_2O$, was readily soluble in water and resulted in the formation of PtMoS[H_2O] upon reaction with NaMoS. Addition of a small amount of water (5%) to MeOH also achieved complete dissolution of $[Pt(NH_3)_4]Cl_2 \cdot H_2O$ during the ion exchange reaction to form PtMoS[5% H_2O]. In contrast, attempts to prepare the ternary molybdenum sulfide in pure methanol encountered difficulties due to the limited solubility of the platinum ammine salt; platinum ammine salt remained in the final product unless extensively washed with MeOH. This problem was obvious after materials had been dried and washed for a second time. XRD characterization of the (dried) filtrate from this washing revealed $[Pt(NH_3)_4]Cl_2 \cdot H_2O$ and NaCl.

Stoichiometries (ignoring inclusion of solvent molecules) determined from microprobe analysis and Mo gravimetric analysis were $Pt_{0.96}Mo_6S_{8.95}$ for PtMoS[H_2O] and $Pt_{1.05}Mo_6S_{9.07}$ for PtMoS[5%H_2O]. Analytical data from ICP and AAS (Table 1) indicated that the stoichiometry was $Pt_{0.86}Na_{0.076}Mo_6S_{8.3}$ for the first material and $Pt_{0.80}Na_{0.071}Mo_6S_{8.1}$ for the second material. A third sample synthesized in pure MeOH had the composition $Pt_{0.93}Na_{0.072}Mo_6S_{8.1}$ by ICP / AAS.

Although $[Pt(NH_3)_4]Cl_2 \cdot H_2O$ is only sparingly soluble in MeOH, the ion exchange reaction performed in pure MeOH apparently went to the same degree of completion as with 5% H_2O or pure H_2O.. Repeated rinsing with MeOH after the ion exchange completely removed the unreacted $Pt(NH_3)_4Cl_2 \cdot H_2O$ salt. However, removal of Na from the material by the simple stoichiometric ion exchange procedure in any of the three methods was not quite complete.

Even with 50% excess Pt salt for the ion exchange reaction, it was still not possible to remove all of the Na.

Sulfur analysis by ICP indicated a lower sulfur stoichiometry than the microprobe data. The results could be systematically low. However, our previous work has demonstrated that oxygen can substitute for sulfur in similarly prepared materials. Fitting of EXAFS results for $SnMo_6S_8$ materials also prepared by the ion exchange method required the inclusion of oxygen, and the stoichiometry was formulated as $SnMo_6O_{0.6}S_{7.4}$ [21].

Surface Area

Surface areas (Table 2) were widely variable but strongly depended on the surface area of the NaMoS starting material. The structure of the material apparently did not change significantly during ion exchange; movement of ions appeared to be possible without significant physical modification of the samples. However, addition of water to the solvent during ion exchange lowered the surface area of the final product. MeOH present within the solvation sphere of the $[Pt(NH_3)_4]^{2+}$ ions and within the pores may have stabilized smaller pores that contribute significantly to the surface area of materials by this technique [22]. Synthesis of the NaMoS starting material in boiling water rather than boiling BuOH typically produced lower surface area materials [23].

As-prepared materials were extremely air sensitive, and even very slight air contamination or exposure significantly reduced the surface area. Samples treated in H_2 at high temperature also had significantly lower surface areas, presumably due to the collapse of smaller pores and sintering.

Characterization

XPS spectra for Mo and Pt for materials prepared by ion exchange reaction in a 5% H_2O MeOH solution and in pure water are shown in Figures 2 and 3, respectively. For both synthesis methods, the Mo 3d region typically exhibited Mo peaks having binding energies (Mo $3d_{5/2}$=228.1 eV) consistent with that characteristic of the cluster, with a very small amount of surface oxide (probably MoO_3) observed occasionally at higher binding energies. Although Mo metal has nearly the same binding energy as that of Mo_6S_8 clusters, the FTIR and XPS data together clearly indicate that the PtMoS materials contain the cluster units. Fitting of the Pt 4f region showed the presence of only a single species having a binding energy shifted 0.3 eV higher than that for Pt metal (71.2, 74.5 eV).

FTIR spectra for PtMoS[H_2O] and $[Pt(NH_3)_4]Cl_2 \cdot H_2O$ are shown in Figure 4. Peaks were observed in both spectra at 1558, 1542, 1340, 1325, 889, and 844 cm^{-1} due to various N-H vibrational modes for the $[Pt(NH_3)_4]^{2+}$ salt. The similarity of the spectra provided evidence that the tetraammine cation was present in the compound. The peak at 383 cm^{-1} was assigned to the Mo-S stretching mode characteristic of Mo_6S_8 cluster units [18,21]. Laser Raman spectroscopy did not reveal formation of MoS_2 for the as-prepared material.

Hydrogen Treatment

High temperature treatment of PtMoS in a flow of pure H_2 for 2 h at 600, 700, 800, 900, and 1000°C was performed in an effort to produce the crystalline Pt Chevrel phase. XRD results (Figure 5) indicated that below about 900°C, a largely amorphous – or at least a very poorly crystalline material – was present. At higher temperatures, however, reflections for Mo and a Pt-Mo alloy became apparent, as well as reflections for an unidentified intermediate phase. At 1000°C, the only major reflections observable were due to Mo metal and a Pt-Mo

compound, Pt_3Mo_2, probably existing as a solid solution containing excess Mo. By contrast, for experiments where excess Pt was used in the ion exchange or where the product was not washed sufficiently to remove excess Pt salt, XRD results indicated that the high temperature treatment produced only Pt and Mo metal. For some samples, reflections characteristic of a crystalline hexagonal Chevrel phase were observed at low intensity. In these cases, conversion to the ternary sodium Chevrel phase, due to residual sodium in the starting material was evidently responsible for these reflections.

LRS was performed on the treated samples in order to detect MoS_2. Although none was detected for the as-prepared material, very small peaks characteristic of MoS_2 (383, 404 cm^{-1}) did appear for the 400-600°C treated materials. Comparison of the size of the observed peaks with those of mechanical mixtures of MoS_2 and NaMoS indicated that the amount of MoS_2 in the treated materials was well below 1%. XPS spectra for the materials treated at 400-600°C indicated that surface Mo was largely in an intermediate oxidation state, with a binding energy too low to be MoS_2. After treatment at 800°C, MoS_2 was not detected by LRS, due to its reduction to Mo metal and H_2S (Fig. 6). XPS spectra for the 800°C treated material indicated virtually all of the surface Mo was in a reduced state consistent with Mo metal.

Weight losses were calculated for the treated samples (Figure 7). During H_2 treatment, the solvent was removed and the ammine ligands associated with the Pt were driven off. The expected and observed weight losses (Table 3) were consistent. At higher temperatures (above 700 to 800°C), the weight loss corresponded to the formation of metallic species.

TPD/TPR Results

TPD/TPR results were largely consistent with those from other characterization techniques. During TPD of PtMoS[H_2O], two peaks arising from H_2O evolution were observed at about

120°C and 300°C (somewhat smaller). H_2O evolution ceased at about 400 °C. The low temperature water peak was probably the result of desorption of loosely bound (physically adsorbed) H_2O. The higher temperature peak was probably chemically bound (or chemisorbed) H_2O. H_2 evolution began at about 400°C and continued to 800°C. H_2O decomposition could lead to the formation of an intermediate oxide-sulfide species with a corresponding release of H_2.

During TPR, a large water peak and a H_2 uptake peak were observed at around 300°C and again at 475°C. H_2O production ended at about 900°C. H_2 uptake was still observable and actually began to increase at about 900°C as H_2S evolution occurred.

Temperatures for the phase changes indicated by TPR and XRD results did not directly correlate for two reasons. First, TPR was conducted in about 10% H_2 in N_2, while H_2 treatment experiments were performed in pure H_2. We have shown in previous TPR studies of LaMoS [22] that treatment in 10% H_2 increases the temperature at which H_2S evolution begins compared to treatment in pure H_2. Second, since TPR is a ramping experiment (while the treatment studies maintained the temperature for 2 h), any slow process in the chemical reactions likely increased the equivalent TPR temperature.

XPS spectra for the material after TPR (Figure 9) indicated that a new Mo species was present having an intermediate oxidation state and comprising the majority of the surface. The presence of a surface Mo oxide was consistent with previous work [22] and did not by itself indicate the destruction of the Mo_6S_8 cluster unit. Some surface MoO_3 was present also. XPS characterization for the as-prepared PtMoS showed a small chemical shift of about +0.3 eV for the Pt $4f_{7/2}$ peaks relative to Pt metal. However, after TPR, the chemical shift decreased to 0.1

eV; this was consistent with the reduction of Pt due to the loss of ammonia ligands, the presence of extra sulfur, and the reduction of the sample to Pt metal or a Pt-Mo alloy.

Thiophene HDS Catalysis

HDS studies (Table 4) indicated that PtMoS activity was comparable to that for a "CoMoS" reference material, based on rates normalized with respect to surface area. Mo_6S_8-based catalysts typically exhibit low selectivity for n-butane, but the PtMoS selectivity was particularly low. This is surprising since Pt metal is known to be an excellent hydrogenation catalyst.. The PtMoS material had higher activity than any other amorphous ternary Mo_6S_8 material yet discovered, while retaining the remarkably low hydrogenation activity.

4. Conclusions

The amorphous sodium salt $Na_2(Mo_6S_8)S$ [NaMoS] has been shown to undergo cation-exchange with $[Pt(NH_3)_4]^{2+}$ in H_2O, in 5% H_2O in MeOH, and in pure MeOH to produce the solvated derivative $[Pt(NH_3)_4]$ $(Mo_6S_8)S{\bullet}x(MeOH/H_2O)$ [PtMoS]. Analytical data show that the displacement of Na was nearly complete (>95%) upon reaction with one mole $[Pt(NH_3)_4]^{2+}$ per mole of NaMoS in these solvents. The high surface area of the starting material NaMoS was retained in the resulting PtMoS. FTIR spectra of the latter indicated retention of the Mo_6S_8 cluster and the $[Pt(NH_3)_4]^{2+}$cations. XPS revealed only one set of Mo 3d and Pt 4f bands with binding energies characteristic of these species in the as-prepared PtMoS. Laser Raman spectra confirmed the absence of MoS_2 in these preparations.

Conversion of PtMoS to the unknown crystalline Chevrel phase $PtMo_6S_8$ by hydrogen reduction at temperatures in the range of 400-800°C was attempted. While XRD showed weak reflections for a Chevrel phase in some samples, $NaMo_6S_8$ may have been formed due to incomplete removal of Na^+ during the ion-exchange process. Several samples of PtMoS

showed formation of Pt, Mo, and perhaps a Pt-Mo alloy upon reduction at temperatures above 800 °C. At lower temperatures, the H_2-treated material remained amorphous, and XPS indicated that the Mo_6S_8 cluster was retained below about 800 °C. In the range of 400-500°C, the weight loss from PtMoS was in agreement with formation of $Pt(Mo_6S_8)S$. HDS studies indicated that these materials will likely be interesting catalysts for organosulfur reactions. In addition, the successful synthesis reported here for the first Mo_6S_8 material containing a platinum group element [in the anionic $(Mo_6S_8)S^{2-}$ network] indicates that other such derivatives containing Ru, Rh, Pd, Os, and Ir also might be prepared by related chemistry.

5. Acknowledgements

We thank Jim Anderegg for assistance in obtaining the XPS data. The microprobe analyses were completed by Dr. Alfred Kracher, Department of Geological and Atmospheric Sciences, at Iowa State University. This work was supported by the U.S. Department of Energy, Office of Basic Energy Sciences, through Ames Laboratory operated by Iowa State University under Contract No. W-7405-Eng-82.

6. References

1. Chevrel, R.; Sergent, M.; Prigent, J. *J. Solid State Chem.*, **1971**, *3*, 515.
2. Chevrel, R.; Hirrien, M.; Sergent, M. *Polyhedron*, **1986**, *5*, 87.
3. Yvon, K. *Current Topics in Materials Science*, Vol. 3, Chapter 2, 1978.
4. Corbett, J. D. *J. Solid State Chem.*, **1981**, *39*, 56.
5. Hughbanks, T.; Hoffmann, R. *J. Am. Chem. Soc.*, **1983**, *105*, 1150.
6. Anderson, O.K.; Klose, W.; Nohl, H. *Phys. Rev. B*, **1978**, *17*, 1209.
7. Fischer, Ø. *Appl. Phys.*, **1978**, *16*, 1.
8. Fischer, Ø.; Maple, M. B. (Eds.). *Superconductivity in Ternary Compounds*, Vol. I and II, Springer-Verlag, Berlin, 1982.
9. McCarty, K. F.; Schrader, G. L. *Ind. Eng. Chem. Prod. Res. Dev.* **1984**, *23*, 519.
10. McCarty, K. F.; Anderegg, J. W.; Schrader, G. L. *J. Catal.*, **1985**, 93, 375.
11. Eckman, M. E.; Anderegg, J. W.; Schrader, G. L. *J. Catal.* **1989**, *117*, 246.
12. Schewe-Miller, I. M.; Koo, K. F.; Columbia, M.; Li, F.; Schrader, G. L. *Chem. Mater.*, **1994**, *6*, 2327.
13. Kareem, S. A.; Miranda, R. *J. Molec. Catal.* **1989**, *53*, 275.

14. Tarascan, J. M.; Waszczak, J. V.; Hull, G. W., Jr.; DiSalvo, F. J.; Blitzer, L. D. *Solid State Commun.*, **1983**, *47*, 973.
15. Tarascon, J. M.; DiSalvo, F. J.; Murphy, D. W.; Hull, G,; Waszczak, J. V. *Phys. Rev. B*, **1984**, *29*, 172.
16. Schöllhorn, R.; Kümpers, M.; Besenhard, J. O. *Mat. Res. Bull.*, **1977**, *12*, 781.
17. Chevrel, R.; Sergent, M.; Pringent, *J. Mat. Res. Bull.*, **1974**, *9*, 1487.
18. McCarley, R. E.; Hilsenbeck, S. J.; Xie, X. *J. Solid State Chem.*, **1995**, 117, 269.
19. Elwell, W. T.; Wood, W. F. *Analytical Chemistry of Molybdenum and Tungsten*; Pergamon Press: New York, 1971, p. 41.
20. Hilsenbeck, S. J.; McCarley, R. E.; Thompson, R. K.; Flanagan, L. C.; Schrader, G. L. *J. Molec. Catal. A: Chemical*, **1997**, *122*, 13.
21. Hilsenbeck, S. J.; McCarley, R. E.; Goldman, A. I.; Schrader, G. L. *Chem. Mater.*, **1998**, *10*, 125.
22. Thompson, R. K.; Hilsenbeck, S. J.; Paskach, T. J.; McCarley, R. E.; Schrader, G. L. *J. Molec. Catal. A: Chemical* (submitted)
23. Hilsenbeck, S. J. Unpublished data.

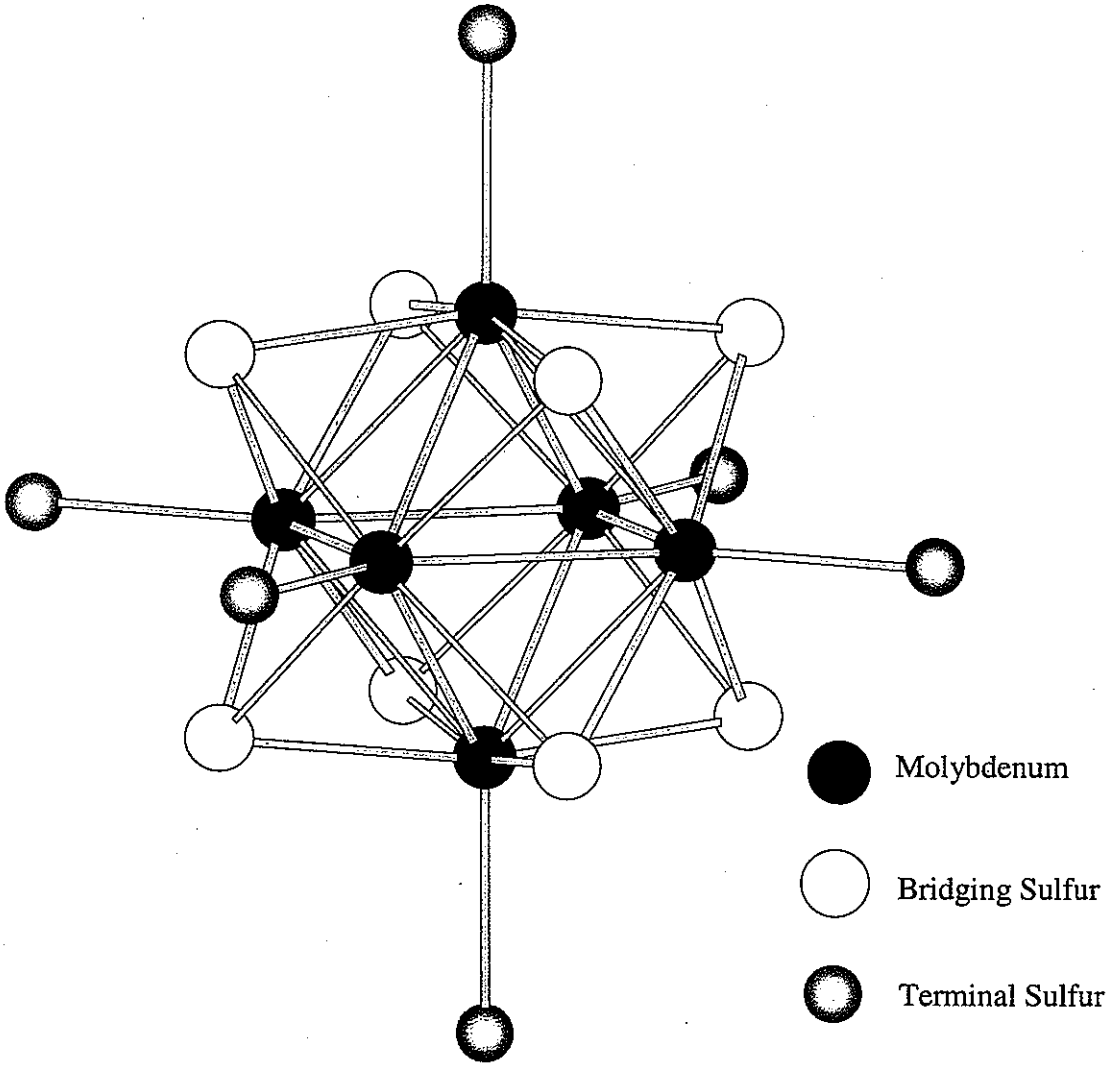

Figure 1. Structure of the Mo_6S_8 hexanuclear cluster unit formed by a molybdenum octahedron and eight triply bridging sulfur atoms capping each face. Six terminal positions are located at the vertices of the octahedron and are occupied by either organic ligands or sulfur atoms.

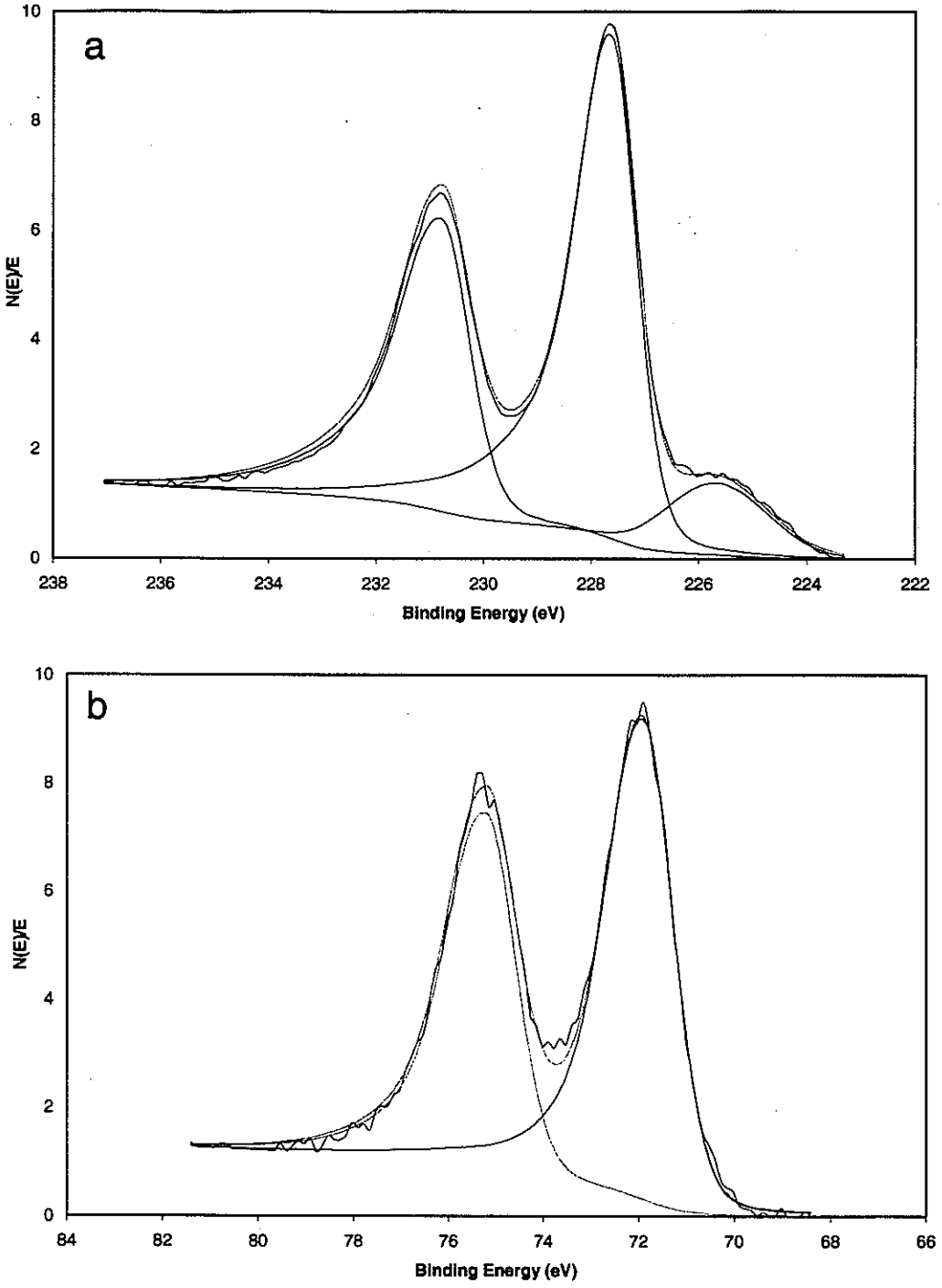

Figure 2. X-ray photoelectron spectra for PtMoS[5% H_2O] synthesized in a 5%H_2O MeOH solution: (a) Mo 3d and (b) Pt 4f regions. Corrected Mo 3d binding energies are consistent with the Mo_6S_8 cluster unit (228.1 eV) in (a). The broad band observed at the lower binding energy side of the Mo 3d doublets arises from the sulfur 2s peak. Only one type of Pt is detected in (b).

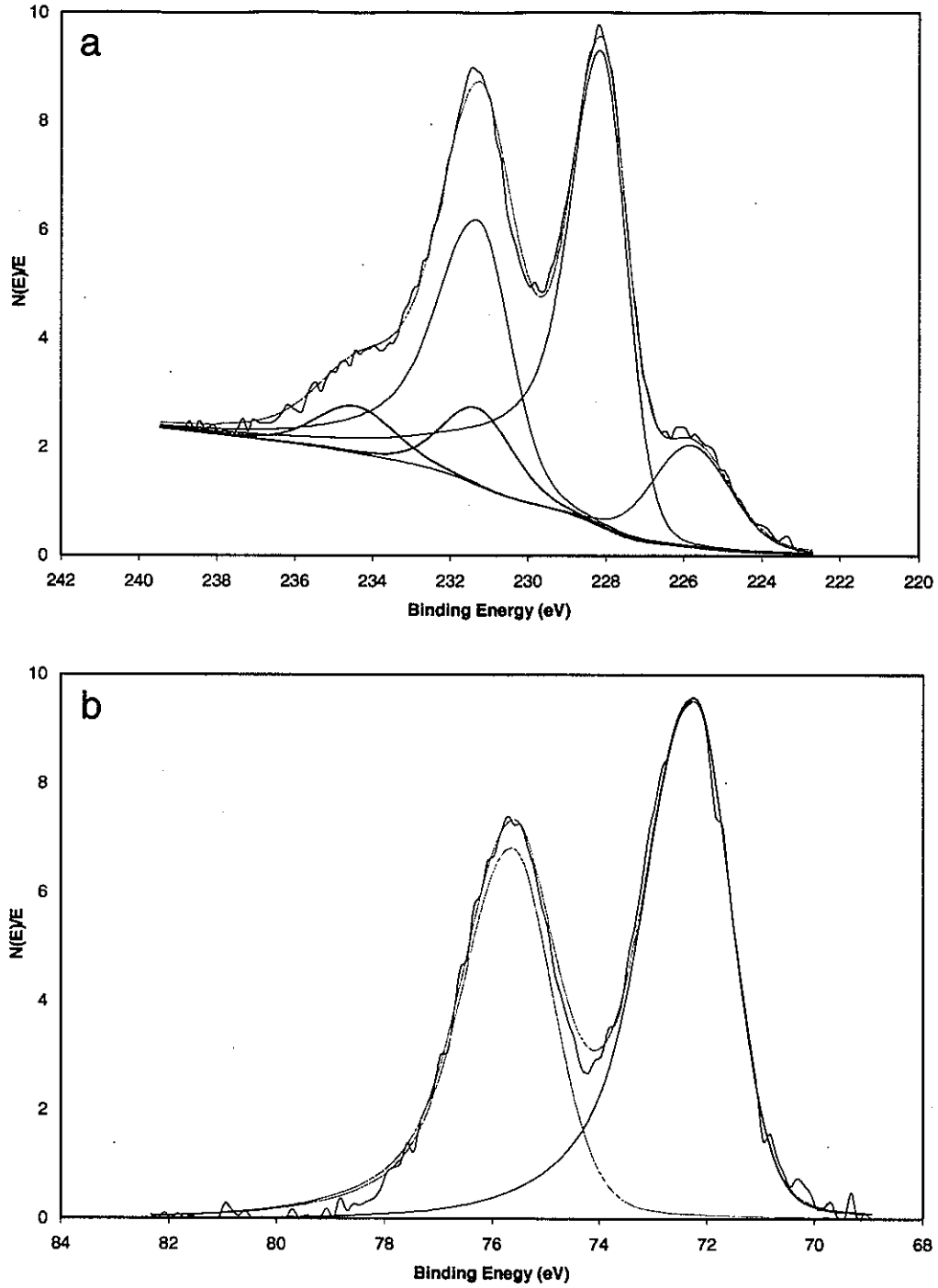

Figure 3. X-ray photoelectron spectra for $PtMoS[H_2O]$ synthesized in pure water: (a) Mo 3d and (b) Pt 4f regions.. Corrected Mo 3d binding energies are consistent with the Mo_6S_8 cluster unit (228.1 eV) and a small amount of surface MoO_3. The broad band observed at the lower binding energy side of the Mo 3d doublets arises from the sulfur 2s peak. Only one type of Pt is detected in (b).

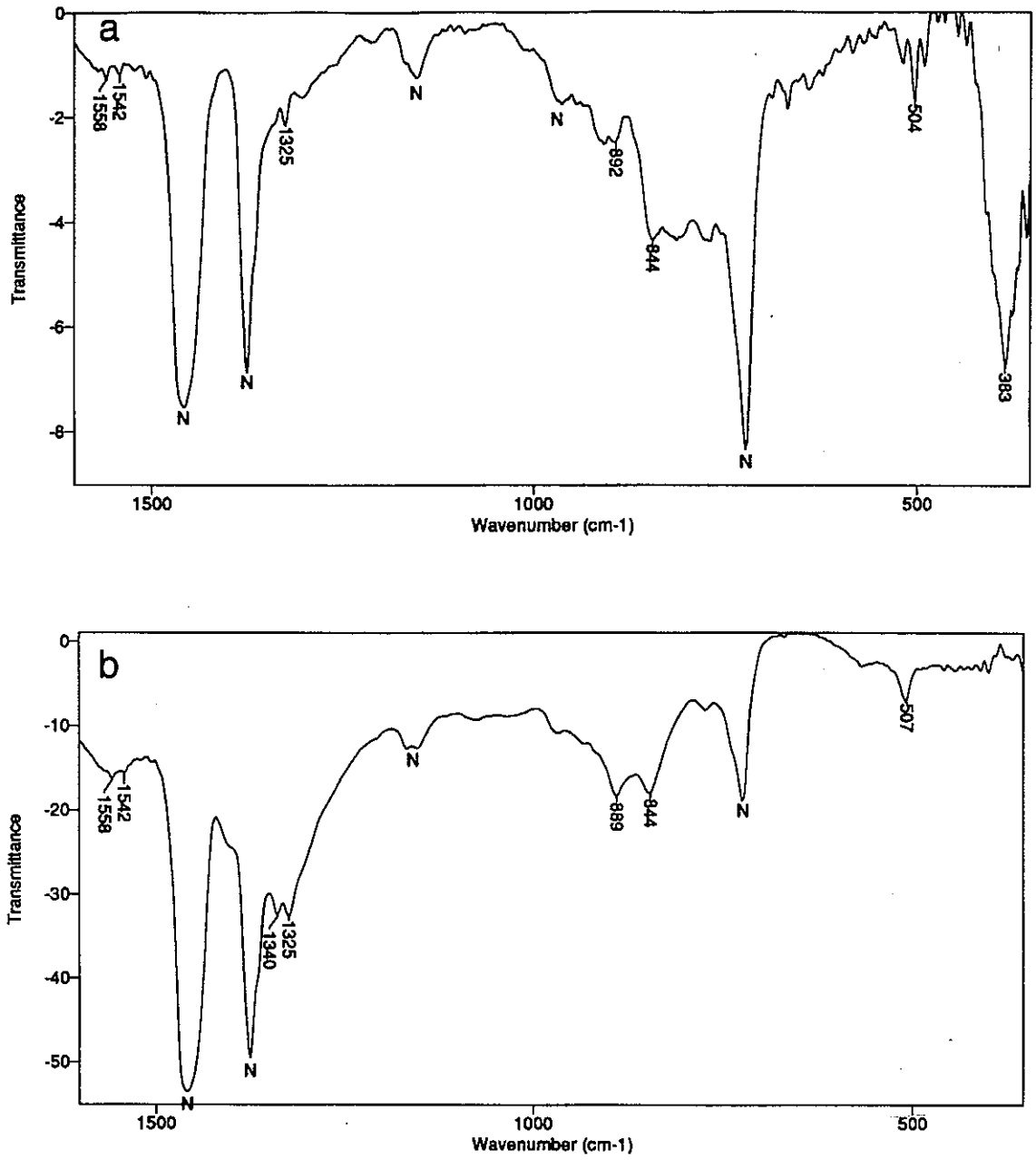

Figure 4. Infrared spectra of (a) PtMoS[H_2O] and (b) [$Pt(NH_3)_4$]$Cl_2 \cdot H_2O$. The peaks arising from the N-H vibrations are indicated at 1558, 1542, 1340, 1325, 889, and 844 cm^{-1}. The peak at 383 cm^{-1} in (a) is indicative of the Mo-S stretching vibration for the cluster. (Peaks marked with an N arise from Nujol.)

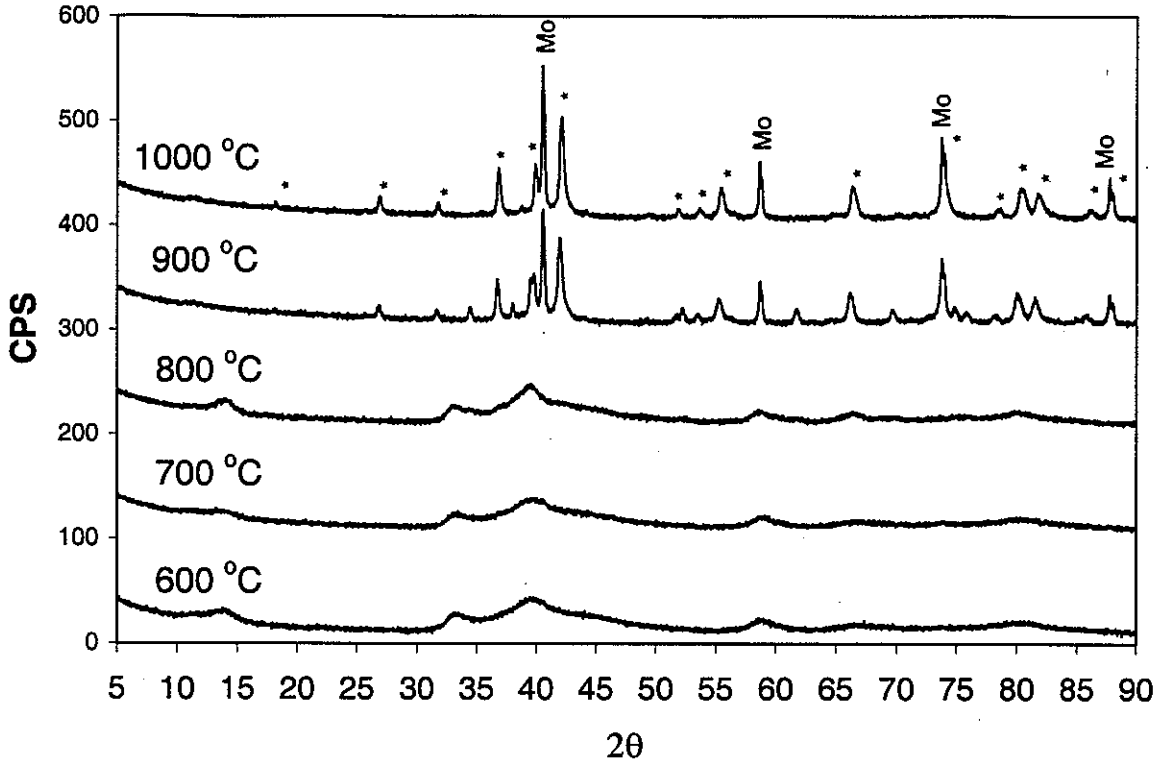

Figure 5. X-ray powder diffraction of PtMoS prepared in pure MeOH and treated in flowing H_2 for 2 h at 600, 700, 800, 900, and 1000°C. Peaks labeled Mo and Pt_3Mo_{2+x} arise from Mo metal and the Pt-Mo alloy, respectively.

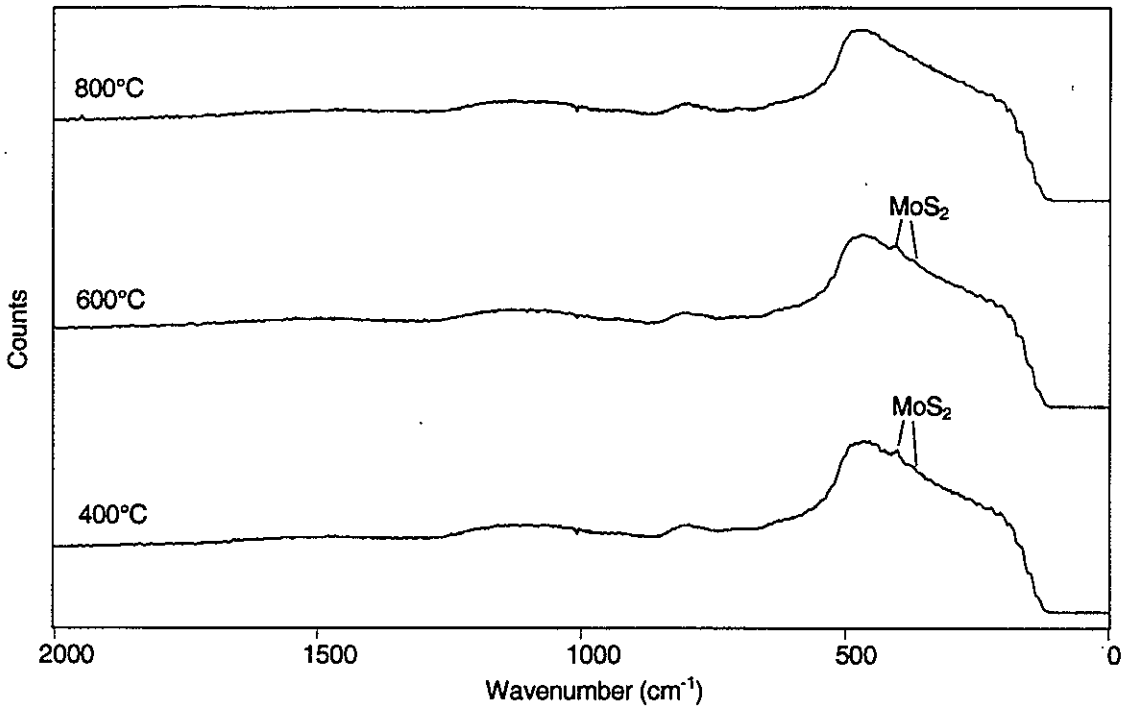

Figure 6. Laser Raman spectra of PtMoS prepared in pure water and treated in pure, flowing H_2 for four hours at 400, 600, and 800°C. The peak at 404 cm^{-1} is due to MoS_2.

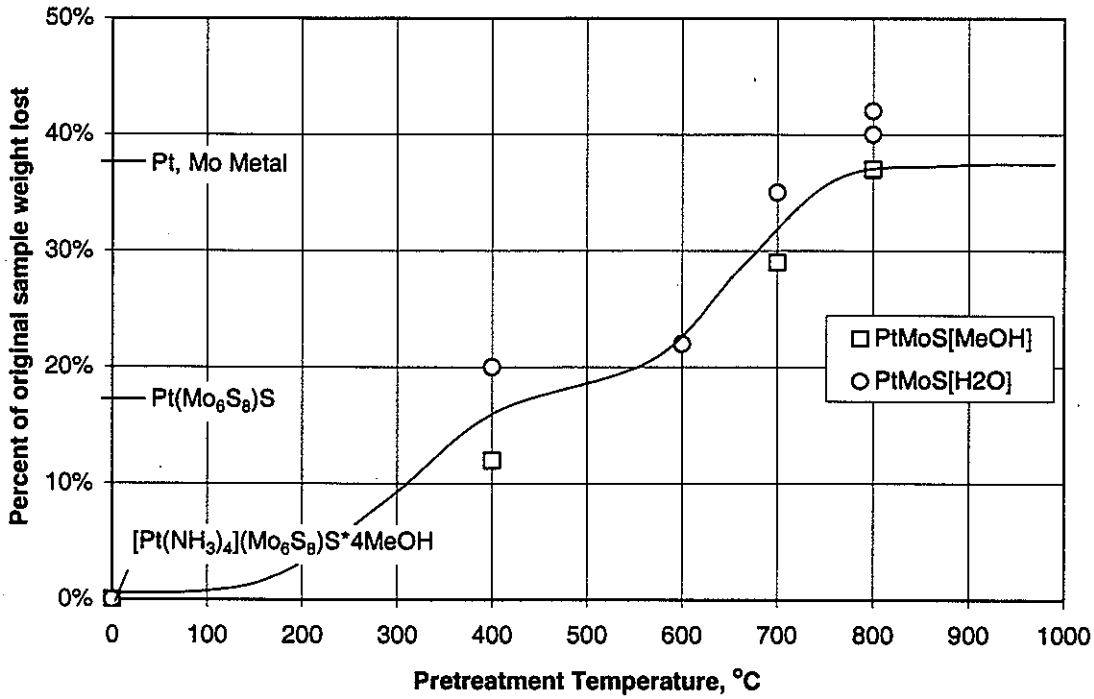

Figure 7. Weight losses during H_2 treatment of PtMoS at various temperatures.

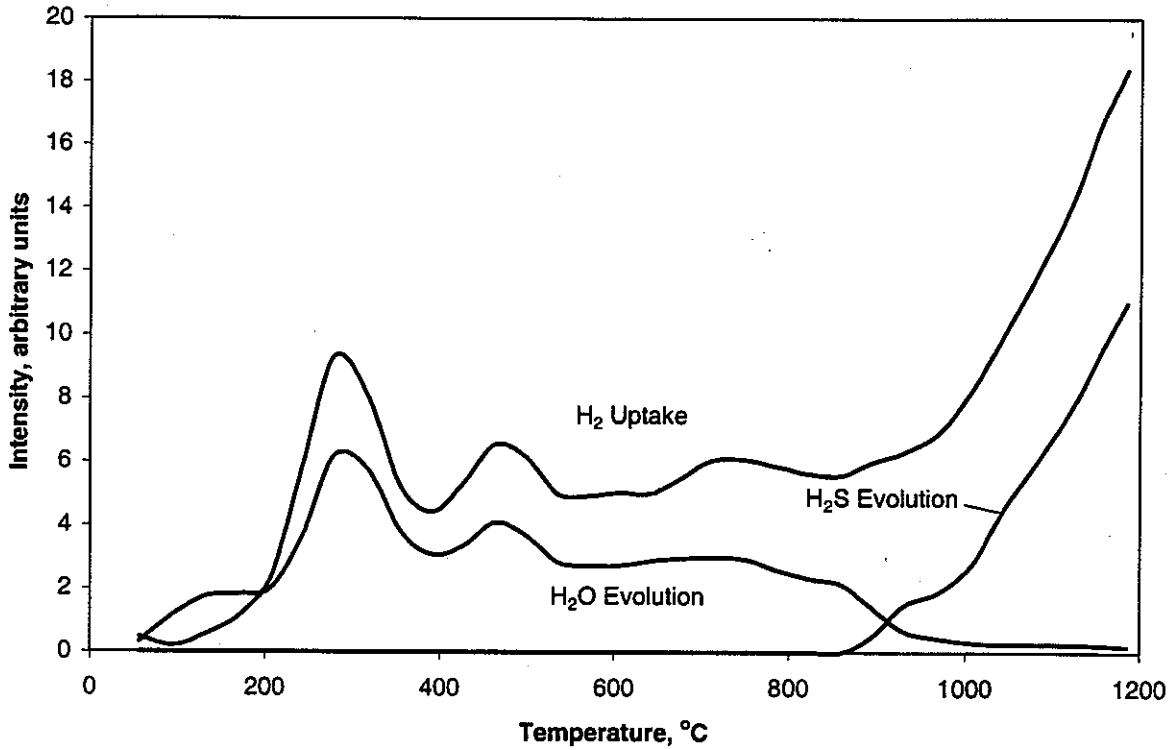

Figure 8. Temperature-programmed reduction of PtMoS[5% H_2O] to 1200°C in flowing 10% H_2 in N_2. The PtMoS[5% H_2O] was prepared by ion-exchange in a 5% H_2O in MeOH solution.

Table 1. Analytical results by ICP and AAS for PtMoS prepared by various ion exchange reactions.

	Pt wt%	Mo wt%	S wt%	Na wt%	Pt/(Mo_6) mol/mol	S/(Mo_6) mol/mol	Na/(Mo_6) mol/mol
Measured (volatile-free basis)							
$Pt(NH_3)_4Mo_6S_9$•[H_2O]	13	46	21	0.14	0.85	8.3	0.075
$Pt(NH_3)_4Mo_6S_9$•[MeOH]	14	46	21	0.13	0.93	8.1	0.072
$Pt(NH_3)_4Mo_6S_9$•[5%H_2O]	13	47	22	0.13	0.80	8.2	0.071
Calculated (volatile-free basis)							
$Pt(NH_3)_4Mo_6S_9$•4[H_2O]	16	48	24	0	1	9	0
$Pt(NH_3)_4Mo_6S_9$•4[MeOH]	16	46	23	0	1	9	0

Table 2. Surface areas by BET (m^2/g) for two different NaMoS starting materials and the PtMoS materials prepared from them by various ion exchange reactions. The surface area of the PtMoS depends largely on the surface area of the NaMoS starting material.

	Preparation A	Preparation B
$Na_2Mo_6S_9$•[MeOH]	39	95
$Pt(NH_3)_4Mo_6S_9$•[H_2O]	14	55
$Pt(NH_3)_4Mo_6S_9$•[5%H_2O]	39	84-87

Table 3. Stoichiometry predicted percent weight losses for various final compositions, given the starting stoichiometry.

	Starting Material	
	$[Pt(NH_3)_4](Mo_6S_8)S$•4MeOH	$[Pt(NH_3)_4](Mo_6S_8)S$•4H_2O
$Pt(Mo_6S_8)S$	16	12
$Pt(Mo_6S_8)$	18	14
$PtMo_6$	39	36

Table 4. Thiophene HDS activities (400°C) after 10h on stream.

	Surface area m^2/g	Thiophene conversion	HDS rate	% C_4 products			
	Before/After reaction	mol%	mol/m^2s (x 10^8)	n-butane	1-butene	*trans* -2-butene[e]	*cis* -2-butene
$PtMoS[H_2O]$	21/6[d]	4.63	3.02	0.9	28.3	48.9	21.9
Reference Materials:							
SnMoS[a]	135/9	3.80	1.90	*f*	42.1	25.0	32.9
LaMoS [$LaCl_3$ prep][b]	201/64	12.12	1.51	17.1	22.7	35.1	25.1
LaMoS [$La(NO_3)_3$ prep][b]	200/54	2.62	0.32	5.5	41.0	32.4	21.1
Co-Mo-S[c]	10.83	0.89	3.36	1.5	36.4	41.1	21.0
MoS_2[c]	3.40	0.88	1.06	1.8	46.0	34.9	17.3

[a]Data from reference 20. [b]Data from reference 19. [c]Data from references 9-12. [d]Surface areas are reported before and after HDS, or after HDS where indicated as a single value. [e]1,3-butadiene has identical retention time. [f]Below detection limit.

CHAPTER 4. SYNTHESIS OF METHANETHIOL FROM METHANOL OVER REDUCED MOLYBDENUM SULFIDE CATALYSTS BASED ON THE MO_6S_8 CLUSTER

A paper submitted to the Journal of Catalysis

Thomas J. Paskach[a,c], Glenn L. Schrader,[a,c] and Robert E. McCarley[b,c]

Department of Chemical Engineering,[a]

Department of Chemistry[b], and

Ames Laboratory-USDOE[c]

Iowa State University

Ames, Iowa 50011

Abstract

Catalysts having structures containing the Mo_6S_8 cluster (crystalline Chevrel phases, amorphous ternary molybdenum sulfides, and ligated molecular clusters) have been discovered to be active for thiol synthesis from methanol and hydrogen sulfide at 250°C and 1 atm. An amorphous lanthanum molybdenum sulfide material was found to be the most selective catalyst (>80% methanethiol) at low conversions. CO_2, CO, CS_2, and CH_4 were the major byproducts in these studies.

1. Introduction

Industrial synthesis of bulk organosulfur chemicals includes the production of mercaptans (thiols), alkylsulfides (thioethers), polysulfides, and thiophenes. Many of the derivatives of these organosulfur chemicals have biological activity and are used extensively in the production of agrochemicals and pharmaceuticals. Low molecular weight thiols such as $C_1 - C_6$ thiols are commercially manufactured on the order of 10^4 ton/yr. For example, methanethiol (MeSH) is used for the production of methionine (an important poultry feed supplement) or methanesulfonyl chloride. Other thiols, especially higher molecular weight compounds, are also used in the manufacture of rubber and plastics and in the production of polysulfides for lubricant additives. However, excessive amounts of some alkylsulfide byproducts are also produced, which necessitates reprocessing or incineration.

Both surface-catalyzed and free radical processing routes are used industrially for thiol manufacture, and significant claims for catalytic selectivity have been discussed in the patent literature (1, 2, 3). Metal oxide catalysts are used for the production of MeSH from methanol (MeOH) and H_2S, including: 1) KOH-promoted commercial hydrodesulfurization (HDS) catalysts which consist of sulfided Ni-Mo, Ni-W, Co-Mo, or Co-W oxides supported on alumina (4), 2) sulfided α- or β-alumina trihydrate on KOH treated γ–Al_2O_3 (5), 3) K_2WO_4 on alumina promoted with KOH, and 4) KOH on alumina (6). Major side products are typically dimethylsulfide (DMS), dimethylether (DME), and methane. Use of secondary alcohol feeds results in formation of olefins *via* dehydration. Solid acid catalysts such as dry cation-exchange resins are used in thiol synthesis from alcohols or olefins and H_2S. These catalysts can be very selective for the production of secondary or tertiary thiols. For α-olefins, the reaction follows Markownikoff addition of SH^- to the double bond. Free-radical

synthesis is used for production of primary thiols from α-olefins and H_2S (anti-Markownikov addition). Conversion assisted by UV radiation is fairly selective to the primary thiol (~92% selectivity), but homogeneous catalysts containing boron which apparently generate radicals are even more selective (up to ~97%).

In our recent research, a new family of materials based on the Mo_6S_8 molecular structure (Fig. 1) have been shown to be effective catalysts for MeSH synthesis from MeOH and H_2S. The categories of materials examined in this work were: 1) crystalline Chevrel phases, MMo_6S_8, where M is a ternary metal such as La; 2) amorphous ternary molybdenum sulfides, $M_x^{+n}(Mo_6S_8)S_{xn/2}$, where M is a ternary metal such as La, Ho, Sn, Pt, or Na; 3) amorphous or crystalline molecular cluster materials, $(Mo_6S_8)L_y$, where L is a ligand such as piperidine (pip) or propylamine ($PrNH_2$); and 4) an amorphous, ligated, ternary material with the formula $Na_{2x}(Mo_6S_8)S_x(py)_y$ [NaMoS(py)] where py refers to a pyridine ligand (7). Crystalline Chevrel phases and various amorphous ternary molybdenum sulfides such as LaMoS have been studied previously in our research and have been found to be active and stable HDS catalysts. In this paper, we provide the first report of the catalytic properties of these Mo_6S_8 cluster materials for thiol synthesis.

2. Experimental

Catalyst Synthesis

Preparations for the various reduced molybdenum sulfides used in this research have been reported previously (8,9,10,11). Amorphous ternary materials (Samples a,b,c and d, Tables 1 and 2) were prepared by a two-step process. In the first step, anhydrous Mo_6Cl_{12} reacted with sodium hydrosulfide (NaSH) and sodium butoxide (NaOBu) under refluxing anhydrous n-butanol (BuOH) to form a black, amorphous sodium salt containing either 2 or 3

Na atoms per cluster. The solid $Na_{2x}(Mo_6S_8)S_x$ (Sample e, Tables 1 and 2, and also referred to as NaMoS) was filtered and washed with anhydrous, degassed MeOH to remove NaCl.

$$Mo_6Cl_{12} + (8+x)NaSH + (4+x)NaOBu \xrightarrow{BuOH} Na_{2x}(Mo_6S_8)S_x + (4+x)BuOH + 12NaCl \quad (1)$$

In the second step, NaMoS was treated with a metal salt [for example $La(NO_3)_3{\cdot}6H_2O$], in anhydrous, degassed MeOH so that ion exchange occurred between the metal atoms and the Na ions to form the amorphous ternary molybdenum sulfide (also referred to as LaMoS).

$$Na_3((Mo_6S_8)S_{1.5} + La^{3+} \xrightarrow{MeOH} La(Mo_6S_8)S_{1.5} \cdot y(MeOH) + 3Na^+ \quad (2)$$

Molecular complexes with the Mo_6S_8 structure were also prepared [Samples h and i, Tables 1 and 2]. For example NaMoS(py) was prepared by adding pyridine to the mixture at the start of reaction 1:

$$Mo_6Cl_{12} + (8+x)NaSH + (4+x)NaOBu \xrightarrow[pyridine]{BuOH} Na_{2x}(Mo_6S_8)S_x(py)_y + (4+x)BuOH + 12NaCl \quad (3)$$

The preparation of the crystalline ligated clusters was achieved by refluxing the liquid ligand-phase in an extractor over the solid NaMoS(py). In each case, the fully ligated cluster was soluble in excess ligand and so was the only product found in the extract (7):

$$2nNa_{2x}(Mo_6S_8)S_x(py)_y(MeOH) \xrightarrow{Ligand} nNa_{4x}(Mo_6S_8)S_{2x}(py)_{6(solid)} + n(Mo_6S_8)L_{6(soln)} \quad (4)$$

Crystalline Chevrel phases (Sample g, Tables 1 and 2) were prepared from their constituent elements by repeated annealing/grinding cycles in sealed fused silica tubes at 1200-1300°C.

Mo_6S_8-based catalysts have generally been found to be oxygen sensitive. Schlenk techniques with a high vacuum line and a Vacuum Atmospheres Company model 8130 drybox with oxygen and moisture gettering capabilities were utilized.

Catalyst Characterization

Catalyst characterization involved infrared spectroscopy (FTIR), laser Raman spectroscopy (LRS), x-ray photoelectron spectroscopy (XPS), and adsorption surface area/pore size measurements.

FTIR spectra were obtained using a Bomem MB-102 spectrometer with CsI optics, at 2 cm^{-1} resolution. Samples were analyzed as mineral oil mulls with special sample holders designed to exclude O_2.

LRS was performed using a Coherent 532-50 diode-pumped solid state laser (532 nm, 50 mW source) with fiber optic couplings and integral source/collection optics. Spectra were taken in a backscattered collection mode. A Kaiser Holospec f/1.8 spectrometer and Princeton Instruments CCD detector (1100x330) with WinSpec software were used for signal analysis. Catalyst samples were analyzed in capillary tubes or the Pyrex reactor tubes for post-reaction LRS characterization due to their oxygen sensitivity.

XPS data were obtained with a Physical Electronics Industries 5500 multitechnique surface analysis system using a monochromatic MgK_α source; binding energies were calibrated with adventitious carbon (C 1s = 284.6 eV). Spectra were fit with peaks consisting of a mixture of Lorenzian and Gaussian character, following Shirley background subtraction. For doublet peak fitting, the peak area ratios and doublet offset value were fixed.

Surface areas were measured with a Micromeretics ASAP 2010C instrument at 77 K. N_2 was used as the adsorbate for amorphous materials whereas Kr was used as the adsorbate for crystalline materials. Brunauer, Emmet, and Teller (BET) calculations were used to determine surface areas for all samples, and the Barret, Johner, and Hallenda (BJH) method

was used for determining pore size distributions for the amorphous samples. Samples were degassed overnight at 150°C under dynamic vacuum prior to analysis.

Catalytic Reactor Studies

H_2S (VLSI grade) was supplied by Scott Specialty Gases. Certified MeOH (Fisher) was degassed in the saturator with bubbling He prior to use. UHP (zero) He (Matheson) was used for the GC carrier and as a reactor feed or product diluent.

The microreactor system (Fig. 2) used 200-400 mg of catalyst fixed in a 6 mm O.D. x 4 mm I.D. Pyrex reactor tube. A 4 mm O.D. x 2 mm I.D. Pyrex tube was inserted in the lower half of the larger tube for catalyst bed support. Small (2-3 mm) plugs of silane-treated quartz wool held the catalyst bed in place. Since the catalyst was air sensitive, the reactor tube was fitted on both ends with Swagelock fittings with high-temperature rubber septa and loaded in the drybox. Installation of the reactor involved piercing the septa with needles under a He purge. The temperature in the reactors was maintained with a Lindberg model 54032 furnace with an Omega 4200 or Eurotherm 815P programmable temperature controller.

Gas feeds were controlled with Brooks model 5850 and 5850E mass flow controllers and model 5878 master controller. MeOH was delivered by saturating a He flow at a controlled temperature with the feed liquid. He was added to the reactor effluent line to dilute the reactor effluent and to prevent condensation. Pressure (approximately 1 atm) was controlled in the reactor by the use of a needle valve on the reactor outlet located downstream of the He addition, which split the flow between the sample loop and the vent/scrubber system.

Product analysis was performed with a Varian model 3600CX gas chromatograph (GC) with a flame ionization detector (FID) and thermal conductivity detector (TCD) in parallel. An Alltech AT-SULFUR (30 m x 0.32 mm, 4 μm film thickness) column was used with a 5 m x 0.32 mm deactivated fused silica guard column. The GC was programmed from 50°C (5 min) to 150°C at 10°C/min and then to 250°C at 20°C/min. All lines from the reactor were also heated electrically over the 150 - 200°C range using Omega 6100 thermostats to prevent product condensation.

GC peaks were identified by trapping products in an amber septum vial in an ice-salt bath, with subsequent analysis by a Finnigan TSQ 700 GC-mass spectrometer system having both electron impact ionization and ammonia positive ion impact ionization modes. The first quadrupole was used as the analyzer and was scanned from m/z 35 to 400 at a rate of 0.5 seconds per scan. The second and third quadrupoles were maintained in at RF-only mode. Unit mass resolution was achieved using FC43 as the calibration and tuning reference. GC retention times were also compared with known standards.

TCD molar response factors were measured with known standards for CO, CO_2, and CS_2. The TCD response factor for COS was assumed to be the same as for CO_2. FID molar response factors were measured for MeOH and estimated for the remaining products using the methods reported by Ackman *et al.* (12,13).

3. Results

Reaction Studies: Activity and Selectivity Comparisons

The activity and selectivity of various catalysts containing the Mo_6S_8 cluster were compared for MeSH synthesis from MeOH and H_2S. For all of the experiments in the comparison studies, the feed rate of MeOH was 1.00 sccm, and the H_2S rate was 3.00 sccm

(H_2S/MeOH ratio of 3). Reactions were carried out for 20 h at 250°C, and average activities and selectivities for the last 2 h have been reported in Tables 1 and 2. Reaction products were MeSH, DMS, DME, CS_2, CH_4, CO, CO_2, and COS, but trace amounts of other products (H_2, ethane, and ethene) were also detected.

All of the materials listed in Tables 1-2 were active catalysts. However, the various Mo_6S_8 materials ranged widely in their specific activities (expressed as the rate of MeOH converted per unit of catalyst weight or per unit surface area after reaction) and selectivities to MeSH and the major byproducts (DMS, CO, CO_2, CS_2, and COS). Activities ranged from 12 to over 400 $\mu mol/h \cdot m^2$, and selectivities to MeSH ranged from 21 to 83%.

For the amorphous ternary materials, MeSH selectivity depended on the ternary metal. Interestingly, amorphous LaMoS had the lowest specific activity but also the highest selectivity for MeSH. Amorphous HoMoS had the highest activity of all the amorphous materials, both on a weight and surface area basis; however, its selectivity to MeSH was slightly lower, at about 72%. Both Ho and La are both considered large ions in the Mo_6S_8 system. Ternary materials containing Na had relatively low selectivity for MeSH and much higher selectivity for COS, CO_x and CS_2.

If activities were compared based on rates expressed on a surface area basis ($mol/m^2 \cdot s$), catalysts with lower surface areas apparently tended to be superior. For example, although the Chevrel material $LaMo_6S_8$ had an activity on a per weight basis of more than an order of magnitude lower than the amorphous LaMoS, the specific activity on a per surface area basis was more than an order of magnitude higher.

Effect of H_2S / MeOH ratio

The effect of the H_2S/MeOH ratio on activities and selectivities was examined using amorphous LaMoS (Table 3). For these studies, the reactor temperature was maintained at 250°C. As the feed rates of MeOH and/or H_2S were changed, He makeup was added to the reactor inlet to maintain a total reactor gas feed rate of 15 sccm. The catalyst was stabilized for 72 h prior to collecting data. The selectivity towards DMS and CO_2 increased noticeably as the H_2S/MeOH ratio was decreased. However, as the H_2S/MeOH ratio was increased, the selectivity towards CS_2 increased steadily. The result of these two combined effects was that the selectivity toward MeSH was much more constant over nearly the entire range of H_2S/MeOH studied. There was a slight maximum, however, at about 3, and the selectivity to MeSH did not drop appreciably until the H_2S/MeOH ratio was significantly below the stoichiometric value of 1 (Table 3). Also of note was that even though H_2S was a reactant, the conversion of MeSH formation decreased with increasing H_2S/MeOH ratios; i.e. excess H_2S tended to suppress the reaction for the values of H_2S partial pressure examined.

Catalyst Stability

Characterization by LRS and FTIR was performed to examine the stability of the Mo_6S_8 cluster. The far IR spectrum of materials incorporating the Mo_6S_8 cluster includes a band at around 385 cm^{-1} arising from the Mo-S stretching vibration; occasionally a weaker band at about 253 cm^{-1} arising from Mo-Mo bond vibrations can also be observed (7). Amorphous materials containing the Mo_6S_8 cluster show essentially no Raman bands, while crystalline molecular compounds and other crystalline phases with the Mo_6S_8 cluster may show one sharp band at about 408-411 cm^{-1}(7). Crystalline (and also to some degree poorly crystalline) MoS_2 is expected to give rise to sharp IR bands at about 385 and 470 cm^{-1} and

sharp Raman bands at about 384 and 408 cm^{-1} (14, 15). Therefore, detection of IR bands at 470 cm^{-1} or Raman bands at both 384 and 408 cm^{-1} indicates the presence of MoS_2. For both of these characterization methods, spectra taken of mechanical mixtures made with fresh catalyst and pure MoS_2 indicated that the detection limit for MoS_2 was less than 10%.

LRS characterization (Fig. 3) after reaction showed that ternary materials involving Sn, Pt, and Na partially converted to MoS_2 after 20 h at 250°C. However, La and Ho ternary materials did not appear to form MoS_2, nor did the ligated crystalline molecular clusters. LRS is particularly sensitive to these species: spectra of mechanical mixtures of 10% MoS_2 in fresh catalysts clearly revealed the large peaks at 383 and 404 cm^{-1}.

All of the amorphous catalysts lost a significant fraction of their surface area under reaction conditions. Crystalline materials did not show much change in surface area, except that the piperidine-ligated crystalline molecular cluster actually showed a significant increase in surface area under reaction conditions.

Expanded Studies of LaMoS and NaMoS(py)

To examine the stability characteristics in greater detail with respect to time and temperature, several additional reactor studies were carried out with amorphous LaMoS and NaMoS(py). These stability studies were conducted for 72 h at 250, 300, and 350°C, with subsequent characterization by, LRS, FTIR, XPS, and adsorption measurements. For these stability studies, 200 mg of catalyst was used, and the H_2S/MeOH ratio was 3. Catalyst contact times based on the feed composition at reactor conditions were on the order of 1 s (Table 4).

The catalysts typically exhibited an initial loss in activity followed by a longer period of slower deactivation (Fig 4). After an initial stabilization period of around 15-20 h,

deactivation was much slower, and after 3 days deactivation had virtually ceased. Selectivity for MeSH generally tended to increase during the experiments, until a steady value was reached (Fig. 5). For each case, MeSH was the dominant product, but other products included CS_2, CO_2, and CO. Also detected were CH_4, DMS, and trace amounts of DME (Table 4). For LaMoS, as temperature and conversion increased, the selectivity to MeSH dropped significantly, but remained above 50% even at 350°C where nearly full conversion was attained. At the elevated temperatures, selectivity for CH_4 increased steadily, as did the amount of CO_2 produced. However, the selectivity for CS_2 was highest at 300°C, while the selectivity for CO was lowest. Between 300 and 350°C, amorphous NaMoS(py) had steady-state selectivity for MeSH of about 40-43%, independent of temperature. For both LaMoS and NaMoS(py), significant differences in selectivity occurred only among CO, CO_2, CS_2, and COS for this temperature range.

N_2 adsorption analysis was performed before and after reaction for LaMoS and NaMoS(py) (Table 4). In all cases, the catalysts underwent significant losses in BET surface area during the reaction, particularly at higher reaction temperatures. Examination of the BJH results for amorphous LaMoS indicated that the decrease of surface area could be attributed to the loss of small pores having diameters of less than about 70 Å (Fig. 6); larger pores were apparently unaffected.

LRS performed on LaMoS and NaMoS(py) before and after reaction at the various temperatures (Fig. 7) clearly showed that MoS_2 was formed during reaction, and that this transformation was more pronounced at above 300°C. Only a slight indication of MoS_2 peaks was observed in the spectra of these catalysts after reaction at 250°C. Additionally, FTIR spectra for the amorphous LaMoS material after reaction clearly showed the formation

of MoS_2 for the samples after reaction at temperatures above 300°C (Fig. 8). Again, there was only a very slight indication that MoS_2 was present at 250°C.

Surface analysis of the LaMoS catalysts by XPS before and after reaction for three days at 250, 300, and 350°C showed substantial changes (Fig. 9). Both the Mo 3d peaks and S 2p peaks shifted to higher binding energies at higher temperatures. Deconvolution of peaks in the Mo3d region for both LaMoS and NaMoS(py) catalysts (before and after reaction) showed the presence of at least four Mo environments (Table 5). Prior to reaction, the major Mo species detected had a the low binding energy characteristic of Mo in the Mo_6S_8 cluster (about 227.3-227.9 eV for the Mo $3d_{5/2}$ peak) (16). A small amount of Mo in a higher oxidation state consistent with MoO_3 (about 231.4-232.9 eV) was also observed in many materials: this was consistent with the formation of MoO_3, likely due to oxygen contamination during the handling procedures.

Following reaction, the catalysts revealed the presence of Mo surface species with intermediate oxidation states, as was observed in our prior HDS studies (17,18). The intermediate Mo oxidation states were +3 to +4. Specifically, Mo^{3+} was observed at binding energies of 228.4-229.0 eV, consistent with Mo_2S_3 (228.7 eV) (18). Mo^{4+} corresponded to binding energies of 229.5-230.2 eV, consistent with MoS_2 (229.5 eV). After reaction the major species was Mo^{3+}, and the low binding energy characteristic of the cluster was not apparent. Following reaction at 250°C, Mo^{4+} was easily detectable; however after reaction at higher temperatures (300-350°C), this species was apparently converted to Mo^{3+}.

XPS spectra for the S 2p region of LaMoS catalysts examined after reaction showed a shift to higher binding energies. However, the binding energy of the S $2p_{3/2}$ peak was still a little too low (161.9 eV) to be considered MoS_2 (162.4 eV) (19).

To further elucidate the transformation of amorphous LaMoS to produce intermediate surface oxidation states, studies were performed in the presence of MeOH or H_2S alone. For these studies, LRS and XPS were performed on amorphous LaMoS that was treated in either MeOH in He or pure H_2S at temperatures ranging from 200-400°C for 4 h. For the samples treated with MeOH only (Fig. 10a), no Mo oxides were detected with LRS. LRS of the samples treated in pure H_2S at 400°C (Fig. 10b) revealed no Mo oxides and a small amount of MoS_2 (404 and 383 cm^{-1}). XPS results (Mo $3d_{5/2}$ region) for LaMoS samples treated with only MeOH in He or only H_2S are summarized in Table 6. After treatment with only MeOH in He at high temperatures, the peak due to the Mo_6S_8 cluster was still present. No conversion to a Mo^{3+} state was detected. However, two higher oxidation state surface species were present (binding energies of ~229.4-230.5 and ~232.8) similar to MoO_2 (229.6) and MoO_3 (232.7) (19). In contrast, XPS characterization of samples treated in pure H_2S appeared to be very similar in the Mo 3d regions to the results for samples after MeSH synthesis at similar temperatures.

4. Discussion

Activity

All of the materials examined in this work seem to be active for MeSH synthesis from MeOH and H_2S. For the amorphous catalysts, the activities initially decreased quickly and then tended to stabilize for an extended time period. This is probably due at least in part to the loss in surface area that the amorphous catalysts experienced. However, specific activity based on catalyst surface areas indicated that those catalysts having the lowest surface areas had the highest specific activity. This was probably an indication that a larger fraction of the surface area was active for catalysis on the materials with lower surface area. This also

supports the idea that the loss of surface area is biased to less accessible surfaces residing in smaller pores.

However, the piperidine-ligated molecular cluster material showed an increase in surface area during reaction. This material at least partially deligated under reaction conditions, as piperidine was detected in the reactor product stream for a few hours after initially reaching 250°C. This is similar to the deligation studies in previous work (20) which indicated that this material deligated at temperatures below 250°C. As the material deligated, the expected tendency would be for it to begin to cross-link at the sites freed up by deligation. If deligation proceeded in a random manner, then rearrangement of clusters upon cross-linking would be rather random as well. Rearrangement of clusters could be expected to continue until three (or more) of the deligated bridging positions on a cluster were linked to another cluster; then the arrangement would be "locked" into place. The resulting arrangement would be less organized than the starting crystalline material and would probably have a slightly higher surface area.

Selectivity

The selectivity of LaMoS catalyst to produce MeSH was maintained even at very low values of H_2S/MeOH ratio. This, combined with the fact that H_2S exhibited negative reaction order, implies that H_2S is very strongly adsorbed on amorphous LaMoS. If the partial pressure of H_2S is excessive, the adsorption of MeOH may be inhibited or blocked, thus reducing the overall reaction rate. Lower requirements for H_2S partial pressures may be attractive since the overall safety of the process may be enhanced.

At the start of each reactor run, a relatively high selectivity toward DMS was observed, but this decreased within a few hours to the steady state value. Related work has

indicated that the formation of DMS on metal oxide catalysts requires different types of surface sites (as characterized by their acidity or basicity) compared to MeSH synthesis (21). These sites may deactivate differently, or at least at differing rates. The initial drop in DMS selectivity could arise if the sites responsible for DMS production were initially deactivated more rapidly than those responsible for MeSH formation.

For NaMOS(py) catalysis, increasing conversion by raising temperature led to a significant increase in CO and CO_2 production and to a slight increase in CH_4 production. As previously mentioned, H_2 was also detected in the reactor effluent in small amounts. It is possible that the Mo_6S_8 materials also catalyze additional reactions:

$$CH_3OH \xrightarrow{Mo_6S_8} CO + 2H_2 \quad (4)$$

$$CO + H_2S \xrightarrow{Mo_6S_8} COS + H_2 \quad (5)$$

$$CO + H_2O \xrightarrow{Mo_6S_8} CO_2 + H_2 \quad (6)$$

$$CH_3OH + H_2 \xrightarrow{Mo_6S_8} CH_4 + H_2O \quad (7)$$

DMS was either not present at all, or present in very small amounts. CO, CO_2, CS_2, or COS are not important side products for reactions with industrial alumina-based catalysts.

Stability

MoS_2 was detected by LRS in amorphous ternary materials containing Na, Pt, or Sn after reaction with MeOH and H_2S, but not for materials containing La or Ho. Formation of MoS_2 was more apparent for the "small ion" materials, probably due to the mobility and loss of the ternary metal from the surface. Destabilization of the Mo_6S_8 clusters could lead to MoS_2 formation.

A small amount of MoS_2 was also detected for LaMoS by LRS and FTIR after reaction for 3 days. The amount of MoS_2 increased with reaction temperature and was clearly detectable by 300°C. Prior HDS work with this catalyst at higher temperatures (400°C) did not show the presence of any MoS_2 in post-reaction characterization. However, for the HDS studies, the partial pressure of H_2S was much lower. In addition, the HDS studies were carried out for only 10 h, and there is a significant difference in the amount of MoS_2 formed at longer reaction times.

XPS analysis of LaMoS and NaMoS(py) revealed interesting changes occurring near the catalyst surface during reaction. By 250°C under reaction conditions with H_2S present, the Mo in the cluster was apparently altered, primarily due to significant conversion to the intermediate Mo^{3+} species and partial conversion to Mo^{4+} (MoS_2). MoS_2 was detected by XPS only at the surface; none was observable by LRS or FTIR. Reaction at higher temperatures (300-350°C) with H_2S present formed only the Mo3+ species at the surface. However, in the bulk, the material seems to substantially convert to MoS_2 as shown by the LRS and FTIR results.

Samples treated in only MeOH in He did not show any conversion to the Mo^{3+} species by XPS, but rather revealed significant conversion to an oxysulfide species, with binding energies consistent with Mo^{4+}. The fact that the Mo peak due to the cluster remained present up to 350°C in samples heated in only MeOH (no H_2S present) — combined with the fact that the Mo^{3+} species was not detected in these samples — indicates that the Mo^{3+} species is most likely a purely sulfide species like Mo_2S_3. These results also imply that this Mo^{3+} species does not form by disproportionation of the Mo and S in the Mo_6S_8 cluster; rather it requires the presence of additional sulfur source, such as H_2S.

XPS results showed the presence of Mo^{4+} at the surface for catalyst treated in pure H_2S at 300-400°C. However, the relative amount of Mo^{4+} seemed to decrease with increasing temperature. This fact, combined with the post-reaction XPS results, seems to indicate that MoS_2 is not the most surface-stable species on these materials; rather it is a more reduced form with Mo^{3+}, perhaps a material like Mo_2S_3. This is somewhat surprising considering their stoichiometries; in excess H_2S one could expect that MoS_2 would be more stable.

Samples treated in pure H_2S did not reveal bulk conversion to MoS_2 (detected by LRS) until the temperature was above 300°C. However, XPS on post-reaction materials showed that the MoS_2 was formed at 250°C and was not present at the surface by 300°C; instead, only the Mo^{3+} species was detected. Under reaction conditions, some surface oxide or oxysulfide formed by oxidation with the alcohol at 250°C, which in the presence of H_2S rapidly converted to MoS_2. However, these studies also have shown that the presence of MeOH is not required to form MoS_2 from LaMoS in the bulk, since a detectable amount formed at 400°C in pure H_2S after only 4 h.

5. Conclusions

Amorphous ternary materials based on the Mo_6S_8 cluster represent a new and promising family of thiol synthesis catalysts. These materials naturally fall into three main categories: amorphous ternary materials, crystalline Chevrel phases, and ligated crystalline molecular cluster materials. The most active, selective, and stable materials for MeSH synthesis were the amorphous ternary materials, where the ternary metal was of the "large ion" type (La, Ho). These materials remained stable for several days and exhibited MeSH

selectivities higher than 80% in the reaction of H_2S with MeOH at 250°C. The ligated crystalline molecular cluster materials had reasonably high activity and were surprisingly stable, even though they did undergo slight deligation at 250°C. The crystalline La Chevrel phase material was also very stable, but had much lower activity (catalyst weight basis) and selectivity to MeSH than its amorphous counterpart. The least stable catalysts examined were the "small ion" amorphous ternary materials, which tended to partially convert to MoS_2 under reaction at 250°C.

6. Acknowledgements

We thank Jim Anderegg of the Ames Laboratory for assistance in obtaining the XPS characterization. We also thank Shane Hilsenbeck for preparing several of the catalysts used in this work. This work was supported by the U.S. Department of Energy, Office of Basic Energy Sciences, through Ames Laboratory operated by Iowa State University under Contract No. W-7405-Eng-82.

7. References

1 Forquy, C. and Arretz, E., *Stud. Surf. Sci. Catal.* **41** (*Heterog. Catal. Fine Chem.*), 91-104 (1988).
2 U.S. Patent 4,233,128 to Societe Nationale Elf-Aquitaine (Production), (1980).
3 U.S. Patent 5,741,934 to S. R. Sandler, P. J. Peerce-Landers, and C. Forquy (1998).
4 U.S. Patent 5,898,012 to Phillips Petroleum Company (1999).
5 European Patent Application 564 706 A1 to Elf Atochem North America, Inc. (1992).
6 U.S. Patent 5,874,630 to Occidental Chemical Corporation (1999).
7 Hilsenbeck, S. J.; Young, V. G.; McCarley, R. E. *Inorganic Chemistry*, **33**(9), 1822-1832 (1994).
8 Hilsenbeck, S. J., McCarley, R. E., Thompson, R. K., Flanagan, L. C., and Schrader, G. L., *J. Mole. Catal. A: Chemical,* **122**, 13-24 (1997).
9 McCarty, K. F., and Schrader, G. L., *Ind. Eng. Chem. Prod. Res. Dev.*, **23**, 519 (1984).
10 McCarty, K. F., Anderegg, J. W., and Schrader, G. L., *J. Catal.*, **93**, 375 (1985).
11 Eckman, M. E., Anderegg, J. W., and Schrader, G. L., *J. Catal.*, **117**, 246 (1989).
12 Ackman, R. G., *J. of Gas. Chrom.*, June, 1964.

13 Ackman, R. G., *J. of Gas. Chrom.*, October, 1968.
14 Chang, C. H. and Chan, S. S., *J. Catal.*, **72**(1), 139-48 (1981).
15 Wieting, T. J. and Verble, J. L., *Phys. Rev. B*, **3**(12), 4286-92 (1971).
16 McCarley, R. E., Hilsenbeck, S. J., and Xie, X., *J. Solid State Chem.*, **117**, 269 (1995).
17 Hilsenbeck, S. J., McCarley, R. E., Goldman, A. I., and Schrader, G. L., *Chem. Mater.*, **10**, 125-134 (1998).
18 Thompson, R. K., Hilsenbeck, S. J., Paskach, T. J., McCarley, R. E., and Schrader, G. L., *J. Mole. Catal A: Chemical*, **161**, 75-87 (2000).
19 Lavasseur, A., Vinatier, P, and Gonbeau, D., *Bull. Mater. Sci.*, **22**(3), 607-614 (1999).
20 Hilsenbeck, S. J., and McCarley, R. E., *Chem. Mater.*, **7**, 499-506 (1995).
21 Mashkina, A. V., *Russ. Chem. Rev.*, **64**(12) 1131-1147 (1995).

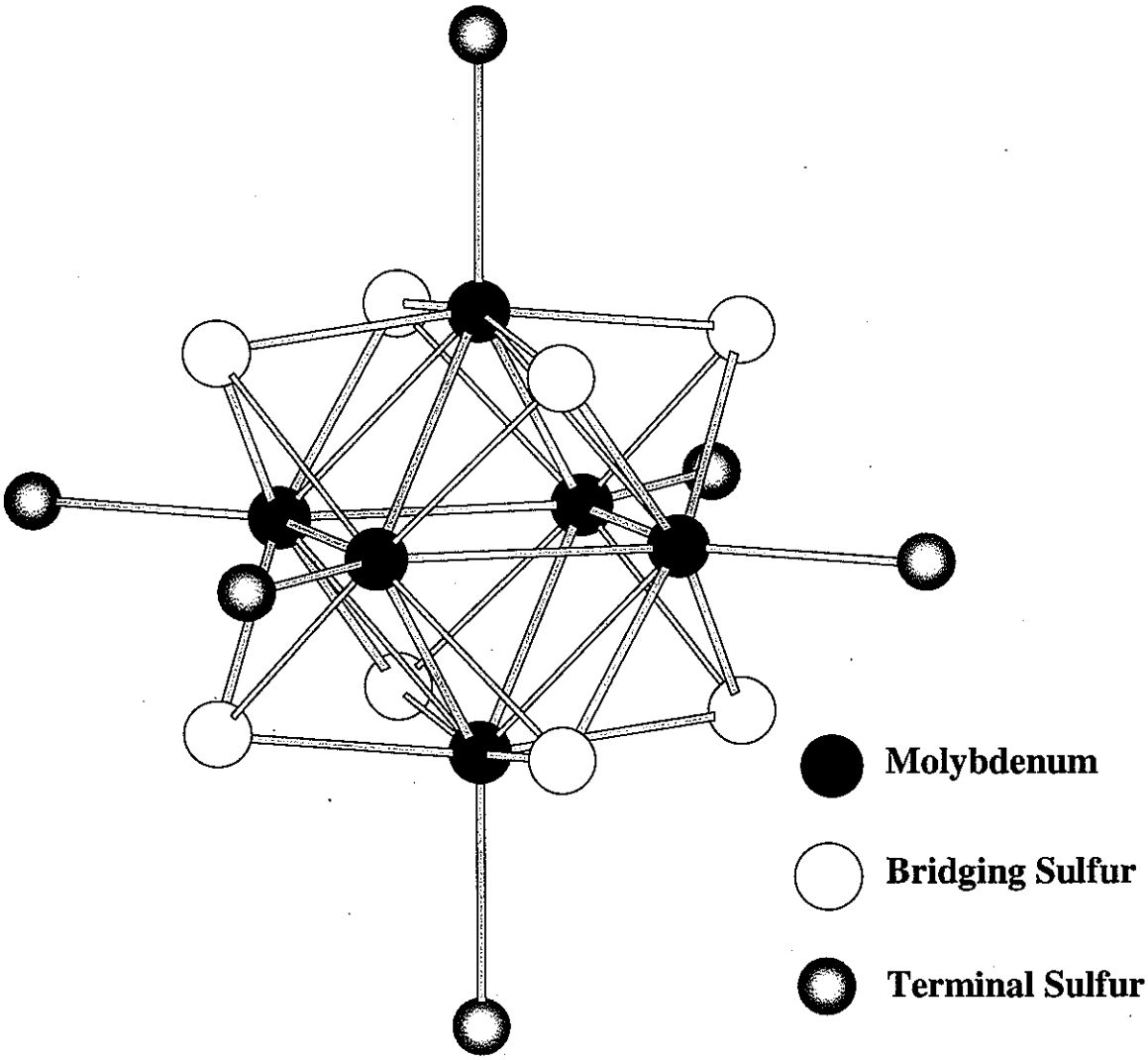

Figure 1. Structure of the Mo_6S_8 hexanuclear cluster unit which is formed by a molybdenum octahedron and eight triply bridging sulfur atoms capping each face. Additionally, six terminal positions are located at the vertices of the octahedron and are occupied by either organic ligands or sulfur atoms

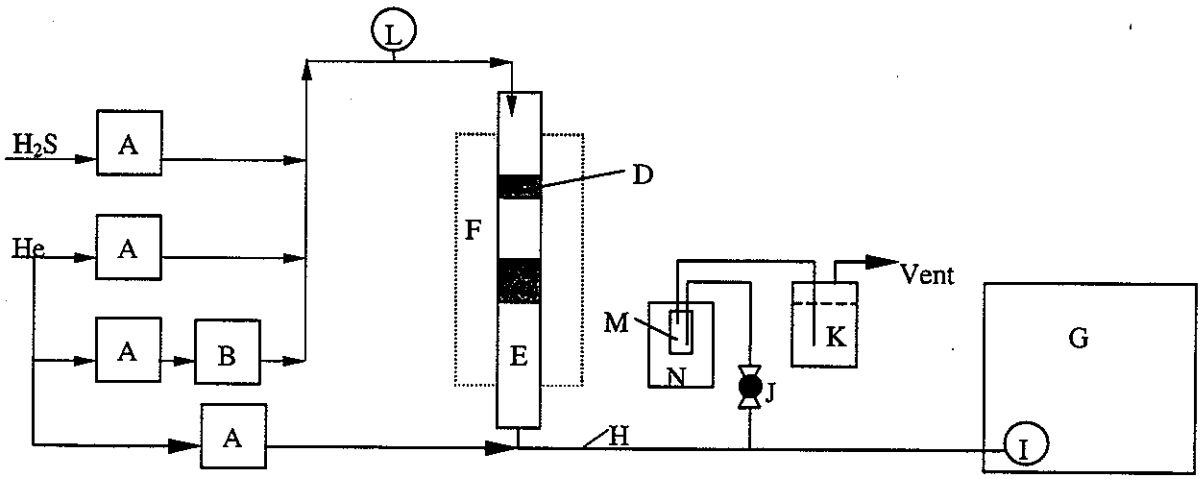

Figure 2. Microreactor system. A: mass flow controllers, B: saturator for MeOH feed, C: catalyst bed with quartz wool plugs on top and bottom, D: quartz wool plug for liquid feed evaporator, E: Pyrex or quartz tube reactor, F: temperature-controlled reactor furnace, G: GC with FID and TCD, H: heat tracing, I: sample injection valve, J: split valve, K: KOH/bleach bubbler, L: pressure gauge, M: trapping vial, N: ice-salt bath.

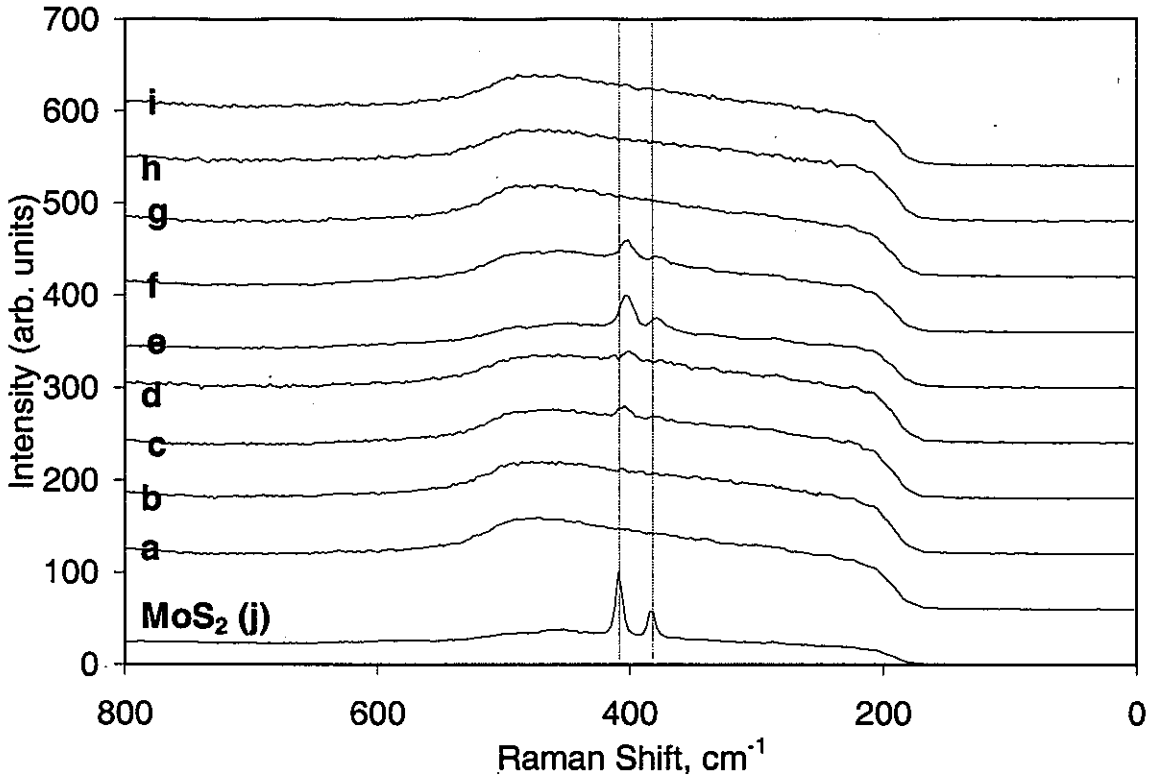

Figure 3. Laser Raman spectra of the various catalysts examined, after 20 hours under reaction conditions (250°C, H_2S/MeOH = 3.00). The bands at 408 cm^{-1} and 383 cm^{-1} arise from MoS_2. Letters indicating the various catalysts are as in Table 1.

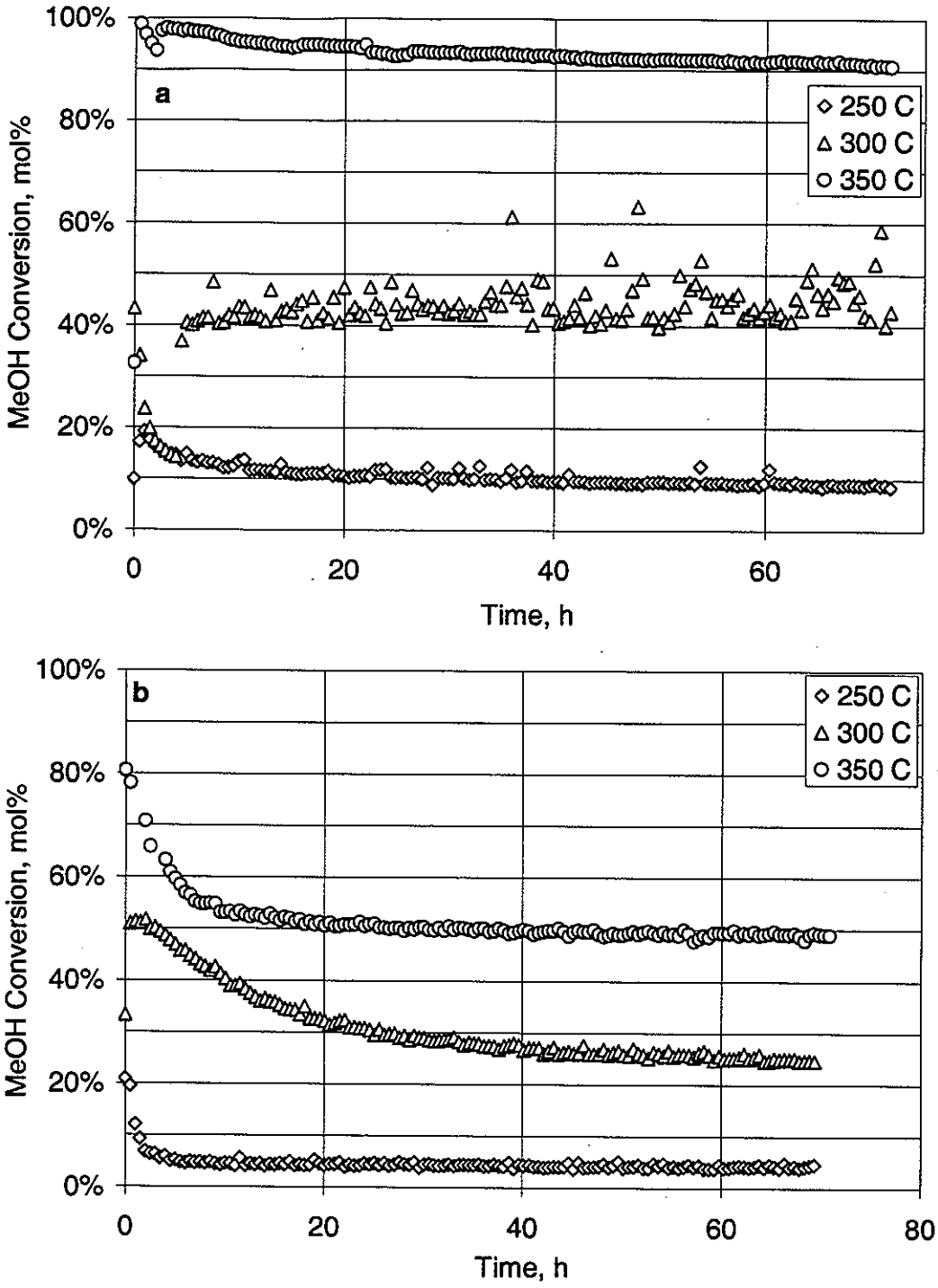

Figure 4. Conversion for H_2S + MeOH over the amorphous catalysts (a) LaMoS and (b) NaMoS(py) at various temperatures, and constant H_2S/MeOH ratio of 3.00.

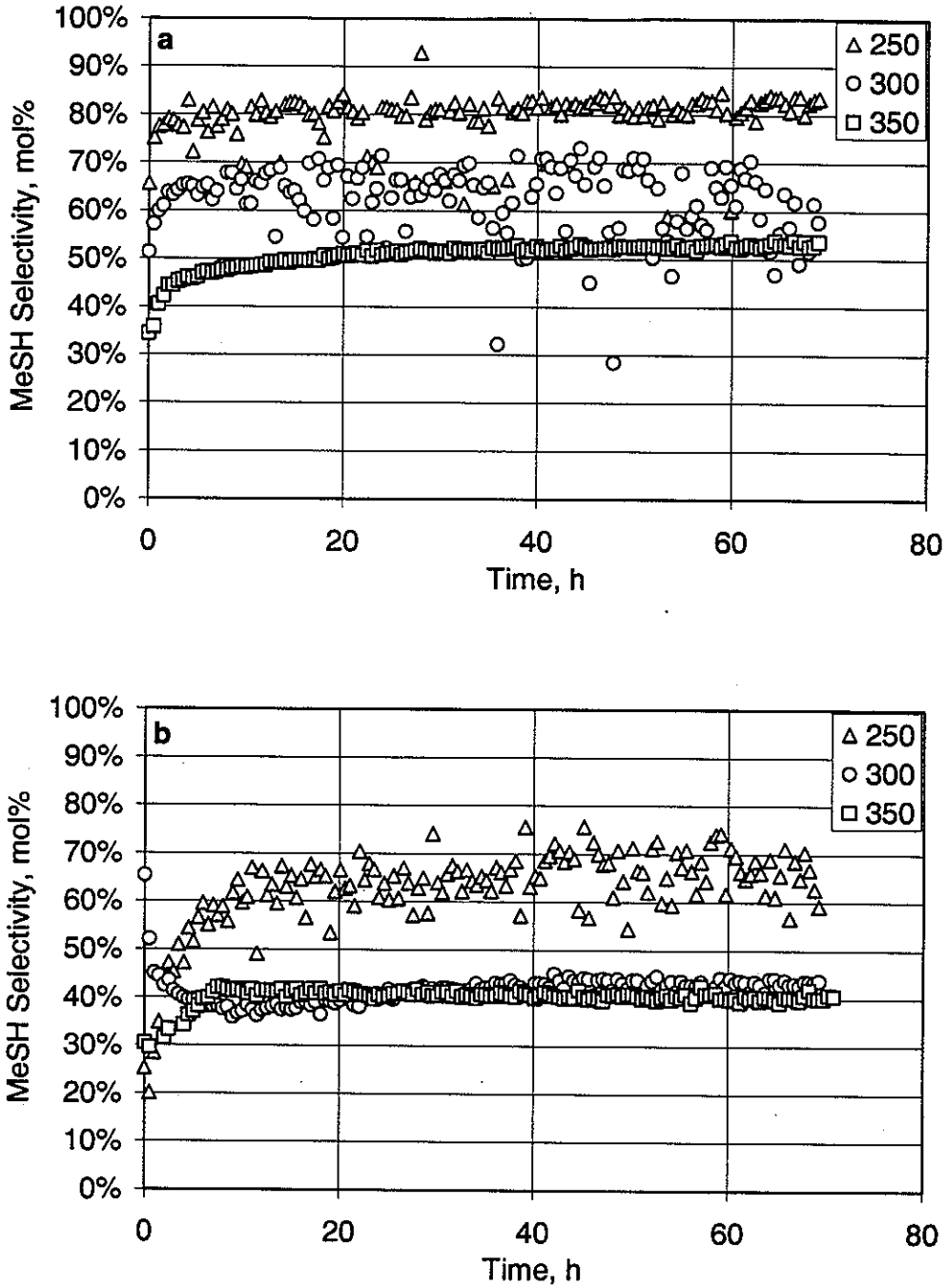

Figure 5. Selectivity to MeSH for H_2S + MeOH over the amorphous catalysts (a) LaMoS and (b) NaMoS(py) at various temperatures, and constant H_2S/MeOH ratio of 3.00.

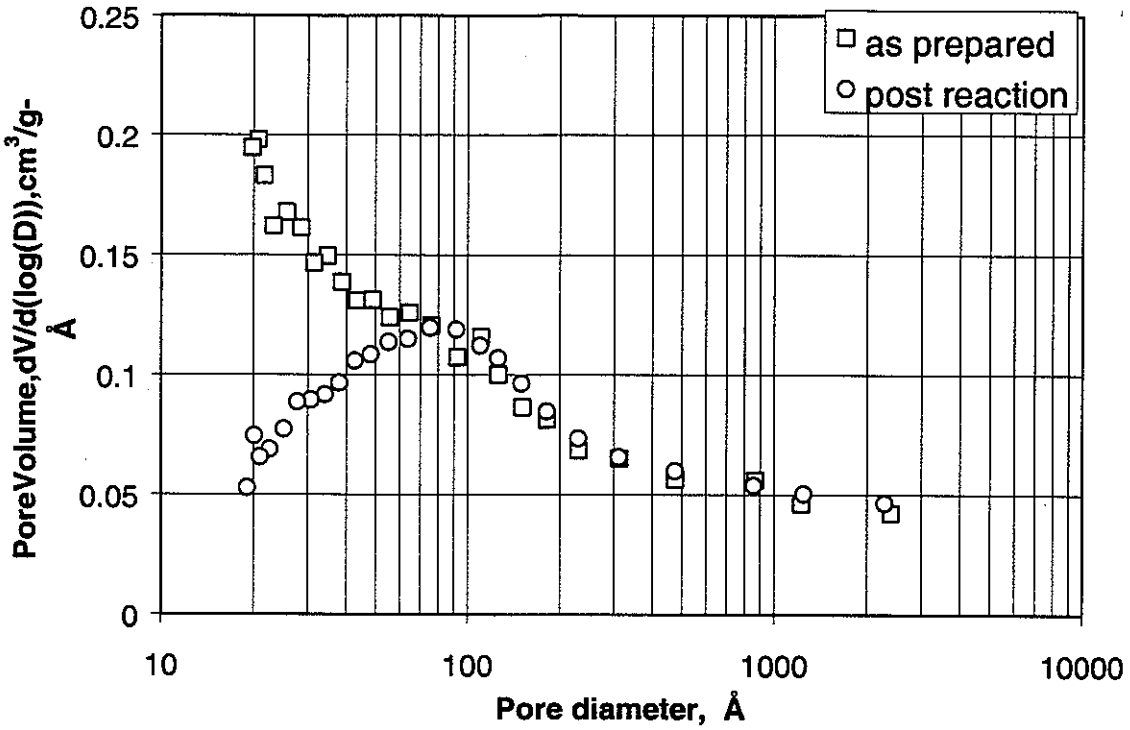

Figure 6. Porosimetry by nitrogen adsorption at 77 K for amorphous LaMoS, before and after reaction. Reaction causes loss of surface area resulting from collapse of pores smaller than about 70 Å.

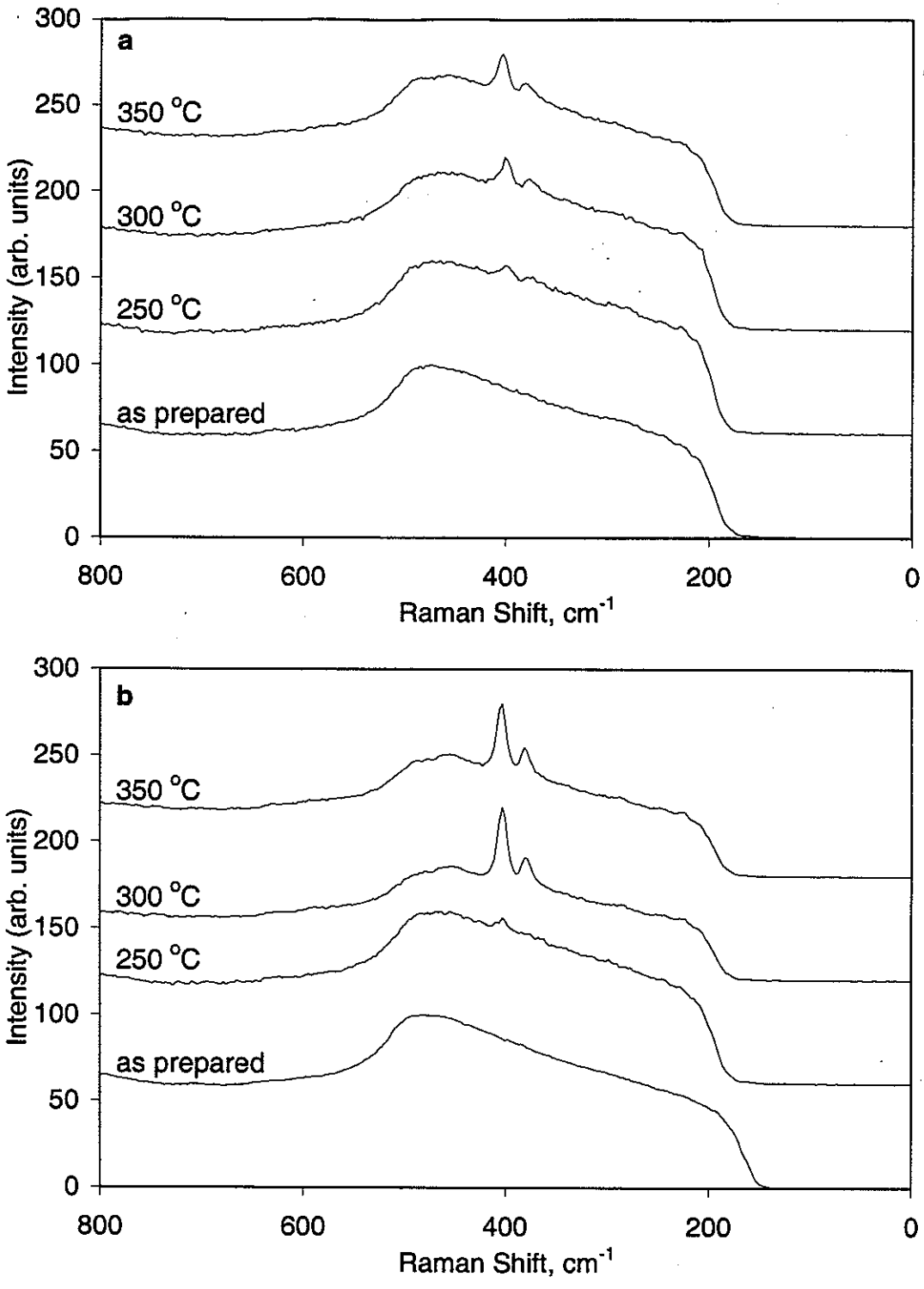

Figure 7. Laser Raman spectra of amorphous catalysts (a) LaMoS and (b) NaMoS(py) before and after reaction for three days at various temperatures, and constant H_2S/MeOH ratio of 3.00. Small amounts of MoS_2 were detected, indicated by peaks at about 383 and 404 cm^{-1}.

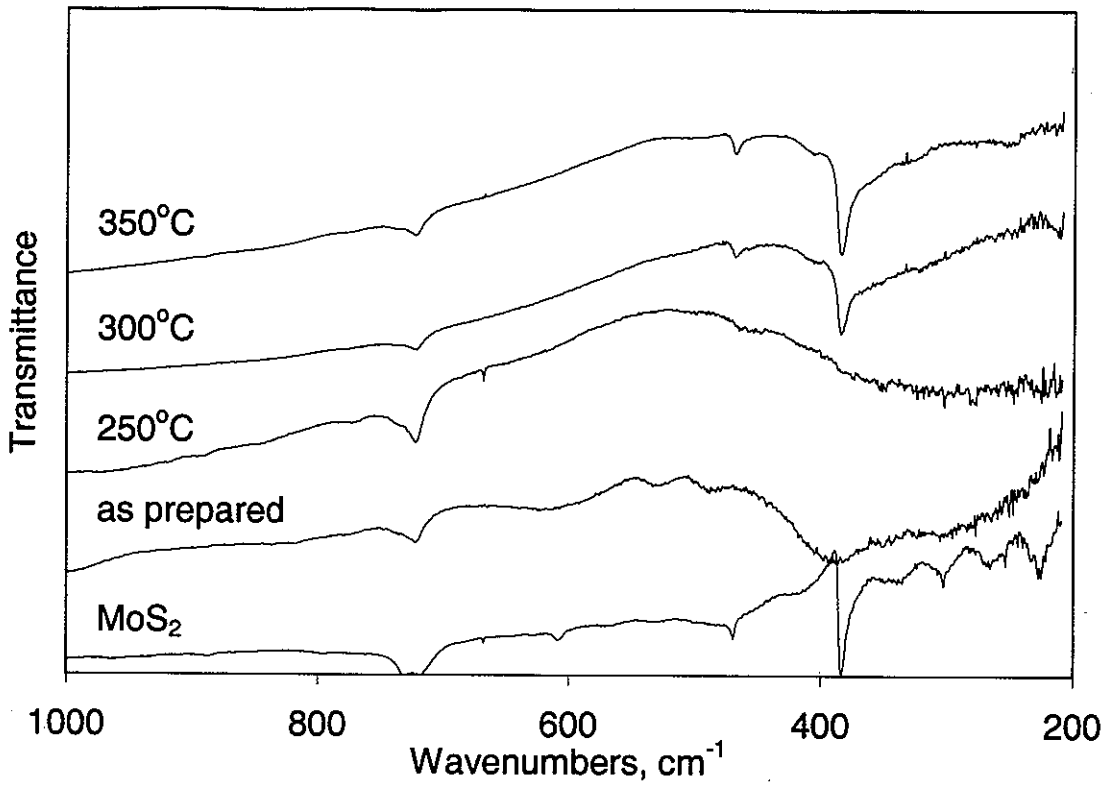

Figure 8. Fourier Transform Infrared Spectra of amorphous LaMoS before and after reaction for three days at various temperatures, and constant H_2S/MeOH ratio of 3.00. Peaks at 670 cm^{-1} arise from the mineral oil mulling agent.

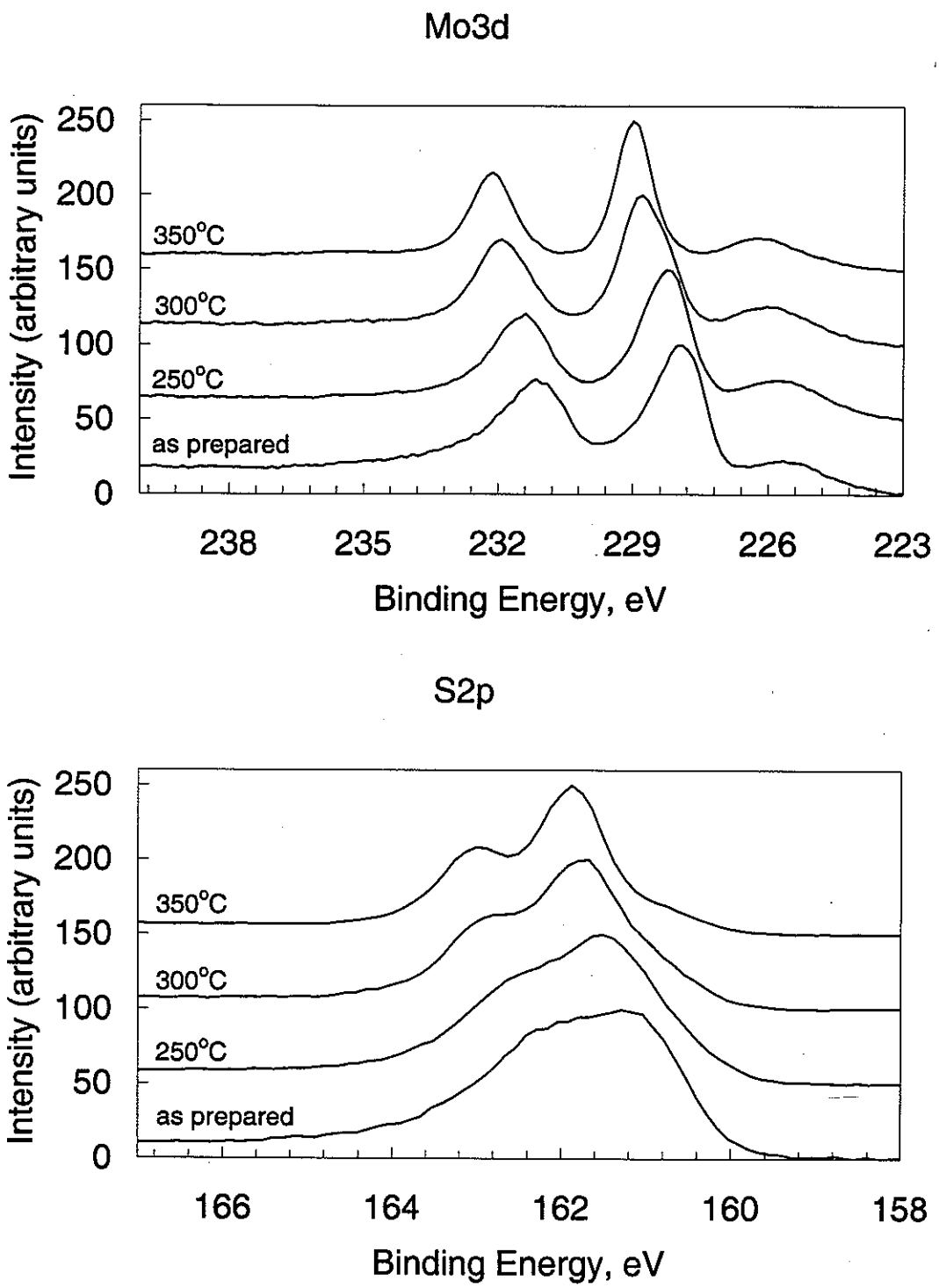

Figure 9. X-ray photoelectron spectra of amorphous LaMoS catalyst for Mo3d, and S2p regions, before and after reaction at various temperatures. Reaction conditions caused a shift in the major Mo and S species to higher binding energies consistent with Mo_2S_3.

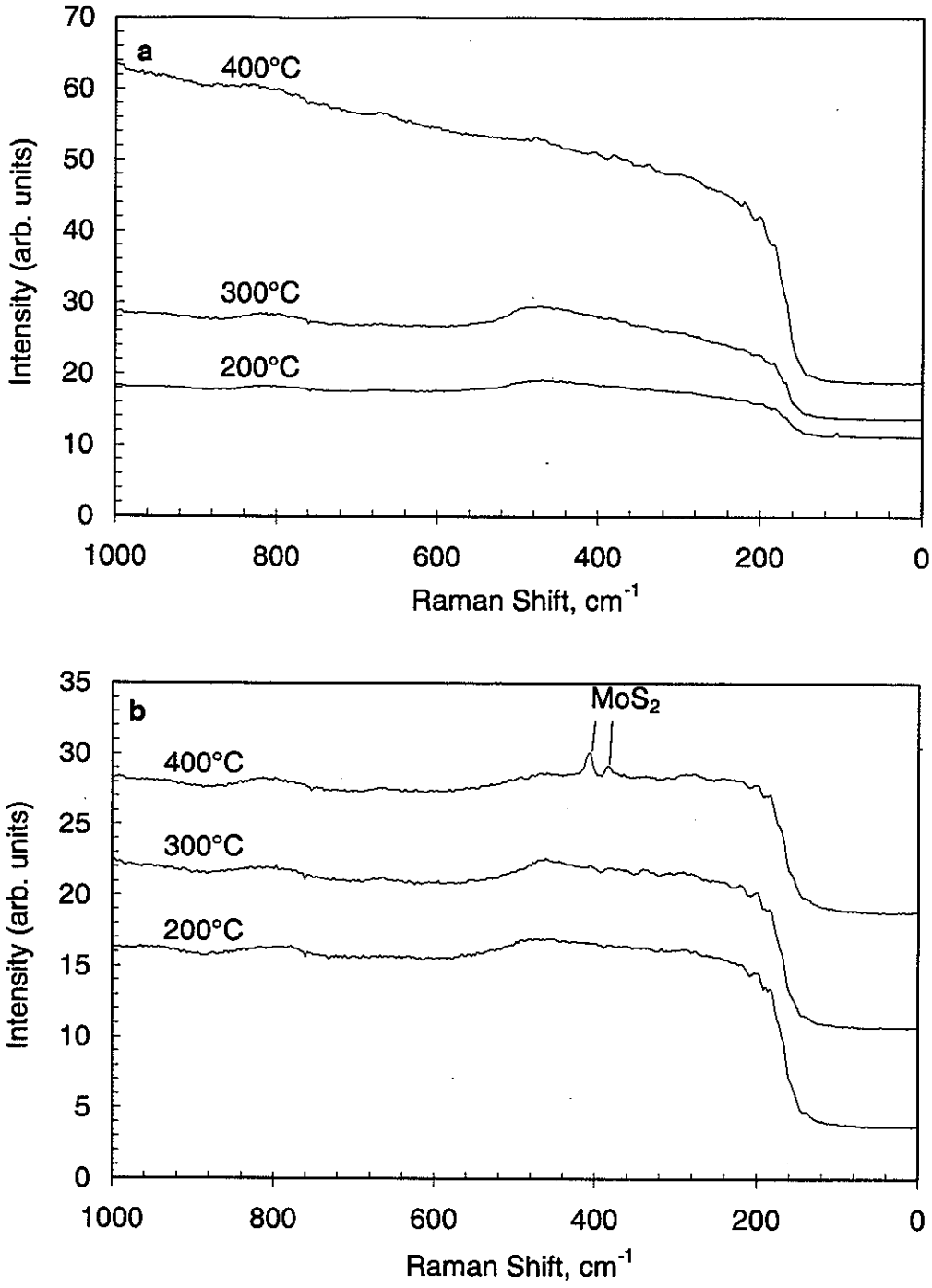

Figure 10. Laser Raman spectra of amorphous LaMoS after treatment in (a) a stream of MeOH in He and (b) a stream of pure H_2S, at 200°C, 300°C, and 400°C for four hours. Weak bands characteristic of MoS_2 (404, 383 cm^{-1}), are present only in the sample treated in pure H_2S at 400°C. No MoO_3 was detected.

Table 1. Activity and surface areas of various amorphous catalysts containing the Mo_6S_8 cluster unit. 250°C, H_2S/MeOH ratio of 3. Data represents the average for the last 2 hours of a 20-hour run.

Label		BET Surface Area, m^2/g		MeOH rate	
		pre-reaction	post-reaction	$\mu mol/h \cdot g_{cat}$	$\mu mol/hr \cdot m^2$
a	$La(Mo_6S_8)S_{1.5}$	170	116	1360	12
b	$Ho(Mo_6S_8)S_{1.5}$	176	14	2031	147
c	$Sn(Mo_6S_8)S$	130	18	375	21
d	$Pt(Mo_6S_8)S$	130	28	523	18
e	$Na_3(Mo_6S_8)S_{1.5}$	135	46	1425	31
f	$Na_2(Mo_6S_8)S(py)_y$	138	38	806	21
g	$LaMo_6S_8$	0.46	0.47	84	178
h	$Mo_6S_8(pip)_y$	0.80	1.47	623	424
i	$Mo_6S_8(PrNH_2)_y$	0.83	0.41	131	317
j	MoS_2	10	8.7	334	38

Table 2. Selectivity of the various amorphous catalysts to the major products of the reaction of H_2S and MeOH at 250°C and H_2S/MeOH ratio of 3. Data represents the average for the last 2 hours of a 20-hour run.

Label		Selectivities, mol% equivalent								
		MeSH	DMS	DME	CH_4	CO	CO_2	COS	CS_2	Other Products
a	$La(Mo_6S_8)S_{1.5}$	83.0	6.4	0.1	0.1	5.0	2.6	0.2	2.5	0.1
b	$Ho(Mo_6S_8)S_{1.5}$	72.2	17.4	0.9	0.4	2.6	2.7	0.1	3.4	0.1
c	$Sn(Mo_6S_8)S$	75.0	11.0	2.7	0.6	8.2	2.5	0.0	0.0	0.0
d	$Pt(Mo_6S_8)S$	75.4	8.0	0.7	0.9	5.5	0.4	1.0	8.1	0.0
e	$Na_3(Mo_6S_8)S_{1.5}$	44.9	0.1	0.0	0.2	13.6	18.3	19.0	3.9	0.0
f	$Na_2(Mo_6S_8)S(py)_y$	51.9	0.3	0.0	0.2	11.9	11.3	15.5	8.9	0.0
g	$LaMo_6S_8$	53.6	0.0	0.6	0.1	38.1	6.5	1.0	0.0	0.0
h	$Mo_6S_8(pip)_y$	59.9	4.7	0.1	0.6	16.2	0.0	4.9	13.7	0.1
i	$Mo_6S_8(PrNH_2)_y$	20.8	0.0	0.1	1.1	65.3	5.2	0.8	5.0	1.7
j	MoS_2	36.5	4.6	8.1	0.0	50.7	0.0	0.0	0.0	0.1

Table 3. Conversion and selectivities for amorphous LaMoS at 250°C reaction temperature, at various values of H_2S/MeOH ratio.

H_2S/MeOH	MeOH Conversion	Selectivities, mol%							
mol/mol	mol%	MeSH	DMS	DME	CH_4	CO	CO_2	COS	CS_2
0.30	19.5	60.0	11.6	0.16	0.59	6.4	15.1	0.1	6
0.50	16.9	68.5	7.2	0.16	0.38	6.3	13.6	0.3	3
1.00	15.3	71.1	4.3	0.14	0.27	6.3	11.4	0.5	6
2.00	13.3	72.0	2.6	0.10	0.20	5.5	9.9	0.6	9
3.00	12.0	72.3	1.9	0.10	0.17	5.3	8.1	0.6	11
4.00	11.1	71.7	1.5	0.06	0.14	4.4	7.4	0.9	14
6.00	10.1	71.4	1.2	0.04	0.12	5.4	6.7	1.2	14

Table 4. Activity and selectivity summary for amorphous catalysts LaMoS and NaMoS(py) at various temperatures and H_2S/MeOH ratio of 3. Data represents the average for the last 5 hours of a 72-hour run.

	LaMoS			NaMoS(py)		
	250°C	300°C	350°C	250°C	300°C	350°C
BET S.A., m^2/g (pre/post reaction)	170 /116	170 / 66	170 / 55	135 / 49	135 / 7.1	135 / 2.7
Approximate contact time, sec	0.87	0.79	0.73	0.87	0.79	0.73
MeOH Conversion						
mol %	8.9	46.3	91.3	4.3	25.0	49.1
$mol/m^2sec \times 10^8$	0.29	2.6	6.2	0.3	13.0	67.0
Selectivities, mol%						
Methane	0.1	0.6	6.1	0.3	1.7	1.9
Ethene/Acetylene	0.0	0.1	0.4	0.0	0.0	0.0
Ethane	0.0	0.0	0.1	0.0	0.0	0.0
Propane	0.0	0.1	0.2	0.0	0.0	0.0
Dimethylether	0.2	0.0	0.0	0.0	0.0	0.0
Methanethiol	82.5	57.2	53.2	64.3	43.1	40.3
Ethanethiol	0.0	0.2	0.2	0.0	0.1	0.0
Dimethylsulfide	5.4	5.6	5.1	0.4	0.1	0.1
CS_2	5.7	20.4	0.8	0.0	0.1	0.0
CO	2.8	2.0	7.9	8.5	16.7	22.1
CO_2	3.4	13.3	25.4	11.6	29.3	30.4
COS	0.1	0.5	0.5	14.9	9.0	5.2

Table 5. X-ray photoelectron spectroscopy summary for the Mo 3d region of both catalysts, before and after reaction for 3 days at various temperatures and H_2S/MeOH ratio of 3.

	Cluster		Mo^{3+}		Mo^{4+}		Mo^{6+} (MoO_3)	
	E_b, eV	frac. (%)	E_b, eV	frac. (%)	E_b, eV	frac. (%)	E_b, eV	frac. (%)
LaMoS								
as-prepared	227.8	70	228.7	18			231.4	12
post-reaction 250 °C			228.4	70	229.5	30		
post-reaction 300 °C			228.7	94			231.6	6
post-reaction 350 °C			229.0	93			232.1	7
NaMoS(py)								
as-prepared	227.3	88	228.4	12				
post-reaction 250 °C			228.4	63	229.2	37		
post-reaction 300 °C			228.8	100				
post-reaction 350 °C			228.8	98	230.2	2		

Table 6. X-ray photoelectron spectroscopy summary for the Mo 3d region of LaMoS catalyst, before and after four-hour treatment with MeOH/He or pure H_2S at various temperatures.

	Cluster		Mo^{3+}		Mo^{4+}		Mo^{6+} (MoO_3)	
	E_b, eV	frac. (%)	E_b, eV	frac. (%)	E_b, eV	frac. (%)	E_b, eV	frac. (%)
as-prepared	227.8	70	228.7	18			231.4	12
MeOH Treatment Temp, °C								
200	227.5	34			229.5	66		
300	227.4	40			230.5	50	232.8	10
400	227.7	27			229.5	64	232.9	9
H_2S Treatment Temp, °C								
200	228.1	100						
300			228.5	76	230.0	24		
400			228.8	86	230.2	14		

CHAPTER 5. SYNTHESIS OF HIGHER THIOLS FROM ALCOHOLS OVER AMORPHOUS $La(Mo_6S_8)S_{1.5}$

Thomas J. Paskach[a,c], Glenn L. Schrader,[a,c] and Robert E. McCarley[b,c]

Department of Chemical Engineering,[a]

Department of Chemistry[b], and

Ames Laboratory-USDOE[c]

Iowa State University

Ames, Iowa 50011

Abstract

Synthesis of ethanethiol (EtSH) and 1-butanethiol (1-BuSH) from ethanol and 1-butanol and hydrogen sulfide (H_2S) have been investigated over amorphous $La(Mo_6S_8)S_{1.5}$ at 200°C. The selectivity of the catalyst for EtSH was greater than 92% at a conversion of 28%, and that for 1-BuSH was 94% at 14% conversion. The reaction pathways for the synthesis of EtSH were investigated, and a proposed reaction mechanism is presented. The reaction of ethylene with H_2S was also found to proceed readily and with excellent (99+%) selectivity) over this catalyst. X-ray photoelectron spectroscopy (XPS) confirmed that Mo was maintained in a very reduced state at the catalyst surface after reaction, though the Mo_6S_8 cluster was not detected in the bulk by Fourier transform infrared spectroscopy.

1. Introduction

Industrial synthesis of bulk organosulfur chemicals includes the production of mercaptans (thiols), alkylsulfides (thioethers), polysulfides, and thiophenes. Many of the derivatives of these organosulfur chemicals have biological activity and are used extensively in the production of agricultural chemicals (agrochemicals) and pharmaceuticals. Low molecular weight thiols such as the $C_1 - C_6$ thiols are commercially manufactured on the order of 10^4 ton/yr. For example, ethanethiol (EtSH) is one of the most diversely applied thiol intermediates for agrochemicals (used for the production of butylate, cycloate, demeton, disulfoton, oxydemeton-methyl, oxydeprofos, dipropetryn, EPTC, molinate, phenothiol, phorate, and sethoxydim), and it is also used as an odorant for propane. Additionally, 1-butanethiol is used extensively as an agrochemical intermediate (1).

The literature on thiol synthesis from alcohols and hydrogen sulfide is dominated by methanol (MeOH) to methanethiol (MeSH) reactions and catalysts. For the production of higher primary thiols, the preferred route depends on the feedstock. Primary alcohol feeds can be effectively converted to primary thiols via surface-catalyzed processing routes, while free-radical synthesis is preferred when starting with α-olefins and H_2S (anti-Markownikov addition). Conversion assisted by UV radiation is fairly selective to the primary thiol (~92% selectivity), but homogeneous catalysts containing boron which apparently generate radicals are even more selective (up to ~97%).

The surface mechanism for methanethiol and dodecanethiol synthesis over alkali modified alumina has been studied by Mashkin et al (2, 3). In their work, adsorbed surface intermediates are proposed: alkoxides (R-O), mercaptides (R-S), H, SH, and OH. These intermediates and serve to explain selectivities to alkylsulfide, alkene, and alkylether.

In our previous work (4), a new family of materials based on the Mo_6S_8 molecular structure (Fig. 1) was shown to contain effective catalysts for MeSH synthesis from MeOH and H_2S. The most selective of these was amorphous $La(Mo_6S_8)S_{1.5}$. However, these catalysts tended to produce significant amounts of CH_4, CO, CO_2, CS_2, and COS, which limited their overall selectivity to MeSH to just over 80%. These very stable single-carbon compounds clearly cannot be produced from higher alcohols without severing carbon-carbon bonds in the molecule. This represented an apparent opportunity to achieve higher selectivities with higher alcohols by eliminating the chemistry of the single-carbon compounds. In this work, the synthesis of C_2 and C_4 thiols from their corresponding alcohols over amorphous $La(Mo_6S_8)S_{1.5}$ has been investigated. The reaction pathway was studied for the EtOH system, and a reaction mechanism has been proposed.

2. Experimental

Preparation of amorphous $La(Mo_6S_8)S_{1.5}$ has been reported previously (5,6,7,8). Amorphous $La(Mo_6S_8)S_{1.5}$ was prepared by a two-step process. In the first step, anhydrous Mo_6Cl_{12} reacted with sodium hydrosulfide (NaSH) and sodium butoxide (NaOBu) under refluxing anhydrous n-butanol (BuOH) to form a black, amorphous sodium salt containing either 3 Na atoms per cluster. The solid $Na_3(Mo_6S_8)S_{1.5}$ was filtered and washed with anhydrous, degassed MeOH to remove NaCl.

$$Mo_6Cl_{12} + 9.5NaSH + 5.5NaOBu \xrightarrow{BuOH} Na_3(Mo_6S_8)S_{1.5} + 5.5BuOH + 12NaCl \qquad (1)$$

In the second step, NaMoS was treated with $La(NO_3)_3 \cdot 6H_2O$ in anhydrous, degassed MeOH so that ion exchange occurred between the La and the Na ions to form the amorphous ternary molybdenum sulfide (also referred to as LaMoS).

$$Na_3((Mo_6S_8)S_{1.5} + La^{3+} \xrightarrow{MeOH} La(Mo_6S_8)S_{1.5} \cdot y(MeOH) + 3Na^+ \quad (2)$$

Mo_6S_8-based catalysts have generally been found to be oxygen sensitive. Schlenk techniques with a high vacuum line and a Vacuum Atmospheres Company model 8130 drybox with oxygen and moisture gettering capabilities were utilized. $La(Mo_6S_8)S_{1.5}$ catalyst was pelletized in the drybox by pressing 200 mg wafers which were subsequently broken and screened to 10-20 mesh prior to use.

Catalyst Characterization

Catalyst characterization involved infrared spectroscopy (FTIR), laser Raman spectroscopy (LRS), x-ray photoelectron spectroscopy (XPS), and adsorption surface area/pore size measurements.

FTIR spectra were obtained using a Bomem MB-102 spectrometer with CsI optics, at 2 cm^{-1} resolution. Samples were analyzed as Nujol oil mulls with special sample holders designed to exclude O_2.

LRS was performed using a Coherent 532-50 diode-pumped solid state laser (532 nm, 50 mW source) with fiber optic couplings and integral source/collection optics. Spectra were taken in a backscattered collection mode. A Kaiser Holospec f/1.8 spectrometer and Princeton Instruments CCD detector (1100x330) with WinSpec software were used for signal analysis. Catalyst samples were analyzed in sealed capillary tubes under Ar or the Pyrex reactor tubes under He for post-reaction LRS characterization due to their oxygen sensitivity.

XPS data were obtained with a Physical Electronics Industries 5500 multitechnique surface analysis system using a monochromatic MgK_α source; binding energies were calibrated with adventitious carbon (C 1s = 284.6 eV). Spectra were fit with peaks consisting of a mixture of Lorenzian and Gaussian character, following Shirley background subtraction. For doublet

peak fitting, the peak area ratios and doublet offset value were fixed. Samples were transferred from the drybox to the XPS instrument under Ar in a special sealed sample container which was opened under dynamic vacuum just before analysis.

Surface areas were measured with a Micromeretics ASAP 2010C instrument at 77 K. N_2 was used as the adsorbate. Brunauer, Emmet, and Teller (BET) calculations were used to determine surface areas for all samples, and the Barret, Johner, and Hallenda (BJH) method was used for determining pore size distributions. Samples were degassed overnight at 150°C under dynamic vacuum prior to analysis.

Catalytic Reactor Studies

H_2S (CP grade) and ethylene were supplied by Matheson. Absolute Ethanol (200 proof, Aaper), certified 1-PrOH (Fisher), and certified 1-BuOH (Fisher) were degassed in the saturator with bubbling He prior to use. (UHP (zero) He (Matheson) was used for the GC carrier and as a reactor feed or product diluent.

The microreactor system (Fig. 2) used 200-500 mg of catalyst fixed in a 6 mm O.D. x 4 mm I.D. Pyrex reactor tube. 4 mm O.D. x 2 mm I.D. Pyrex tube was inserted in the lower half of the larger tube for catalyst bed support. Small (2-3 mm) plugs of silane-treated quartz wool held the catalyst bed in place. Since the catalyst was air sensitive, the reactor tube was fitted on both ends with Swagelock fittings with high-temperature rubber septa and loaded in the drybox. Installation of the reactor involved piercing the septa with needles under a He purge. The temperature in the reactors was maintained with a Lindberg model 54032 furnace with an Omega 4200 or Eurotherm 815P programmable temperature controller.

Gas feeds were controlled with Brooks model 5850E mass flow controllers and model 5878 master controller. Liquid feeds were delivered by saturating a He flow at a controlled

temperature with the feed liquid. He was added to the reactor effluent line to dilute the reactor effluent and to prevent product condensation. Pressure (approximately 1 atm) was controlled in the reactor by the use of a needle valve on the reactor outlet located downstream of the He addition, which split the flow between the sample loop and the vent/scrubber system.

Product analysis was performed with a Varian model 3600CX gas chromatograph (GC) with a flame ionization detector (FID) and thermal conductivity detector (TCD) in parallel. An Alltech AT-SULFUR (30 m x 0.32 mm, 4 μm film thickness) column was used with a 5 m x 0.32 mm deactivated fused silica guard column. The GC was programmed from 50°C (5 min) to 150°C at 10°C/min and then to 250°C at 20°C/min. All lines from the reactor were also heated electrically over the 150 - 200°C range using Omega 6100 thermostats to prevent product condensation.

GC peaks were identified by collecting gas-phase samples of reactor products in a septum flask with subsequent analysis by a Finnigan TSQ 700 GC-mass spectrometer system having both electron impact ionization and ammonia positive ion impact ionization modes. The first quadrupole was used as the analyzer and was scanned from m/z 35 to 400 at a rate of 0.5 seconds per scan. The second and third quadrupoles were maintained in at RF-only mode. Unit mass resolution was achieved using FC43 as the calibration and tuning reference. GC retention times were also compared with known standards. FID molar response factors were measured for EtOH and estimated for the remaining products using the methods reported by Ackman *et al.* (9,10).

The reactor system was controlled using remote setpoint programs from a personal computer running DASYLab data acquisition and control software, and an IOtech

Daqboard/2000 interface card. The liquid saturator pressure values were read into DASYLab, and then fed into a MicroSoft EXCEL spreadsheet using an open dynamic data exchange (DDE) link. DASYLab also simultaneously acquired and stored all reactor operating data to disk. The spreadsheet contained an algorithm for estimating the molar rate of liquid feed delivery, and computed the proper setpoints for the mass flow controllers to maintain the desired values of key reactor control parameters, e.g. total molar flow and H_2S/Alcohol molar ratio. DASYLab in turn, read these values from the spreadsheet via a second DDE link. DASYLab then converted the values to appropriately scaled voltage signals, which were then sent out to the mass flow controller setpoint inputs to control the process.

Temperature-programmed desorption (TPD)

TPD was performed on 500 mg of catalyst under flowing He at 10.00 sccm. Temperature was ramped at 1.0°C/min, which provided a good combination of signal-to-noise ratio and resolution of desorption peaks. Prior to the TPD experiment, the catalyst was treated under flowing He at 400°C to desorb any volatile surface species. The catalyst was cooled to room temperature under He flow and then exposed to a mixture of 2-5 mol% of the desired adsorbate in He for 10-20 minutes, followed by a He purge. Detection of desorption products was obtained using the FID on the GC for EtOH and EtSH, and using the thermal conductivity detector (TCD) for H_2O and H_2S.

3. Results

Catalyst Activity and Selectivity

EtOH + H_2S

The reaction of EtOH over amorphous LaMoS occurred readily at 200°C, with EtSH as the main product of the reaction (Table 1). Small amounts of DES and ethylene were also produced, as well as traces of butene isomers and several other unidentified products.

1-BuOH + H_2S

Amorphous LaMoS was also found to catalyze the reaction of 1-BuOH with H_2S selectively (>90%) to 1-butanethiol (1-BuSH) at 200°C and at molar ratios of H_2S/1-BuOH ranging from 1.5 to 10. Other products in the reaction (Table 2) were butenes, dibutylsulfide (DBS), 2-butanol (2-BuOH), and 2-butanethiol (2-BuSH). Various C_8 thiophene isomers were also produced, accounting for 1-5% of the selectivity and are not listed in the table. Increasing the contact time resulted in higher conversion of 1-BuOH accompanied by an increased selectivity to butenes, offset by a decreasing selectivity to 2-BuOH.

Reaction pathway studies

The main reaction of EtOH and H_2S was studied in greater detail, in an effort to elucidate the major reaction pathways. Experiments were performed to examine the dependence of product yields on the molar ratio of H_2S to EtOH in the reactor feed and the inverse space velocity. Additional studies were performed by feeding proposed reaction intermediates to the reactor, as well as several TPD studies.

Effect of H_2S/EtOH molar feed ratio

The effect of the molar feed ratio of H_2S to EtOH (H_2S/EtOH) was examined at 195°C. The H_2S/EtOH ratio was varied from 0.5 to 15, while maintaining a constant overall

inverse space velocity by using a He diluent. Excess H_2S tended to suppress the overall average reaction rate, so that at each temperature, the EtSH yield was maximized at lower values (0.5-1) of the H_2S/EtOH (Fig. 3). Additionally, the yield of acetaldehyde and other products decreased with increasing H_2S/EtOH, but the effect was more pronounced. The net result was that EtSH selectivity increased with increasing H_2S/EtOH (and thus H_2S partial pressure) up to >94% at H_2S/EtOH equal to 15 (Table 3).

EtOH Only Feed

After running the reaction of EtOH + H_2S for about 18 hours, the flow of H_2S was stopped. EtSH production decreased apparently exponentially, but EtSH was observed in the reactor effluent for more than 20 hours after H_2S was cut out (Fig. 4). During the time when H_2S was not fed to the reactor, the main products of the reaction were acetaldehyde and ethylene, and many other unidentified products were observed in smaller quantities. The conversion of EtOH, and therefore the acetaldehyde yield, was much higher without H_2S present, but the rate of catalyst deactivation was also increased. When H_2S was again admitted to the reactor, the original yields were restored after about 15 hours.

The total amount of EtSH detected after eliminating H_2S from the feed was calculated to be 660 μmol by integrating the product yield curve over time. If the molecular cross-sectional area of H_2S is 0.13 nm^2/molecule, this much H_2S would take up on the order of 100 m^2/g of catalyst surface area. Since the post-reaction surface area of the catalyst is around 80-100 m^2/g, this suggests that under reaction conditions, virtually the entire surface of the catalyst was covered by H_2S.

To determine which, if any, of the observed species in the reactor effluent were reaction intermediates, and also as an initial effort to obtain reaction rate data, the reaction of

EtOH and H_2S was examined as a function of time. The total reactor feed rate was changed while keeping a constant H_2S/EtOH ratio of 1.0, and the yields were plotted as a function of inverse space velocity (Figs. 5-6). At the largest value of the inverse space velocity, EtOH conversion of nearly 40% was obtained. Also note that the concentration of acetaldehyde went through a maximum at short contact time.

Ethylene + H_2S

Ethylene was reacted with H_2S over amorphous LaMoS at 200°C. During this experiment, the molar ratio of H_2S to ethylene was varied from 0.5 to 10. The overall reactor feed rate (and therefore the approximate contact time) was held constant by adjusting a He feed to the reactor. The reaction produced ethanethiol at more than 98% selectivity, with a maximum in selectivity at a value of H_2S/ethylene of 2.0. Interestingly, the conversion ethylene increased with increasing partial pressure of H_2S over the entire range studied (Fig. 7). Side products observed were butenes and 2-methyl-1-propanethiol (tert-butyl thiol) (Fig. 8).

Acetaldehyde + H_2S

Acetaldehyde was reacted with H_2S over amorphous LaMoS at 200°C. During this experiment the molar feed ratio of H_2S to acetaldehyde was kept constant at 10.0. Initially, acetaldehyde was converted virtually completely and mainly to EtSH, though also detected were some ethanol and butenes as well as at least 15 unidentified products. The catalyst deactivated very quickly as reflected by a precipitous loss in acetaldehyde conversion to less than 50% in only two hours on stream (Table 4). After the reaction was completed, a significant amount of a reddish-brown tar-like substance was found in the reactor effluent lines. Analysis by GC/MS showed the substance was a mixture of compounds, having

between 4 and 7 carbon atoms and 3-4 sulfur atoms per molecule. The main constituent was a cyclic compound, 5-methyl-3H-1,2-dithiole-3-thione, ($C_4H_4S_3$).

TPD

To determine the relative strength of adsorption for the main reactants and products, temperature-programmed desorption (TPD) studies were performed for the main species present: EtOH, H_2S, H_2O, and EtSH, as well as the possible intermediates, ethylene and acetaldehyde. Interestingly, additional products were observed on desorption of the main adsorbate, which gave some additional insight into the adsorption characteristics of the desorbing species. TPD studies were also performed with ethylene and acetaldehyde.

The TPD results for ethanol (Figure 9) showed only one large ethanol desorption peak centered at 70° C, which is close to the normal boiling point of ethanol (78°C). Additionally, a small, clear peak for EtSH was observed between 190° and 200° C. Acetaldehyde was observed desorbing in a very broad peak centered at about 60-70° C, but stretching between 20° and 200° C. The acetaldehyde peak had a large shoulder indicating it was probably made up of two overlapping desorption peaks. Deconvolution of the acetaldehyde desorption peak indicated two peaks, a larger one centered at about 70° C and a smaller one centered at about 150° C. Ethylene was observed desorbing from the catalyst also, in a very broad band covering nearly the entire experiment.

The TPD experiment for adsorbed EtSH (Fig. 10) revealed a broad peak at about 70°C, again with a distinct shoulder. Deconvolution of the peak indicated two peaks, a larger one centered at about 67°C, and a smaller one centered at about 161°C. Very small peaks were observed for 1-propanethiol and 2 propanethiol (very broad, from about 60-200°C, and 250-400°C, respectively). These probably arose from impurities in the ethanethiol reagent

used for the experiment. A smaller ethylene peak was also observed centered at about 250°C. However, it was very broad, ranging over virtually the entire temperature range of the experiment.

TPD of adsorbed H_2S (Fig. 11) was very interesting in that a large amount of water was observed desorbing. Desorption of water peaked at about 150°C and then tailed off through the rest of the experiment. Desorption of H_2S did not begin until about 350°C, and the rate of desorption was still increasing at 400°C.

TPD for adsorbed H_2O (Fig. 12) revealed a peak at about 100°C which tailed off gradually up to about 300°C. A small amount of H_2S was observed beginning to desorb at about 350°C, apparently left over from the previous H_2S TPD experiment.

TPD of adsorbed ethylene (Fig. 13) yielded a very broad band from about 30°C up to about 290°C. Of note was the fact that the total intensity of ethylene detected in the desorption was very small compared to the amount observed desorbing during TPD of EtOH and EtSH. A small amount of 2-methyl-1-propanethiol (tert-butyl thiol) was also detected, desorbing above about 340°C.

Acetaldehyde TPD (Fig. 14) yielded a rich array of desorption products, most of which have not been identified. Acetaldehyde itself desorbed in two peaks, a large one that began immediately upon initiation of heating, and a smaller one centered at about 180°C. Also detected were desorption peaks for EtSH (100°C and 190°C) and EtOH (190°C). The numerous unidentified products observed desorbing from the surface were mostly in very small amounts.

Catalyst Stability

Catalyst was characterized after the reaction of EtOH and H_2S for 5 days on stream, to determine the stability of the Mo_6S_8 cluster. The far IR spectrum of materials incorporating the Mo_6S_8 cluster includes a band at around 385 cm^{-1} arising from the Mo-S stretching vibration; occasionally a weaker band at about 253 cm^{-1} arising from Mo-Mo bond vibrations can also be observed (11). Amorphous materials containing the Mo_6S_8 cluster show essentially no Raman bands(11). Crystalline (and also to some degree poorly crystalline) MoS_2 is expected to give rise to sharp IR bands at about 385 and 470 cm^{-1} and sharp Raman bands at about 384 and 408 cm^{-1} (12, 13). Therefore, detection of IR bands at 470 cm^{-1} or Raman bands at both 384 and 408 cm^{-1} would indicate the presence of MoS_2. For both of these characterization methods, spectra taken of mechanical mixtures made with fresh catalyst and pure MoS_2 indicated that the detection limit for MoS_2 was less than 10%.

Results of LRS characterization did not indicate any presence of MoS_2 on either the catalyst as-prepared or after being exposed to reaction conditions with EtOH and H_2S at 200°C for five days. FTIR characterization of the as-prepared catalyst showed the Mo-S stretching vibration absorbance peak at 383 cm^{-1} characteristic of the Mo_6S_8 cluster. However, the band was not clearly visible in the samples post-reaction (Fig 15).

Nitrogen adsorption surface analysis on the catalyst revealed the loss of significant surface area (Table 5). Similar to previous work (4) with methanethiol synthesis at 250°C over these catalysts, the loss of surface area was accompanied by an increase in average pore diameter and a decrease in total pore volume. However, with the lower temperatures employed in this work (200°C), the loss of smaller pores was less dramatic.

XPS spectra (Fig. 16) of catalyst taken before and after reaction indicated only subtle changes in the oxidation state of the Mo at the catalyst surface. Both before and after reaction, the major Mo species detected had the low binding energy characteristic of Mo in the Mo_6S_8 cluster (about 227.3-227.9 eV for the Mo $3d_{5/2}$ peak) (14). A small amount of Mo in a higher oxidation state consistent with MoO_3 (about 231.4-232.9 eV) was observed in the as-prepared sample, likely due to oxygen contamination during the handling procedures.

4. Discussion

Reaction Studies

The reactions of the higher alcohols EtOH, 1-PrOH, and 1-BuOH all occurred readily over amorphous LaMoS, and the reactions involving 1-PrOH and 1-BuOH produced the primary thiol in high selectivity.

Ethanethiol synthesis reaction pathways

The desorption temperature for a particular species can be related to the heat of adsorption for that species, if the order of the reaction is assumed. Generally speaking, however, the higher the desorption temperature, the larger is the heat of adsorption, and so the more strongly adsorbed is the particular species. Based on this idea, the strength of adsorption (chemisorption) of the species in the proposed reaction scheme is ethanol, acetaldehyde, ethanethiol, and hydrogen sulfide. The fact that hydrogen sulfide is very strongly adsorbed is therefore of key importance in determining the dominant reaction pathway. Hydrogen sulfide had the ability to limit the overall reaction rate, but it apparently tended to suppress the rates of the non-selective side reactions more than the desired reaction.

Ethylene + H_2S reaction

The selectivity to ethanethiol was maximized at a value of H_2S/ethylene of about 2.0. This was because the selectivity to butenes decreased, while the selectivity to 1-methyl-2-propanethiol increased, with increasing H_2S/ethylene. Therefore, the total selectivity to butenes and 1-methyl-2-propanethiol was minimized at a value of H_2S/ethylene of 2.0.

While it is difficult to comment on the actual reaction rate for these data, it is possible to conclude that the average rate of ethanethiol production in the reactor did increase with increased H_2S partial pressure, in sharp contrast to the inhibiting effect of H_2S exhibited with the EtOH feed. This suggests that either 1) ethylene is not an important intermediate in the EtOH reaction, or 2) if ethylene is an important intermediate, then the rate controlling step in the overall reaction occurs no later in the mechanism than the formation of ethylene, and it is inhibited by excess H_2S.

It is also very interesting to note that the reaction of ethylene with H_2S to produce ethanethiol over LaMoS is so selective, and occurred so readily. This reaction by itself could be commercially as important or even more imporant than the reaction of EtOH with H_2S over these catalysts.

Given all of the above information, we have hypothesized a reaction mechanism for the system involving hydrogen sulfide and ethanol at 200°C and 1 atm:

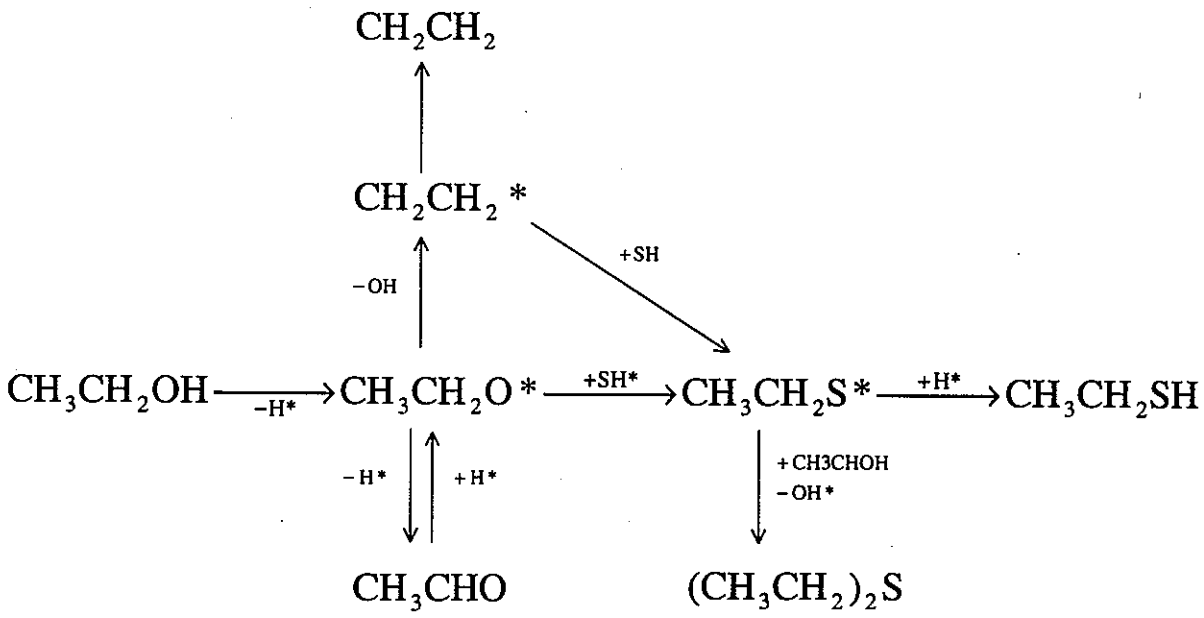

and additionally the following reactions are expected:

$H_2S \longrightarrow SH^* + H^*$ and $OH^* + H^* \longrightarrow H_2O$

where the asterisk (*) refers to an adsorbed species.

In this scheme, ethanol first adsorbs to the catalyst surface dissociatively, as an adsorbed ethoxy species and an adsorbed hydrogen species. The adsorbed ethoxy group can react to form acetaldehyde by the loss of another hydrogen atom, or to ethylene by the loss of hydroxide. However, the main pathway is the conversion to an adsorbed ethyl mercaptide group via exchange of hydroxide and sulfhydryl (SH). The adsorbed ethyl mercaptide then can react with adsorbed hydrogen to form ethanethiol.

At low H_2S partial pressures, (or in its absence), the main reaction pathway is the formation of acetaldehyde, favored over the formation of ethylene by a factor of about 10:1. If even a small amount of H_2S is present, however, the reaction to form ethanethiol is strongly favored. Excess H_2S tends to suppress the rate of EtSH formation, suggesting

saturation kinetic models such as those proposed by Hougen and Watson might be the most appropriate for the main reaction. For example, a simplified model for the main reaction

$$CH_3CH_2OH + H_2S \longrightarrow CH_3CH_2SH + H_2O$$

where all species adsorb dissociatively, and conditions of low conversion are considered (P_{H_2O} and P_{EtSH} are small) is

$$r_{EtSH} = \frac{k\sqrt{K_{EtOH}P_{EtOH}}\sqrt{K_{H_2S}P_{H_2S}}}{\left(1+\sqrt{K_{EtOH}P_{EtOH}}+\sqrt{K_{H_2S}P_{H_2S}}+\sqrt{K_{H_2O}P_{H_2O}}+\sqrt{K_{EtSH}P_{EtSH}}\right)^2}$$ when the surface

reaction is rate controlling. If H_2S is strongly adsorbed, this equation reduces to

$$r_{EtSH} = \frac{k\sqrt{K_{EtOH}P_{EtOH}}}{\sqrt{K_{H_2S}P_{H_2S}}},$$ or equivalently

$$r_{EtSH} = k' P_{EtOH}^{0.5} P_{H_2S}^{-0.5}.$$

Clearly, to show the appropriateness is not possible with the limited data currently available for this system.

The side path involving ethylene is interesting since the separate experiment with ethylene feed showed that the reaction with ethylene and H_2S is very clean, producing almost exclusively ethanethiol. Since it has been established in the TPD experiments that ethylene can adsorb on the catalyst, this may offer an explanation as to the source of the non-selective products, butene and tert-butyl thiol:

$$CH_2CH_2 * + CH_2CH_2 \longrightarrow C_4H_8 *$$

$$CH_3CH_2SH * + CH_2CH_2 \longrightarrow (CH_3)_2CHCH_2SH *$$

At low values of H_2S partial pressure, the formation of butene was faster, but at higher values of H_2S partial pressure, tert-butyl thiol was faster. This could be because at

lower H_2S partial pressures, more adsorption of ethylene is possible, while at higher partial pressures, more adsorbed ethanethiol is present. It is unlikely that the major pathway for the formation of tert-butyl thiol is from the reaction of butene and H_2S. This is because the surface concentration of ethylene should be much lower at higher H_2S partial pressures, preventing the formation of butene in the first place. This idea is supported by the selectivity data, which goes through a maximum at a value of H_2S/Ethylene of about 2.0. This would not be expected unless the rate of butene formation was inhibited by increased H_2S partial pressure.

In the experiment where the reactor residence time was varied, the yield of acetaldehyde went through and apparent maximum at very short residence times. This indicates that the formation of acetaldehyde is very fast. The fact that the concentration of acetaldehyde decreased with time indicates that it is possibly an intermediate product in the overall reaction scheme. However, it is also possible that the reactions whereby acetaldehyde is formed from surface ethoxy species, and the reverse reaction whereby ethoxy species is formed from acetaldehyde, are fast and approach equilibrium. In that case the observed concentration of acetaldehyde could go through a maximum even if acetaldehyde itself were not a direct intermediate in the main pathway. This is because the gas phase concentration of acetaldehyde would always directly depend on the surface concentration of ethoxy species. Indeed, when ethanol alone is fed into the reactor at 200°C, acetaldehyde was formed at 10-12% yield, which was fairly close to the predicted equilibrium yield of 15%.

The main reaction pathway in the scheme presented above depends strongly on the amount of H_2S that is present; at low partial pressures of H_2S the routes to acetaldehyde and

ethylene are favored, and at high partial pressures of H_2S the route to ethanethiol is strongly favored. Without any H_2S present, the yield of acetaldehyde (11-12%) from EtOH approached equilibrium conditions (15%), indicating a very fast reaction. At low partial pressures of H_2S, particularly at a value of H_2S/EtOH equal to 1, acetaldehyde is either a direct intermediate to the ethanethiol product, or more likely is representative of the surface concentration of adsorbed ethoxy species.

Acetaldehyde as feed to the reactor with H_2S initially reacted primarily to ethanethiol and the reaction was apparently very fast. However, examining the required stoichiometry of the overall reaction:

$$CH_3CHO + H_2 + H_2S \longrightarrow CH_3CH_2SH + H_2O$$

suggests that there was an effective hydrogen shortage on the catalyst surface. This may help to explain the source of the observed tar-like substance found in the reactor effluent lines, which was made up of refractory compounds having low H/C atomic ratios. The H_2 required for EtSH formation could have been produced by dehydrogenation and sulfur insertion reactions to form the cyclic compounds. For example, the overall stoichiometry for producing $C_4H_4S_3$ from acetaldehyde would produce three free hydrogen molecules:

$$2CH_3CHO + 3H_2S \longrightarrow C_4H_4S_3 + 2H_2O + 3H_2$$

The effective hydrogen shortage is not a good scenario for the catalyst activity since these types of reactions would tend to produce heavier species that would remain on the surface of the catalyst, blocking access to active sites.

Catalyst Stability

Post-reaction characterization of the catalyst by LRS and FTIR did not show any formation of MoS_2. Additionally, XPS characterization suggested that the main species of Mo present at the surface of the catalyst was Mo in cluster units, in a very reduced state. This is in contrast to previous work (4) with methanethiol synthesis, where there was a significant shift of Mo to higher oxidation states at the catalyst surface. The restructuring seen previously appeared to be temperature activated, where higher temperatures up to 400°C also favored MoS_2 formation. With the higher alcohol feedstocks employed in this work, conversion to the thiols occurred more easily. Reactant conversions were adequate to allow study of these systems at 200°C. This was probably an important factor in maintaining the more reduced Mo oxidation state at the catalyst surface.

5. Conclusions

Amorphous $La(Mo_6S_8)S_{1.5}$ has been shown to be an active, selective, and stable catalyst for thiol synthesis from higher alcohols and H_2S. In contrast to our previous work with methanol, thiol selectivity is not limited by production of carbon oxides or CS_2, and reasonable reaction temperatures could be lower (200°C). The reaction pathway of EtOH and H_2S appears to proceed via a surface-adsorbed intermediate, which can desorb as ethylene or acetaldehyde. Reaction with 1-BuOH favored the formation of 1-BuSH with high selectivity (>90%).

Due to the strength of H_2S adsorption, a compromise must be made between acceptable conversion and selectivity when choosing the appropriate H_2S partial pressure, since excess H_2S suppresses the overall reaction but increases EtSH selectivity. Application of these catalysts would probably require increasing the conversion to nearly 100%, either by

increasing the reactor temperature or contact time. This may lower the selectivity beyond what has been reported here.

This catalyst was also shown to very effectively catalyze the reaction of ethylene and H_2S to form EtSH, with selectivities as high as 99% at fairly low H_2S/ethylene ratios. This could be a very interesting area for future research.

Under reaction conditions with EtOH and H_2S, the catalyst appears to be stable for extended periods (up to five days), and formation of MoS_2 was not detected. However, changes to the physical structure did occur including reduction of surface area due to loss of smaller pores.

6. Acknowledgements

We thank Jim Anderegg of the Ames Laboratory for assistance in obtaining the XPS characterization. This work was supported by the U.S. Department of Energy, Office of Basic Energy Sciences, through Ames Laboratory operated by Iowa State University under Contract No. W-7405-Eng-82.

7. References

1 Roberts, J. S., Kirk-Othmer Encyclopedia of Chemical Technology, 4th Ed., John Wiley & Sons, NY (1997), Vol. 24, 19-34.

2 Mashkin, V. Yu., *Applied Catalysis A: General*, 109 (1994), 45-61.

3 Mashkin, V. Yu., Chernomyrdina, N. A., Mashkina, A., V., *Kinetics and Catalysis*, **36**(5), (1995), 639-643.

4 Paskach, T. J., McCarley, R. E., Schrader, G. L., *J. Catal.* (submitted JCAT-01-0450) (2001)

5 Hilsenbeck, S. J., McCarley, R. E., Thompson, R. K., Flanagan, L. C., and Schrader, G. L., *J. Mole. Catal. A: Chemical*, **122**, 13-24 (1997).

6 McCarty, K. F., and Schrader, G. L., *Ind. Eng. Chem. Prod. Res. Dev.*, **23**, 519 (1984).

7 McCarty, K. F., Anderegg, J. W., and Schrader, G. L., *J. Catal.*, **93**, 375 (1985).

8 Eckman, M. E., Anderegg, J. W., and Schrader, G. L., *J. Catal.*, **117**, 246 (1989).

9 Ackman, R. G., *J. of Gas. Chrom.*, June, 1964.

10 Ackman, R. G., *J. of Gas. Chrom.*, October, 1968.
11 Hilsenbeck, S. J.; Young, V. G.; McCarley, R. E. *Inorganic Chemistry*, **33**(9), 1822-1832 (1994).
12 Chang, C. H. and Chan, S. S., *J. Catal.*, **72**(1), 139-48 (1981).
13 Wieting, T. J. and Verble, J. L., *Phys. Rev. B*, **3**(12), 4286-92 (1971).
14 McCarley, R. E., Hilsenbeck, S. J., and Xie, X., *J. Solid State Chem.*, **117**, 269 (1995).

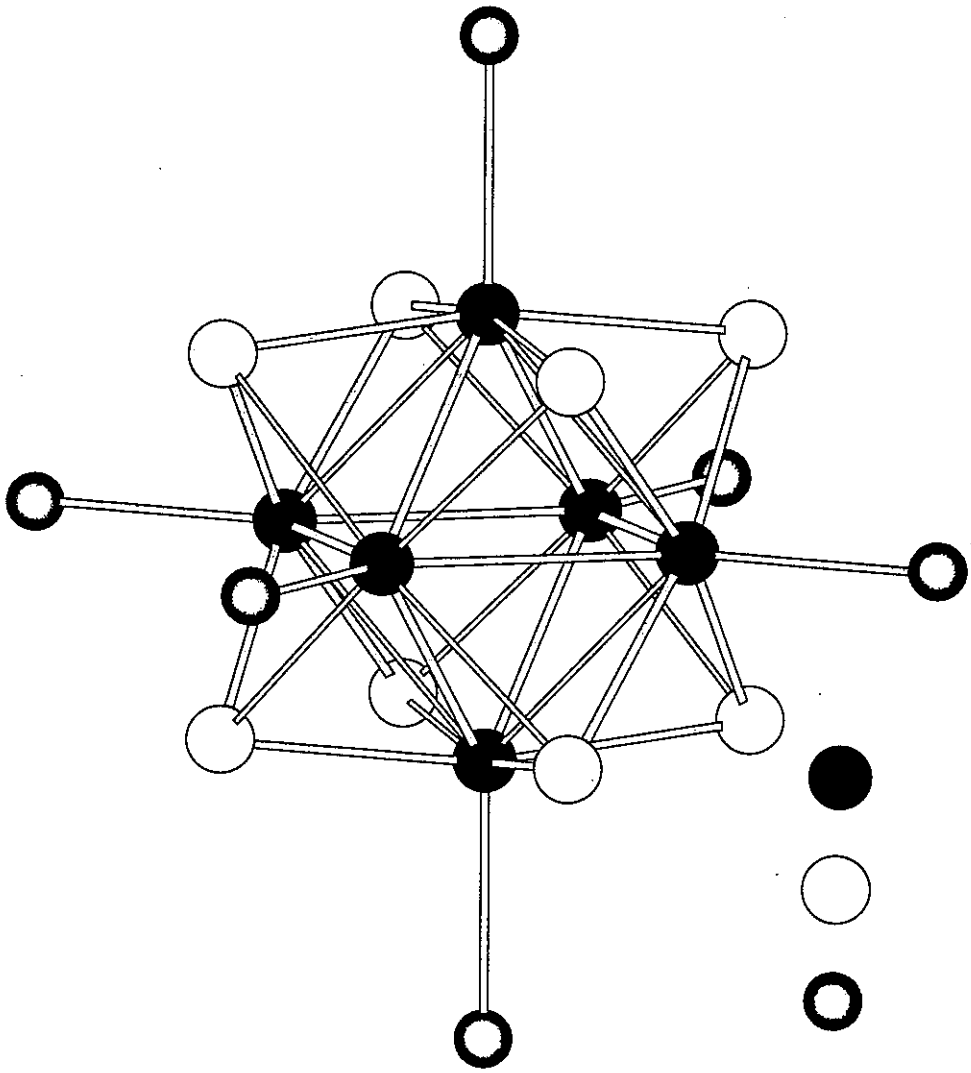

Figure 1. Structure of the Mo_6S_8 hexanuclear cluster unit which is formed by a molybdenum octahedron and eight triply bridging sulfur atoms capping each face. Additionally, six terminal positions are located at the vertices of the octahedron and are occupied by either organic ligands or sulfur atoms.

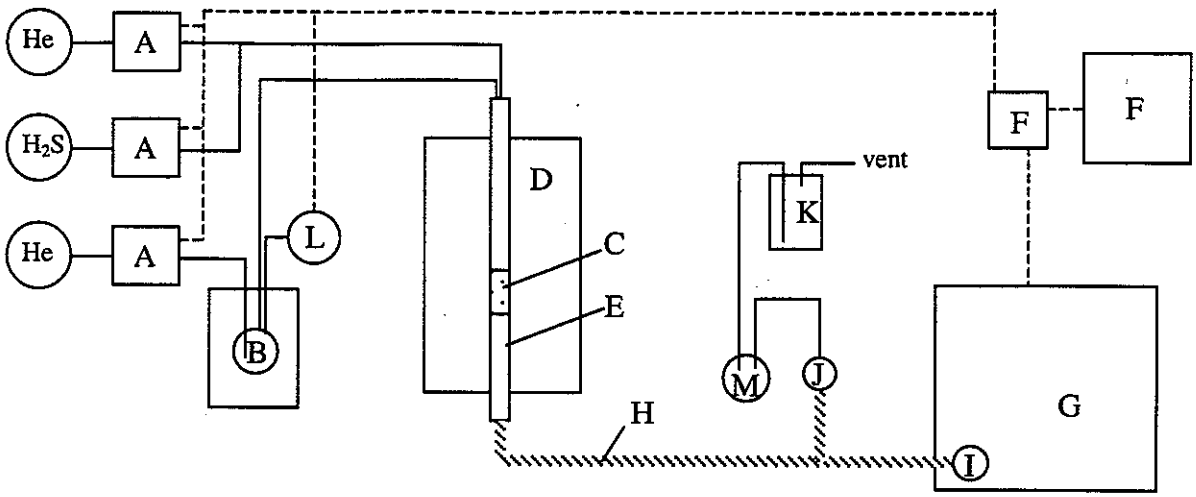

Figure 2. Microreactor system. A: mass flow controllers, B: saturator for liquid feeds, C: catalyst bed with quartz wool plug on bottom, D: temperature-controlled reactor furnace, E: Pyrex or quartz tube reactor, F: control computer and analog/digital in/out interface, G: GC with FID and TCD, H: heat tracing, I: sample injection valve, J: split valve, K: KOH/bleach bubbler, L: pressure transmitter, M: trapping vial.

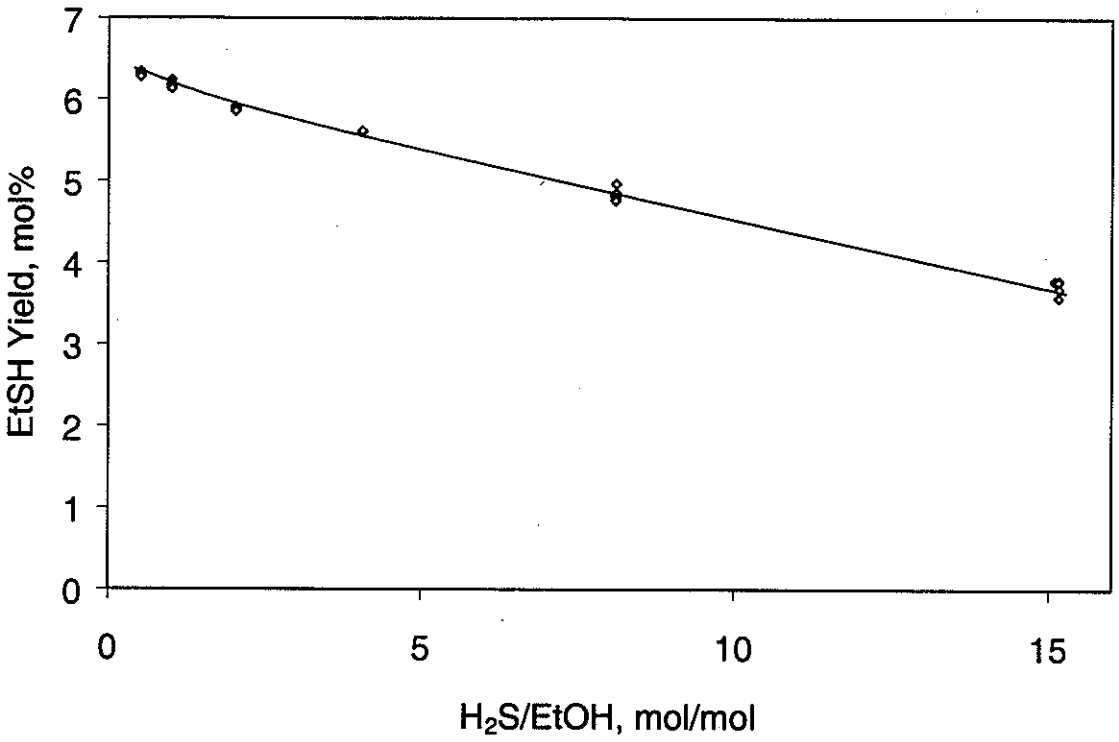

Figure 3. The effect of increasing H_2S/EtOH on EtSH yield at 200°C and constant inverse space velocity.

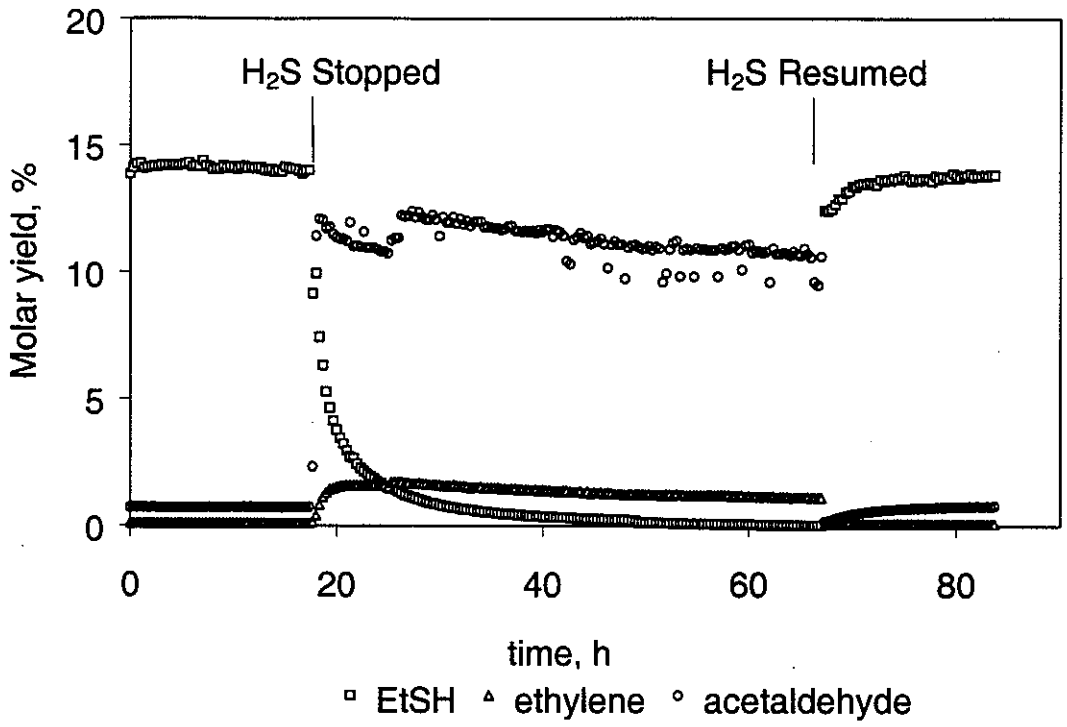

Figure 4. Effect of temporarily removing H_2S from the reactor feed on product yields.

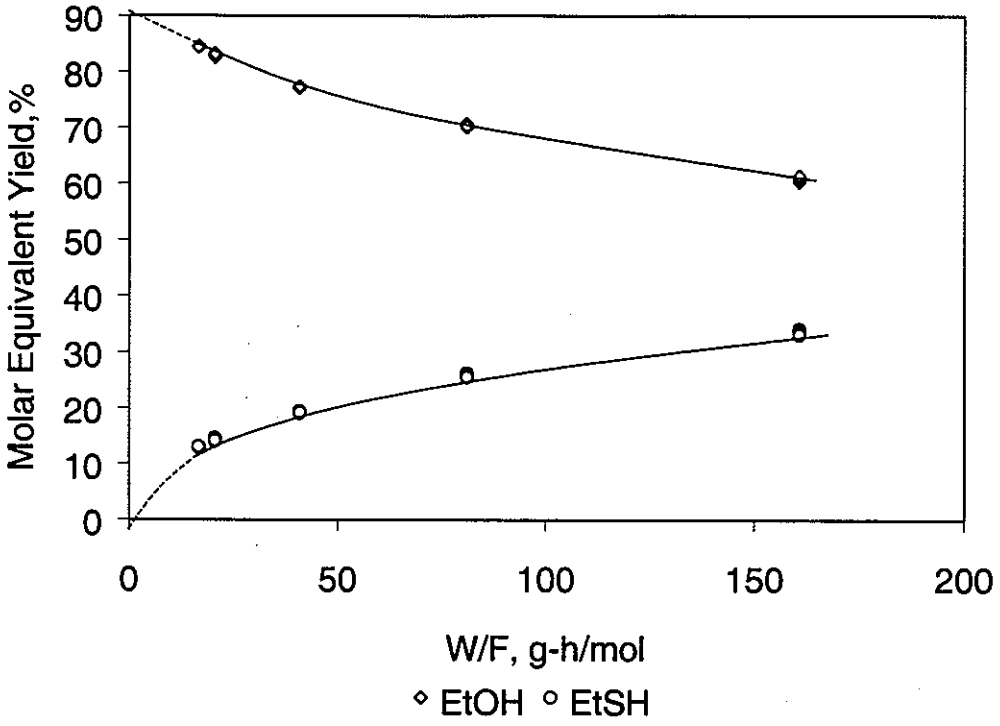

Figure 5. Yield of EtSH and EtOH as a function of the inverse space velocity at 200°C and a H_2S/EtOH feed ratio of 1.0.

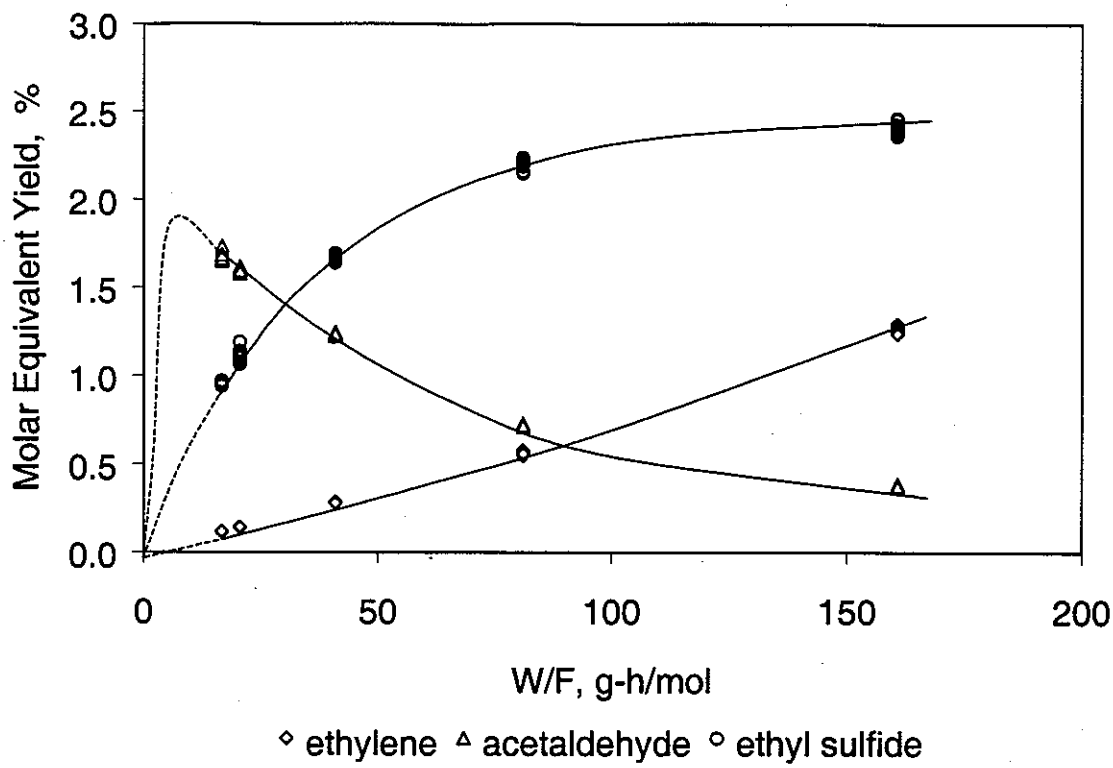

Figure 6. Yield of nonselective products as a function of the inverse space velocity at 200°C and a H_2S/EtOH feed ratio of 1.0.

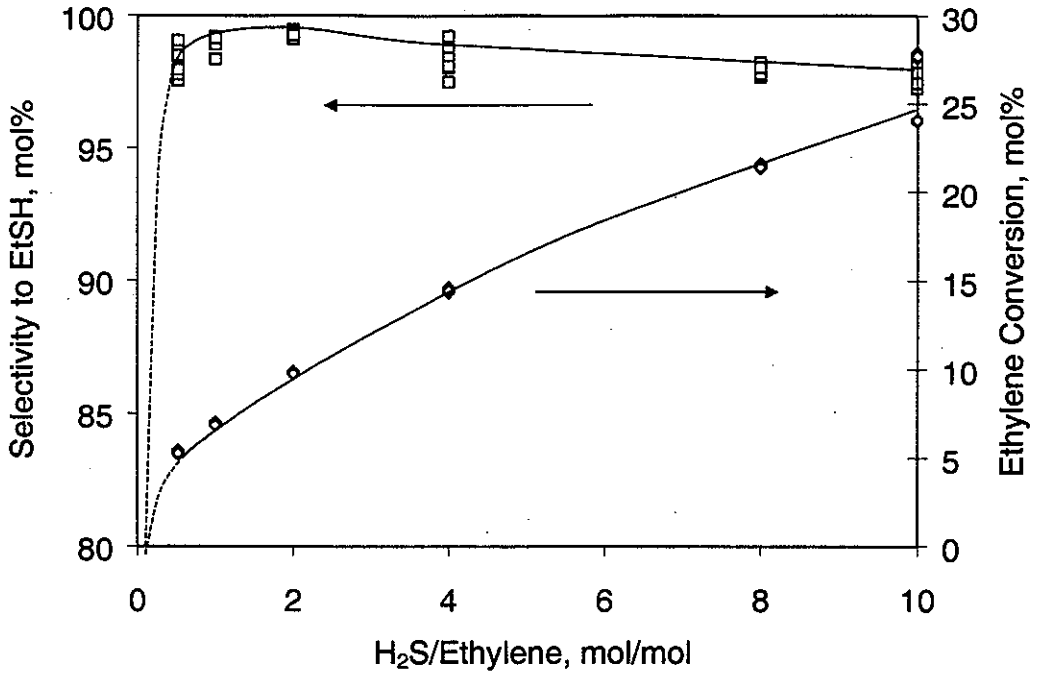

Figure 7. The effect of H_2S/Ethylene on ethylene conversion and EtSH selectivity at 200°C and constant inverse space velocity.

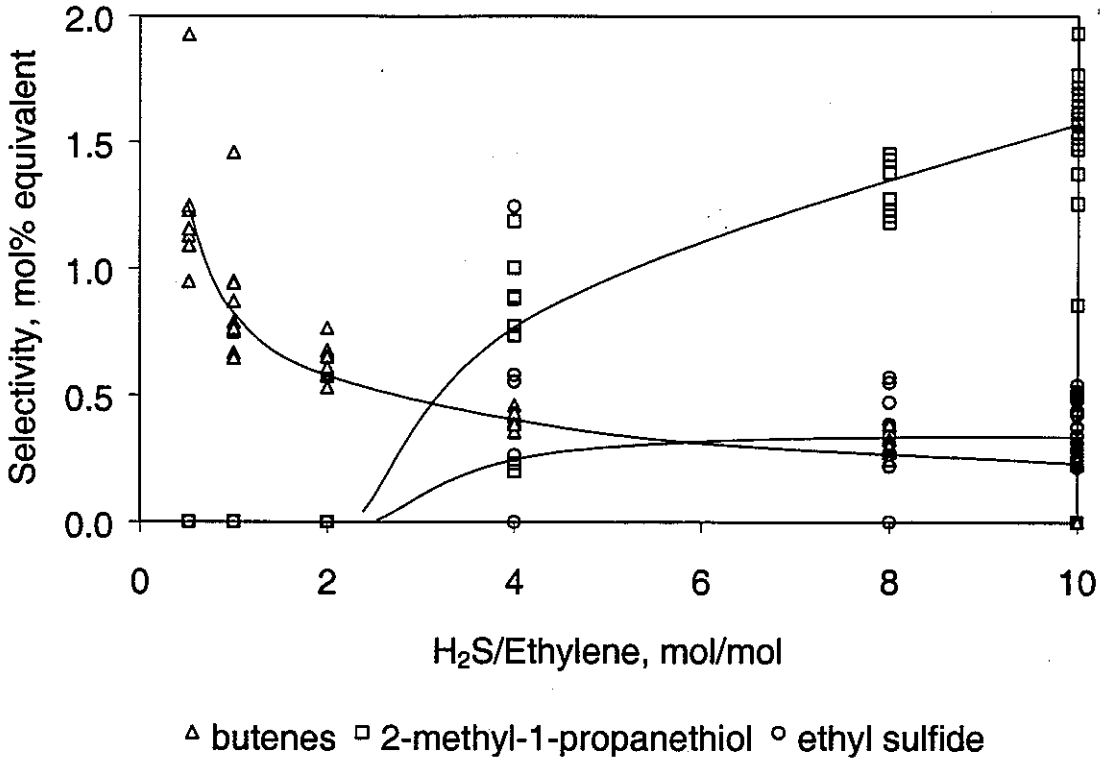

Figure 8. The effect of H_2S/Ethylene on selectivity to side products at 200°C and constant inverse space velocity.

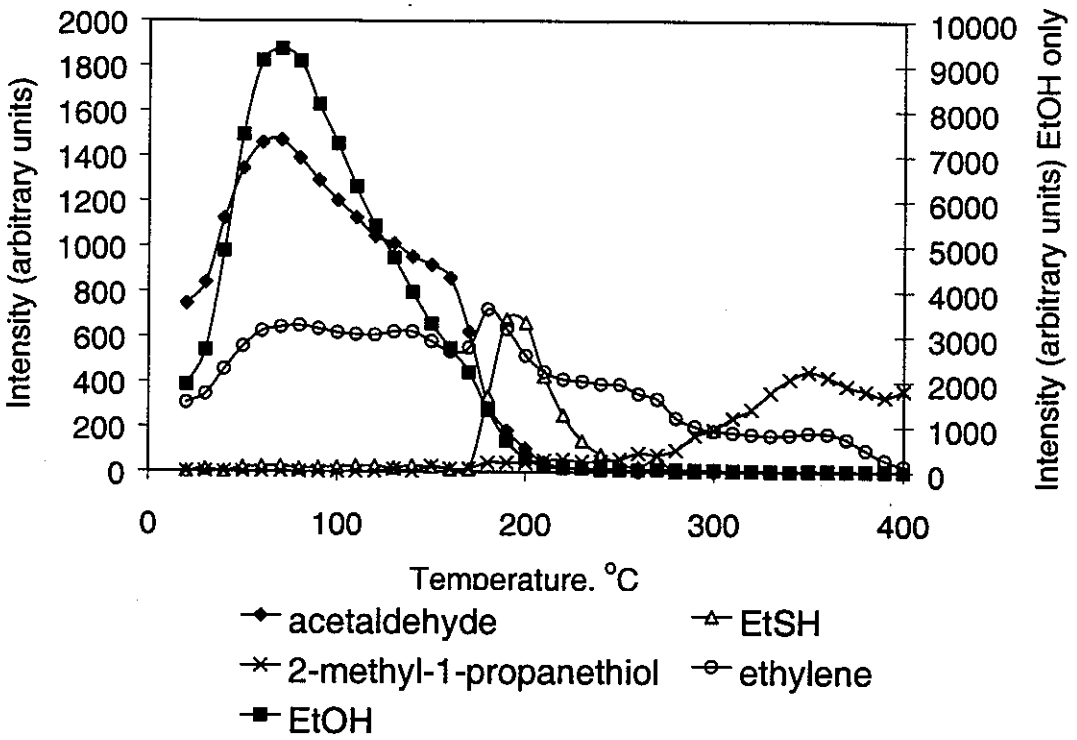

Figure 9. TPD products of adsorbed EtOH

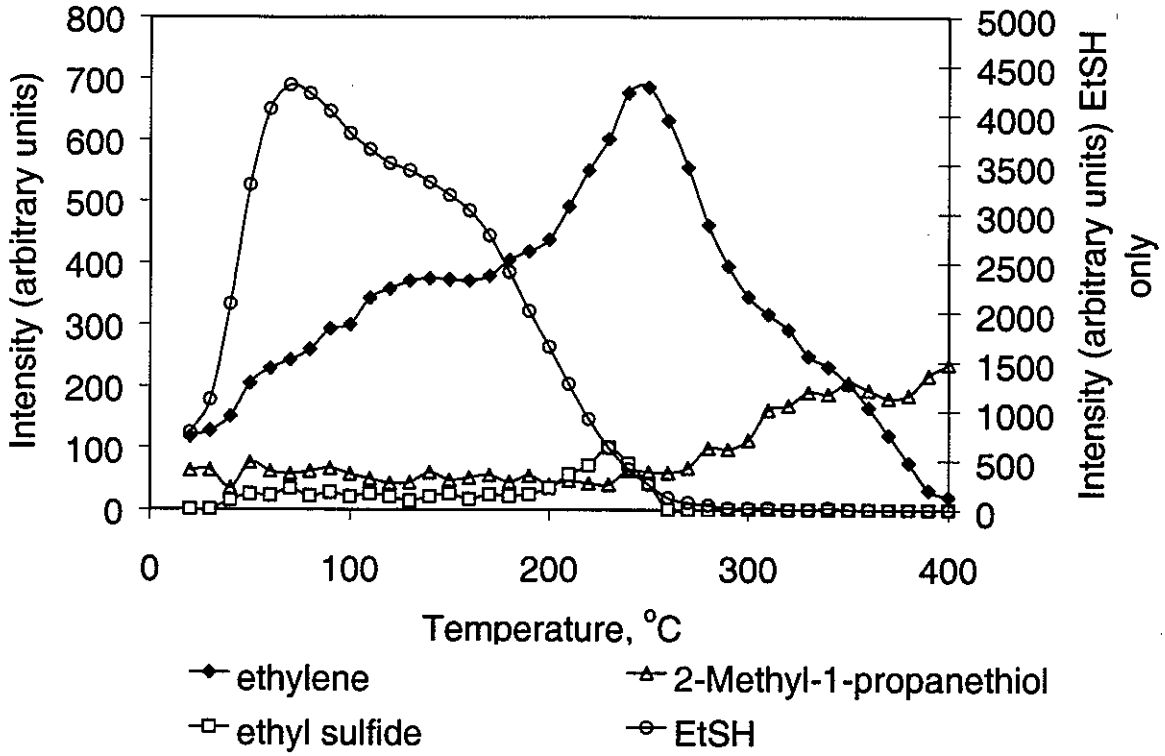

Figure 10. TPD products of adsorbed EtSH

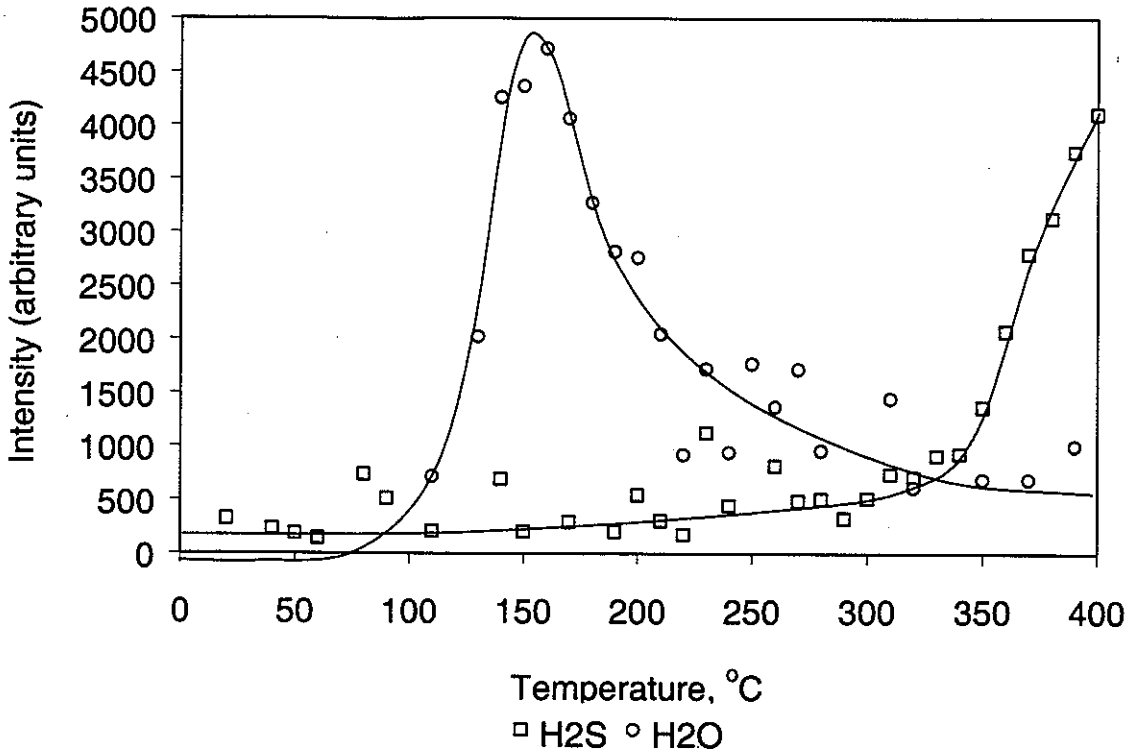

Figure 11. TPD products of adsorbed H_2S

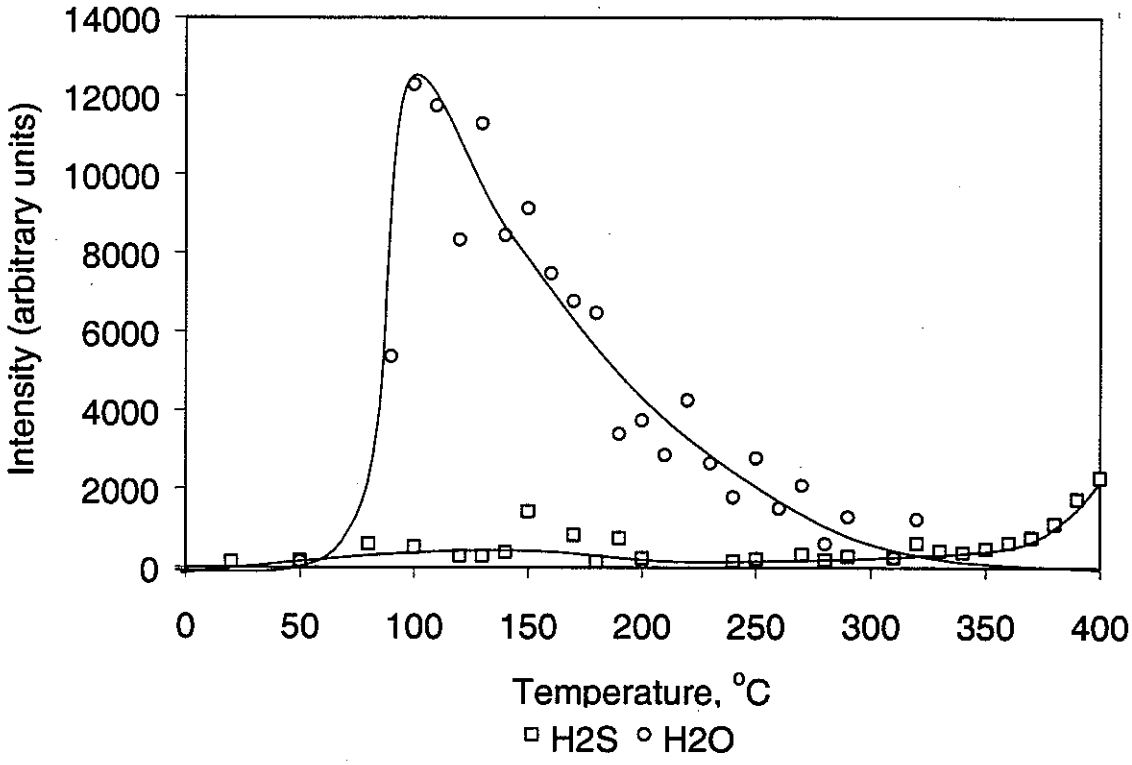

Figure 12. TPD products of adsorbed H_2O

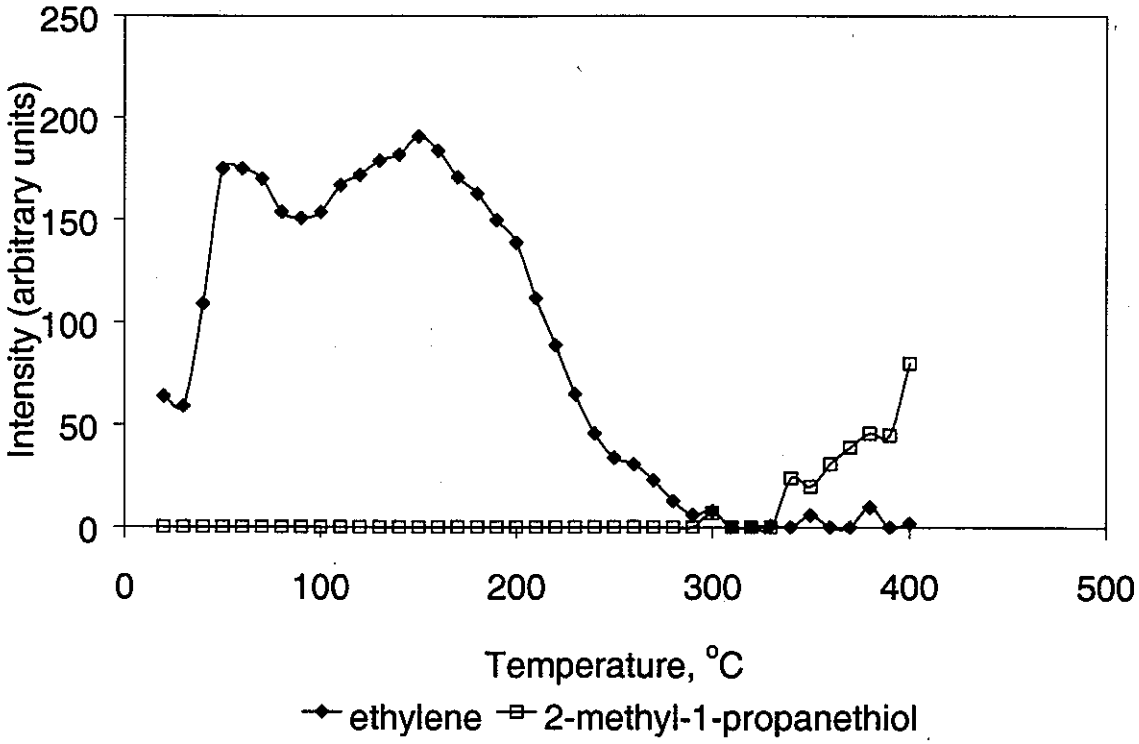

Figure 13. TPD products of adsorbed ethylene

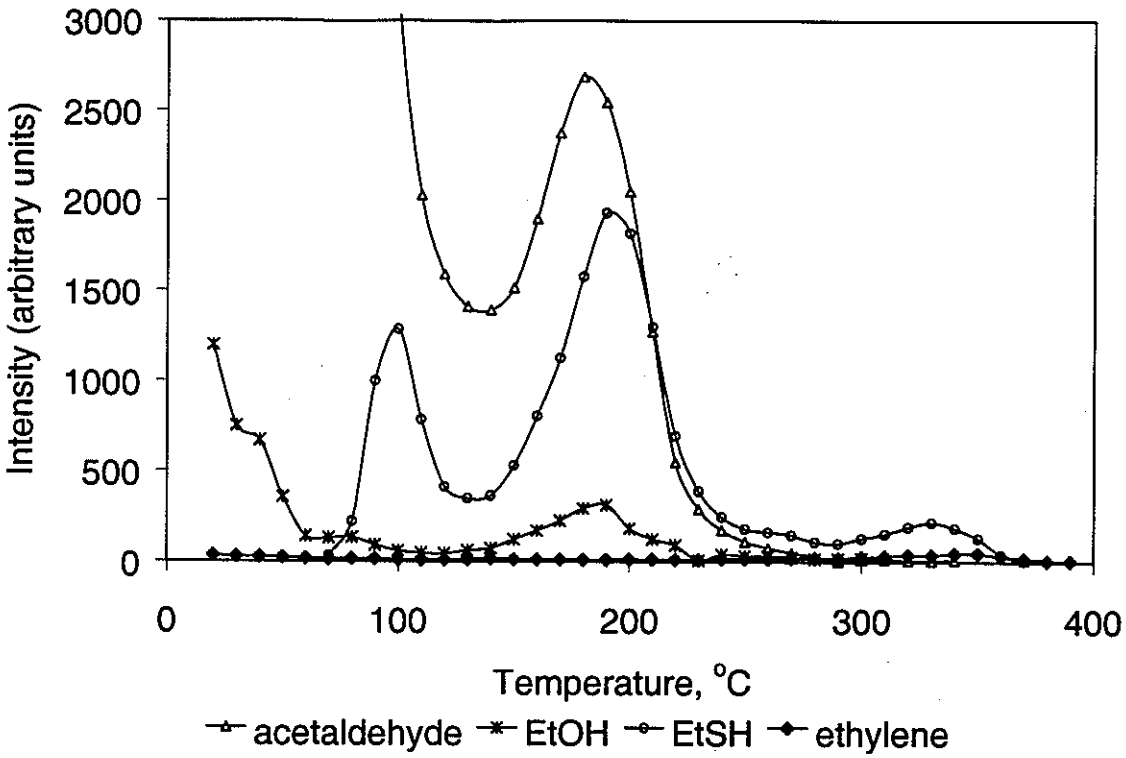

Figure 14. TPD products of adsorbed acetaldehyde

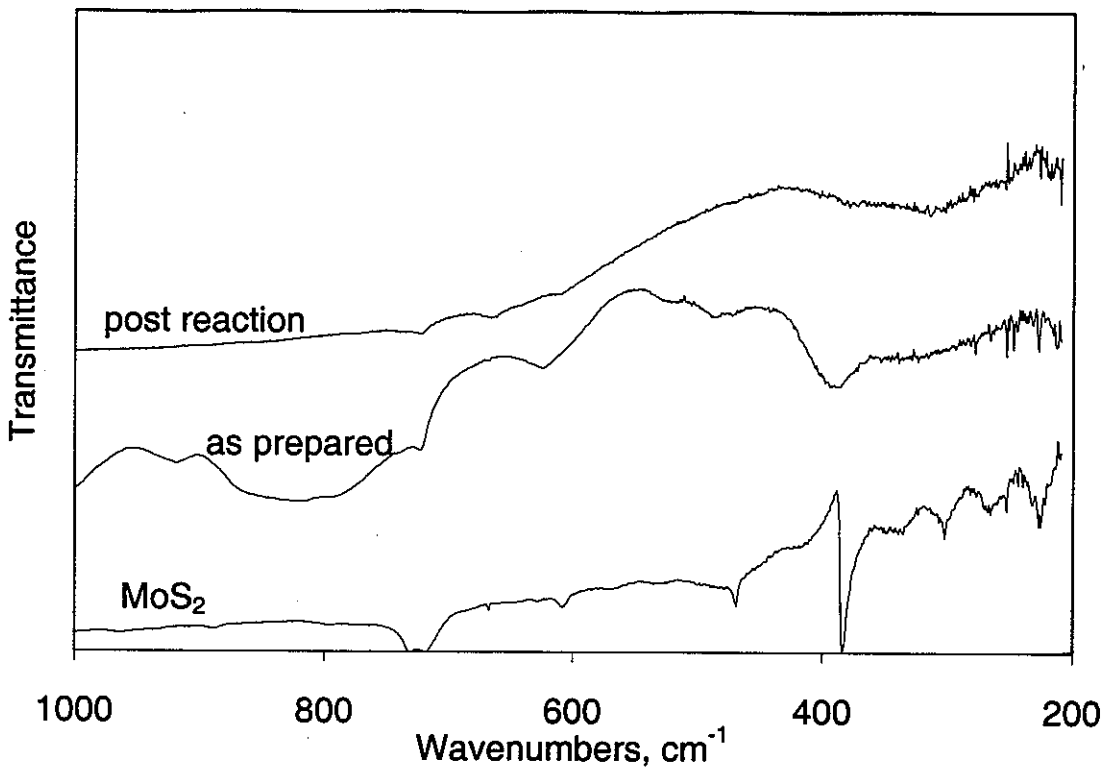

Figure 15. FTIR spectra of LaMoS before and after reaction. The peak at 383 cm^{-1} results from the Mo-S stretch in the Mo_6S_8 cluster, and is not readily apparent in the post-reaction sample.

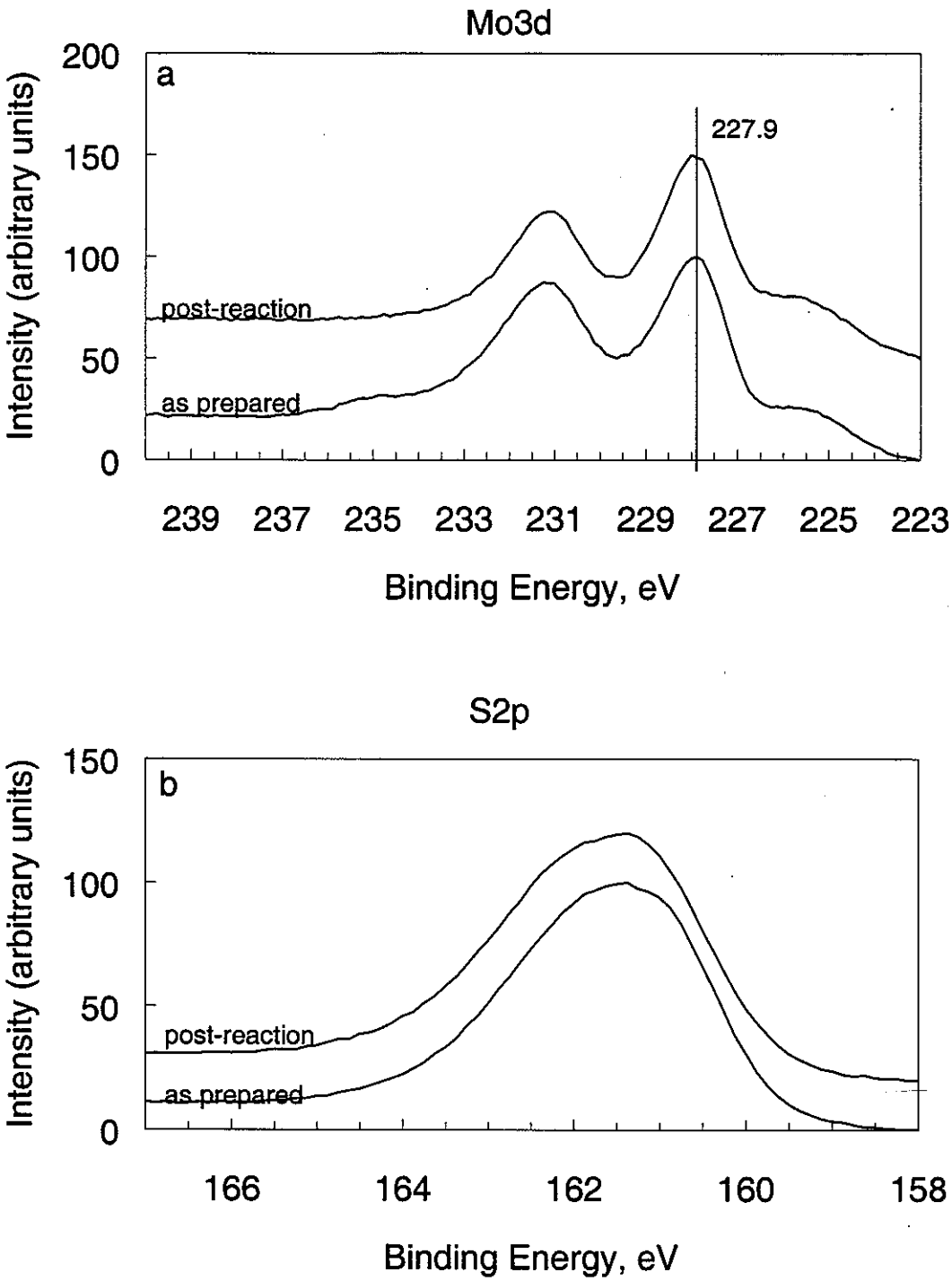

Figure 16. X-ray photoelectron spectra of amorphous LaMoS catalyst for Mo3d, and S2p regions, before and after reaction at 200°C. There is no shift in the oxidation state of the major Mo species, and no change apparent at all for S species.

Table 1. EtOH conversion and selectivies to various products at 200°C and a H_2S/EtOH ratio of 10.0.

EtOH conversion, mol%	28.4
Selectivities, mol% equivalent	
EtSH	92.6
DES	2.8
Ethene	2.4
Butenes	0.5
Acetaldehyde	0.0
Other Products	1.7

Table 2. Conversion and selectivities for the reaction of 1-BuOH with H_2S at 200°C over amorphous LaMoS.

Contact time	**H_2S/1-BuOH**	**BuOH Conversion**	**Selectivities, mol%**					
sec	mol/mol	mol%	1-BuSH	DBS	2-BuSH	2-BuOH	butenes	other products
1.66	1.5	6.3	89.5	2.3	0.0	2.7	2.4	3.1
1.66	3.0	14.1	94.5	0.4	0.4	1.0	1.9	1.7
1.66	5.0	14.6	94.9	0.3	0.6	0.6	2.2	1.4
1.66	10.0	13.0	95.4	0.2	0.8	0.4	2.0	1.2
0.55	3.0	4.7	92.3	1.2	0.0	2.8	1.6	2.1
0.83	3.0	5.3	90.1	2.7	0.0	2.0	1.9	3.4
1.66	3.0	14.1	94.5	0.4	0.4	1.0	1.9	1.7
3.32	3.0	16.3	91.3	0.9	0.6	1.1	2.5	3.6

Table 3. EtOH conversion and product distributions as a function of H_2S/EtOH feed ratio at 200°C and constant inverse space velocity.

H_2S/EtOH	**EtOH conversion**	**Yields, mol%**			**Selectivities, mol%**		
mol/mol	mol%	EtSH	Acetaldehyde	Other products	EtSH	Acetaldehyde	Other products
0.5	9.7	6.3	2.5	0.9	65.1	25.7	9.2
1.0	8.7	6.2	1.7	0.8	71.2	19.9	8.9
2.0	7.7	5.9	1.1	0.7	76.3	14.8	8.8
4.1	6.8	5.6	0.7	0.5	82.4	10.3	7.3
8.1	5.5	4.8	0.3	0.3	88.6	6.4	5.1
15.1	3.9	3.7	0.0	0.2	94.4	1.0	4.6

Table 4. Acetaldehyde conversion and product selectivities as a function of time on stream at 200°C and a H_2S/acetaldehyde feed ratio of 10.0.

Time on stream	Acetaldehyde conversion	Approximate selectivity, mol%			
h	mol%	EtSH	EtOH	Butenes	Other products
0.7	99	67	5	3	24
1.0	99	71	7	2	21
1.3	94	73	7	2	18
1.6	55	74	8	1	17
4.3	41	55	1	1	43
14.3	26	51	1	1	47
24.3	15	13	2	0	85

Table 5. Results of nitrogen adsorption analysis for catalyst as prepared and after exposure to reaction conditions for 5 days at 200°C.

	Surface area	**Total pore volume**	**Average pore diameter**
	m^2/g	cm^3/g	Å
As prepared	170	0.274	83
Post reaction	86	0.232	98

CHAPTER 6. CONCLUSIONS AND RECOMMENDATIONS

General Discussion

Compounds containing the Mo_6S_8 cluster represent a new and interesting family of catalysts for organosulfur chemistry. A wide variety of materials can be made, with different morphologies and ranging ternary metals. Using the low-temperature pathway for their synthesis, a novel material was made containing Pt. This material represented the first time a Mo_6S_8 material was made that contained a noble metal. That material, ,PtMoS, was shown to have very high activity for hydrodesulfurization of thiophene, with a high selectivity to butene products.

All of the major families of compounds: amorphous ternary materials: ligated molecular clusters, and Chevrel phases, have been shown to have be activite for MeSH synthesis from MeOH and H_2S, though there was significant selectivity to carbon oxides, COS, and CS_2. Of those materials studied, amorphous LaMoS

Recommendations for Future Research

Clearly there are several opportunities for future work in the area of organosulfur synthesis over these compounds. First, there is still plenty to be learned regarding the mechanism for ethanethiol synthesis over these catalysts. This could be done using the existing apparatus, although the addition of a second liquid feed capability would improve its versatility greatly by allowing the addition of products or intermediates during the main reaction of EtOH and H_2S. One of the main difficulties with the pathway studies where a pure intermediate or product is fed to the reactor is that the conditions at the catalyst surface may be significantly different from that during the normal reaction. Spiking small amounts of intermediates or products into the feed of a normal reaction would not expected to perturb

the usual catalyst surface conditions so greatly. This would give a more reliable indication of the role of the intermediates or products in inhibiting or enhancing the various reaction pathways.

Additionally, actual *in-situ* studies of the catalyst may be possible using FTIR or solid-state NMR during the reaction. These would have the benefit of seeing changes in the catalyst in real time, and possibly even the direct detection of surface intermediates.

Probably the most promising new application for amorphous LaMoS could be in the area of EtSH synthesis starting with ethylene. Again, very nice mechanism studies could be performed on this reaction since it is so clean.

There also still exists a huge potential of exploiting the ability to make such a wide range of ternary catalysts containing the Mo_6S_8 cluster. Some of these would have advantages for forming supported catalysts, especially those like the molecular clusters that are soluble in common solvents.

APPENDIX A. TYPES OF ORGANO-SULFUR COMPOUNDS, NOMENCLATURE, PHYSICAL PROPERTIES

The literature in organosulfur chemistry often uses the common names for these compounds, so a review of the nomenclature of these compounds is included here for convenience.

A ***thiol*** contains the sulfhydryl group (–SH) and can form the same types of derivatives as alcohols: thioacetals, thioesters, etc. Thus, the naming conventions are similar to those for alcohols; it is possible to have normal or branched thiols, primary, secondary, or tertiary thiols, dithiols, trithiols, etc. Thiols which also have a hydroxy group are called ***mercaptoalcohols***, e.g. 1-thio-4-butanol[1]. The common name for thiol is ***mercaptan***, and these terms are typically used interchangeably, even within a single source. Common names for the ***thioethers*** are ***alkylsulfides***; e.g. dimethyl thioether is normally referred to as methyl sulfide or dimethylsulfide.

Sulfur is similar to oxygen in that it can form a five-membered aromatic ring structure, and this is named ***thiophene***. The naming conventions here are similar to furan, i.e. start numbering with 1 for the sulfur atom, and 2-5 clockwise for the 4 carbon atoms in the ring.

Polysulfides are formed when the –SH group is oxidized to form –S-S- chains of two or more sulfur atoms. Disulfides are the most common, and are named with the alkyl groups, e.g. dimethyl disulfide, CH_3-S-S-CH_3.

Thiiranes (also commonly called episulfides) refer to the 3-membered, sulfur-containing ring structured compounds analogous to oxiranes (epoxides or alkene oxides). Naming conventions again follow those for the analogous oxygen compound.

In addition to the engineering controls, other measures were taken to assure safety in handling H_2S:

1. A buddy system was employed whenever the H_2S cylinder was opened, where a second person would some distance from the person opening the cylinder.
2. The system was pressure tested (leak checked) on a periodic basis.
3. Only trained personnel were allowed to operate the reactor system.
4. A detailed standard operating procedure (SOP) manual was prepared for this project. It described procedures for startup, shutdown, and emergencies, so the reactor system could be operated safely. This manual was kept in the laboratory at all times, and reviewed on a regular basis.

APPENDIX C. DETERMINATION OF REACTION EQUILIBRIUM CONSTANTS

The determination of equilibrium constants for chemical reactions depends on the relation $K_{eq}(T) = \exp\left(\frac{-\Delta G^{o}_{rxn,T}}{RT}\right)$.

Since values of the Gibbs energy are normally only listed in tables for pure compounds at 25°C, calculations must be performed in order to determine these values at other temperatures. Using the equation

$\Delta G = \Delta H - T\Delta S$,

it is obvious we can calculate the Gibbs energy by knowing the values of the enthalpy and the entropy of reaction at the reaction temperature. These values are calculated by their defining equations: $\Delta H_{rxn,T} = \sum_i \nu_i \Delta H_{f,i,T}$ and $\Delta S_{rxn,T} = \sum_i \nu_i \Delta S_{f,i,T}$.

However, since the values of the enthalpy and entropy are tabulated for pure substances only at 298 K, we need heat capacity information so that they can be calculated at reaction temperature by the relations $\Delta H_{f,i,T} = \Delta H^{o}_{f,298} + \int_{298}^{T} Cp(T)dT$ and $\Delta S_{f,i,T} = \Delta S^{o}_{f,298} + \int_{298}^{T} \frac{Cp(T)}{T} dT$.

The heat capacity relationship is sometimes a polynomial, but more precise relationships have been suggested, such as in the DIPPR database[2]:

$$Cp(T) = A + B\left(\frac{\frac{C}{T}}{\sinh\left(\frac{C}{T}\right)}\right)^2 + D\left(\frac{\frac{E}{T}}{\cosh\left(\frac{E}{T}\right)}\right)^2$$

Then the equations for enthalpy and entropy can be determined by performing the integrations above:

$$\Delta H(T) = AT + BC\coth\left(\frac{C}{T}\right) - DE\tanh\left(\frac{E}{T}\right) + const,$$

$$\Delta S(T) = A\ln(T) + B\left[\left(\frac{C}{T}\right)\coth\left(\frac{C}{T}\right) - \ln\left(\sinh\left(\frac{C}{T}\right)\right)\right] - D\left[\left(\frac{E}{T}\right)\tanh\left(\frac{E}{T}\right) - \ln\left(\cosh\left(\frac{E}{T}\right)\right)\right] + const.$$

Once these values are known, calculation of the Gibbs energy and therefore the equilibrium constants at the reaction temperature is straightforward.

The values of equilibrium constants quoted here were actually determined using the HYSYS (3) simulation software, which makes use of similar correlations for heat capacity.

References.

1 Morrison and Boyd, Organic Chemistry, Fifth Ed., Allyn and Bacon, Inc., 1987.

2 T. E. Daubert and R. P. Danner, Physical and Thermodynamic Properties of Pure Chemicals Data Compilation, Hemisphere Publishing Corp, NY (1989).

3 HYSYS is a trademark of Hyprotech, Ltd, Calgary, Alberta, Canada.

ACKNOWLEDGEMENTS

I would like to thank my major professor, Glenn Schrader for his constant guidance and support, and for allowing me freedom in my research. I would also like to thank Prof. Bob McCarley, who was always willing to share valuable insights. I would like to thank my colleages, Dr. Kirk Thompson, Dr. Craig Fontenot, and especially Dr. Will Schroeder, for their willingness to listen to my ideas and offer their own. I would also like to thank Prof. Peter Reilly, for encouraging me to enter graduate school. But most of all, I would like to thank my wife, Jeanne, for her constant support, encouragement, and love.

This work was performed at Ames Laboratory under Contract No. W-7405-Eng-82 with the U.S. Department of Energy. The United States government has assigned the DOE Report number IS-T 1939 to this thesis.